MASSACHUSETTS INSTITUTE OF TECHNOLOGY
LINCOLN LABORATORY

ELF PROPAGATION STUDY (PHASE II – FALL 1971)

D. P. WHITE
D. K. WILLIM

Group 66

TECHNICAL NOTE 1972-1

15 FEBRUARY 1972

LEXINGTON MASSACHUSETTS

The work reported in this document was performed at Lincoln Laboratory, a center for research operated by Massachusetts Institute of Technology. The work was sponsored by the Department of the Navy under Air Force Contract F19628-70-C-0230.

ABSTRACT

An experimental measurement program has been undertaken to determine the parameters for propagation in the 40 and 70 Hz range. A transmitter in Wisconsin (WTF) transmitted simple sinusoidal signals for two eight-hour periods per day for 20 days. The radiated power was 1/4 watt at 45 Hz and 1/2 watt at 75 Hz. Receiver sites were located in Utah, Nova Scotia and Hawaii.

Subject to the constraints detailed in the text, estimates of the attenuation rates and the mode excitation factors have been determined with high accuracy. The daytime attenuation rates were found to be higher than those estimated previously on the basis of theoretical calculations. The nighttime excitation factor was also found to be a few dB smaller than previously expected. A careful analysis shows that directional differences in the attenuation rates ($|\alpha_{EW} - \alpha_{WE}|$) are <u>less</u> than 0.2 dB |Mm for both the 40 and 70 Hz range.

Accepted for the Air Force
Joseph R. Waterman, Lt. Col., USAF
Chief, Lincoln Laboratory Project Office

NOTATION

α	true attenuation rate (dB/Mm) of only propagating mode
α'	true attenuation rate (nepers/Mm)
α_{eff}	approximation for α when *total* field strengths are used rather than the *direct* field components
f_C	calibration frequency (Hz)
f_S	signal frequency (Hz)
$\mathcal{E}$	excitation factor of only propagating mode ($\mathcal{E} \triangleq 1/h\sqrt{\sigma_e (c/v_{ph})}$)
v_{ph}	phase velocity of only propagating mode
$H_N^2(f)$	atmospheric noise (dBH/$\sqrt{Hz}$) referred to an equivalent H_φ field
G( )	voltage gain in system
$V_{C.M.}$	calibration monitor voltage (mv.)
A	voltage associated with the *received field strength* measured at the input to correlators.
B	voltage associated with the *injected calibration signal* measured at the input to correlators.
$\mathcal{A}$	voltage at the antenna output associated with the received H_φ
β	injected calibration signal voltage measured across the input transformer
P_1	voltage attenuation ratio (associated with noise processing circuit)
d	distance from transmitter to receiver
r_e	earth's radius - 6.378 Mm
$\mid \ \mid$	magnitude of a quantity
E[ ]	expectation

SUBSCRIPTS

c	cosine component
s	sine component
C	calibration frequency
S	signal frequency
H	Hawaii
U	Utah
NS	Nova Scotia
u	unbiased estimator
b	biased estimator
$\mathcal{D}$	direct component
$\mathcal{R}$	round-the-world component
T	total field component (or associated with gain of cascaded tape recorders)
I	integrated (usually refers to the integrated noise)
i, j	indices
D	daytime
N	nighttime
C. M.	calibration monitor
EW(WE)	propagation direction - from East to West (from West to East)
m	<u>mid</u> or center frequency in a selected group of frequencies

SUPERSCRIPTS

$\widehat{(A^2)}$	estimator for the true value of A^2
$\overline{(A^2)}$	single average
$\overline{\overline{A^2}}$	double average

TABLE OF CONTENTS

APPENDICES

I. INTRODUCTION

For the period 15 March through 9 April 1971, the test facility transmitter at Clam Lake, Wisconsin was scheduled to transmit a simple sinusoidal signal for two eight hour periods per day. The EW antenna consists of a horizontal dipole, center fed with the ends grounded. The dipole is a single wire transmission line hung on conventional telephone poles. The total length of the EW antenna is 22.5 km and the line current was 300 A (rms). The electrical axis of the EW antenna is approximately 116° S. E. (There is in addition a similar N. S. antenna which was not utilized in these tests.) The transmissions were specified to be the odd frequencies from 41 to 49 Hz and from 73 to 77 Hz. Receiver sites were located at Wendover-Utah, Maitland Bridge-Nova Scotia and Pohakuloa Test Range-Hawaii (Fig. 1). The measurements were completed without significant equipment failures or data loss for the duration of the tests. About 120 analog magnetic tapes (40/site), each with eight hours of recorded signal were collected. These tapes have been processed through the laboratory playback facility and the results are compiled in this report.

It must be realized at the outset that the transmitted signal levels were extremely low. For example, the total radiated power at 45 Hz was only 1/4 watt and at 75 Hz only 1/2 watt. Since the Hawaii site is 6.53 Mm away, to obtain good estimates of the signal strength one needs to perform the detection with equivalent bandwidths of the order of a few ten thousandths of a Hz (i.e., integration times of the order of hours). Furthermore, to calculate good estimates of the attenuation

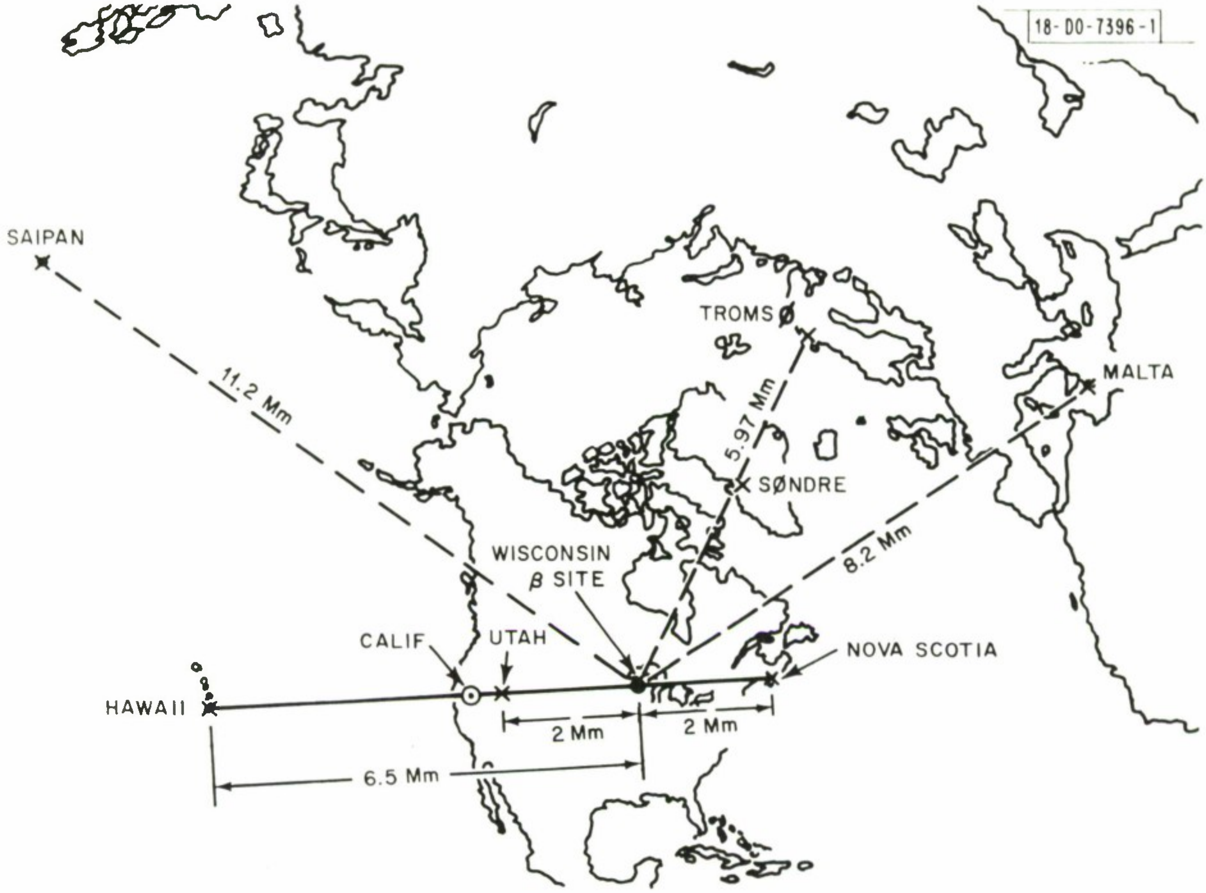

Fig. 1. Receiver site locations (past, present and future).

rate α it is necessary to average several such (properly weighted) estimates at each receiver site.

The propagation parameters of interest are the attenuation rate α and a term denoted as the excitation factor, $1/(h\sqrt{\sigma_e c/v_{ph}})$ (See Eq. 1, Section II for the definition of terms). These two quantities vary with frequency, time and possibly with propagation direction. It is an a priori hypothesis based on our previous limited experimentation that both of these quantities differ significantly from all day to all night path conditions but remain fairly constant during either period. The propagation direction dependence for $30 < f < 80$ Hz is believed to be so slight that an extremely precise experiment would be necessary to resolve directional differences.

A number of comprehensive reviews on the status of measurements and theoretical estimates of the propagation parameters at the lower ELF range have been written [1,2,3]. Basically, the shortcomings of past parameter estimates fall into two classes:

(1) Theoretical estimates depend on an accurate representation of the conductivity profiles of the D, E and lower F regions (including effects of ions and the earth's magnetic field). Small differences in the chosen models lead to estimates of the propagation parameters so varied that an ELF communications system could not be sized on theoretical predictions alone.

(2) The experimental measurements are based almost entirely on spectral decomposition of individual large lightening pulses. Using two receiver sites and an equation <u>similar</u> to equation 1 (but modified to account

for a vertical rather than a horizontal dipole source) the ratio of field strengths at the two sites is taken in order to estimate $\alpha(f)$. This method is rather unsuccessful for the following reasons. First the point of origin of the particular lightening stroke analyzed is imperfectly known. In addition it is not known whether the stroke orientation is cloud to cloud (horizontal) or cloud to ground (vertical). The geometrical configuration of the receivers with respect to the lightening stroke may be such that small uncertainties in either the stroke's position or in the signal strength estimate may give large differences in values of α. Second, for information concerning propagation at frequencies less than 100 Hertz, one needs to analyze the long tail of the stroke in question which tends to be corrupted with return strokes from the same burst and the bursts of other strokes. Therefore, the S/N ratios tend to be extremely unfavorable for $f < 100$ Hz. Third, on the tail of the sferic there may be included a component of signal which has traveled around the world and adds to the direct path component. This will give an additional source of error in estimation of α.

It should be noted that recent sferic measurements (Hughes and Thiessen [4]) have suggested that the diurnal difference in attenuation rates is about 1.5 dB/Mm at 50 Hz (daytime attenuation being the higher). If one assumes a nighttime attenuation rate of .7 dB/Mm then α_D would be of the order of 2.2 dB/Mm. (An earlier paper by Hughes [5] suggested that significant differences in α_{EW} and α_{WE} exist.) In order to determine whether the first results of Hughes (i.e., $\alpha_D \sim 2.2$ dB/Mm) were valid we deployed receivers in Hawaii and California in an attempt to measure α_{EW}

[6]). This experiment was completed in July 1970. The results from the test were somewhat ambiguous since only the California data could be utilized, making this a one station measurement. The Hawaii data was not useable since the summer noise was considerably higher than expected. (The transmitted signal strength was also some 6 dB lower than at present.) As a rule of thumb for the accuracies that were needed in that experiment to measure α, a S/N ratio of at least 15 dB is required. Because of low transmitted signal and high noise conditions,even after a 3.2 hour coherent integration the S/N_I ratio in Hawaii was only 8 dB. Consequently, we were forced to base our conclusions on a one station (California) measurement and make assumptions concerning the mode excitation factor $(1/(h\sqrt{\sigma_e c/v_{ph}}))$ for day and night conditions in order to deduce a probable range of values for the attenuation rate for day and night. The tentative result based on the hypothetical excitation factors was that α_D was reasonably close to .75 dB/Mm at 45 Hz while the value of α_N was probably closer to 2 dB/Mm. This high value of α_N was not expected and was a strong factor in planning the recent propagation tests. The recent tests (with the two station - Utah and Hawaii sites) have led to a different interpretation of these California results. Specifically one of the main results of this experiment was that the nighttime mode excitation factor is about 2.3 dB lower than originally predicted and that the nighttime attenuation rate is about .9 dB/Mm (at 45 Hz). Hence the low nighttime signal strengths in California were due to a worse excitation factor than originally estimated rather than a high attenuation rate; in this perspective the earlier tests and the present tests are totally

compatible.

This report has a dual purpose. First it is a compilation of the results of the recent experiment. Second it is intended for use as a handbook in that it describes in considerable detail the receiver design considerations, the mechanics of the system calibration and the methods by which the data is analyzed and estimates of α and the excitation factor are determined. Since this type of experiment is to be repeated a few more times by both Lincoln Laboratory and Navy laboratories this report should serve as a useful reference with regard to standardization of experimental technique.

For those interested only in the detailed results of the recent experimental phase it is probably sufficient to read the main text (Sections I through VI). The conclusions are presented in Section VI. Appendices A through I serve as reference material.

The primary goal of the recent experimental phase was to measure α_{EW} (attenuation rate in an east to west direction) using data from Hawaii and Utah. We believe we have determined this value satisfactorily. A second goal was to use the data from Utah and Nova Scotia to look for small differences (i. e., $\pm .2$ dB/Mm) in $(\alpha_{EW} - \alpha_{WE})$. We were able to achieve this goal as well.

All field strengths are expressed in terms of H_φ (φ denotes a horizontal component normal to the propagation direction). The magnitude of the vertical E field is related to H_φ through

$$|E_V| = \eta \left(\frac{c}{v_{ph}}\right) |H_{\varphi}|$$

where $\eta = 377\Omega$ and v_{ph} is the phase velocity.

II. THEORY

The equations determining the ELF electromagnetic field components produced by a specified source at the surface of a spherical earth and confined by the presence of a concentric and *vertically* inhomogeneous ionosphere have been extensively investigated over the last decade. One basic formulation is in terms of a zonal harmonic series. The use of this method is illustrated in a series of calculations performed by Johler and Lewis [7] for a specified ionospheric model and frequency of operation. The disadvantage of this formulation is that the equations (which have a few hundred significant terms in the series) are not readily amenable to confirmation within a reasonable experimental program. In addition, because of the complexity of the series it is difficult to develop a physical insight into the nature of the propagation and hence it is difficult to extrapolate the results to other frequencies or models where the ionosphere has markedly different characteristics over different portions of the propagation path (i.e., daytime versus nighttime effects). A more useful (and physically revealing) formulation results from use of the Watson transformation (Wait [8, 9]) which converts the series of zonal harmonics to a more rapidly converging infinite series of radial harmonics. When the receiver is located in the far field ($\frac{2\pi d}{\lambda} > 1$) but sufficiently removed from the region of the transmitter's antipode, and the attenuation rate is greater than a few tenths of a dB/Mm, the series of radial harmonics can be replaced to first order by the simple expression (for a horizontal electric dipole transmitter source at the earth's surface) representing the *direct* ($\mathcal{D}$) contribution to the

H_{φ} field

$$(H_{\varphi})_{\mathfrak{A}} = \frac{ILf}{2\eta} \sqrt{\frac{2\pi\mu_o}{c}} \cos\Phi \left\{\frac{1}{h\sqrt{\sigma_e(\frac{c}{v_{ph}})}}\right\} \left\{\frac{1}{\sqrt{d}} \sqrt{\frac{d/r_e}{\sin d/r_e}}\right\} e^{-\alpha' d} \tag{1}$$

$$\times\ e^{j(k_o(\frac{c}{v_{ph}})d - \omega t + \pi/4)}$$

where

IL	current moment of the transmitter
Φ	angle between axis of horizontal antenna and propagation path direction
σ_e	ground conductivity at transmitter
h	effective height of ionosphere
v_{ph}	phase velocity for the only propagating mode
η	120π
r_e	earth's radius
k_o	$2\pi/\lambda$
d	shorter great circle distance between receiver and transmitter $d < \pi r_e$
α'	attenuation rate (nepers/m) for the only propagating mode.

For greater accuracy one must add to the field shown in equation 1 another magnetic field component ($\mathfrak{R}$ component) which travels around the world along the longer segment of the same great circle path. This component is given by

$$(H_{\varphi})_{\mathfrak{R}} = F e^{-\alpha'(2\pi r_e - d)} e^{j[k_o(\frac{c}{v_{ph}})(2\pi r_e - d)]} \tag{2}$$

where

$$F = \frac{ILf}{2\eta}\sqrt{\frac{2\pi\mu_o}{c}}\cos\Phi\left\{\frac{1}{h\sqrt{\sigma_e\left(\frac{c}{v_{ph}}\right)}}\right\}\left\{\frac{1}{\sqrt{r_e}}\;\frac{1}{\sqrt{\sin\frac{d}{r_e}}}\right\} \tag{3}$$

$$\times\; e^{-j(\omega t - \frac{\pi}{4})}.$$

These direct and round the world components add at each point to give a standing wave pattern as illustrated in Fig. 2. It can be shown (Jones [10]) that the minimums of the standing wave H_φ pattern are located at a distance ρ' from the antipode where

$$\rho' = \frac{(4n+3)\lambda}{8(c/v_{ph})} \qquad n = 0, 1, 2, \ldots \tag{4}$$

and the standing wave length is

$$\lambda_{sw} = \rho'_{n+1} - \rho'_n = \frac{\lambda}{2(c/v_{ph})}\,. \tag{5}$$

It should be made clear that the total field $(H_\varphi)_T$ as expressed by the sum of equations 1 and 2 was derived under the set of assumptions

a) The ionosphere is variable only in the vertical direction. No lateral inhomogeneities (i.e., day-night transitions) are allowed.

b) The ionosphere is isotropic, that is, the earth's magnetic field is assumed to be zero. This is a reasonable approximation provided that a significant amount of the electromagnetic energy does not get into the altitude region where the mean free path between electron-neutral collisions becomes comparable to the electron gyro radius. During daytime conditions this appears to be the case but for nighttime conditions the magnetic field probably has some minor effect on the directional behavior of the attenuation

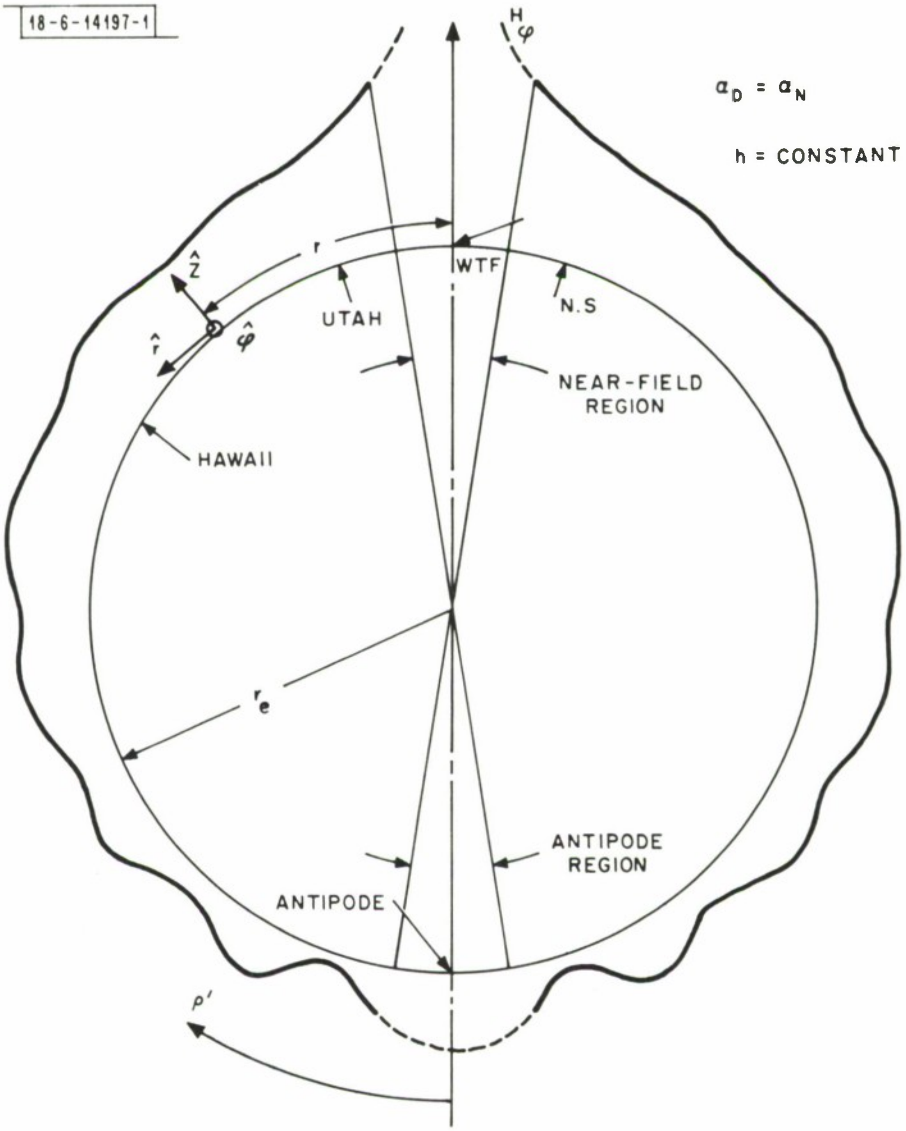

Fig. 2. Standing wave pattern in an idealized uniform earth-ionosphere cavity.

rate.

c) The three parameters h, α and v_{ph} are expected to reflect the behavior of the lower ionosphere (and to lesser extent the variable ground conductivity) on the ELF propagation. Only an extensive experimental program will show if these parameters are sufficient to characterize the bulk of the propagation data.

d) α, h and v_{ph} are all frequency dependent.

The form of equations 1 and 2 suggests that a good approximation for the total field strength $(H_\varphi)_T$ in a more realistic model for the earth-ionosphere cavity where the changes in α and v_{ph} can be both locally and directionally varying is (Fig. 3)

$$(H_\varphi)_\mathcal{S} = F' e^{-\int_0^d \alpha'_\mathcal{S}(r)dr} e^{jk_0 \int_0^d (c/v_{ph})_\mathcal{S} dr} \tag{6}$$

and

$$(H_\varphi)_\mathcal{R} = + F' e^{-\int_0^{2\pi r_e - d} \alpha'_\mathcal{R}(r)dr} e^{jk_0 \int_0^{2\pi r_e - d} (c/v_{ph})_\mathcal{R} dr} \tag{7}$$

and

$$(H_\varphi)_T = (H_\varphi)_\mathcal{S} + (H_\varphi)_\mathcal{R} . \tag{8}$$

F' differs from F in the following way: $h\sqrt{(c/v_{ph})\sigma_e}$ is replaced by an effective number $(h\sqrt{(c/v_{ph})\sigma_e})_{eff}$ which can only be determined from experimental data.

The primary objective of this measurement program was to estimate the magnitude of $\alpha_\mathcal{S}(r)$. With CW signals of the type radiated by the WTF, one can by experiment estimate the magnitude of the total horizontal magnetic field

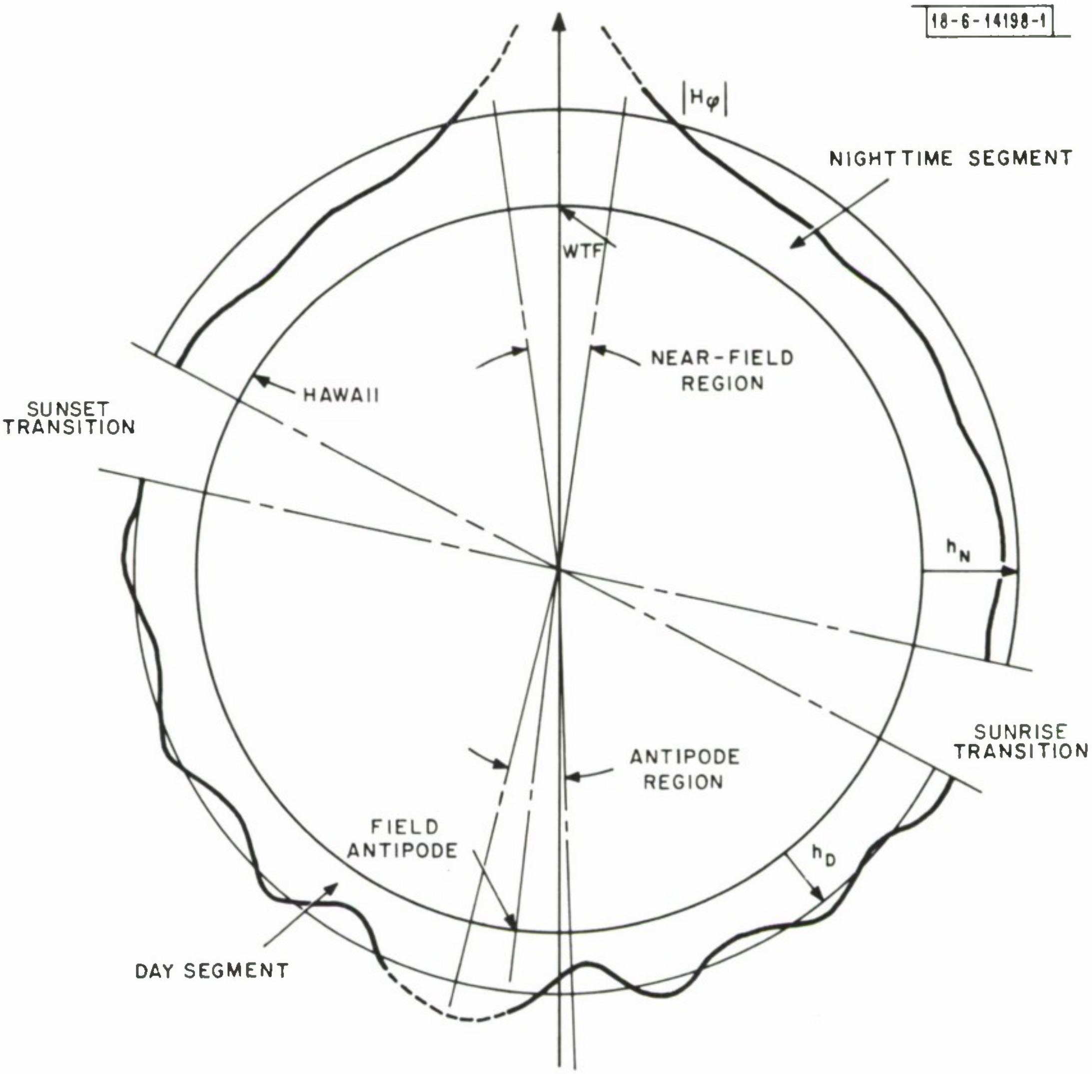

Fig. 3. Pictorial representation of the standing wave pattern in a realistic model of the earth-ionosphere cavity.

$(H_{\varphi})_T$. The difficulty comes in relating the estimates of $(H_{\varphi})_T$ and the function $\alpha_{\mathcal{D}}(r)$. The <u>first hypothesis</u> then is that the exponential terms in equations 6 and 7 are approximately constant over the estimate's determination time. Accordingly since the estimation period is of the order of a few hours and the direct path length is at least a few megameters then

$$\int_{d_{r1}}^{d_{r2}} \alpha_{\mathcal{D}}(r,t)dr \simeq C_1, \qquad \int_{d_{r1}}^{d_{r2}} (c/v_{ph})_{\mathcal{D}}\, dr \simeq C_3 \tag{9}$$

and

$$\int_{2\pi r_e - d_{r2}}^{2\pi r_e - d_{r1}} \alpha_{\mathcal{R}}(r,t)dr \simeq C_2, \qquad \int_{2\pi r_e - d_{r2}}^{2\pi r_e - d_{r1}} (c/v_{ph})_{\mathcal{R}}\, dr \simeq C_4$$

for all $t_b \leq t \leq t_e$ where t_b and t_e are the beginning and end of the estimation period. d_{r2} and d_{r1} denote the locations of two receivers on the same great circle path as the transmitter. From prior experiments [6] it has been determined (as far as poor S/N ratios will allow) that as long as the entire direct path segment is in daytime (or nighttime) conditions the received signal strength is approximately a constant value over a period of several hours. The only observable signal changes come when the sunrise (or sunset) terminator intercepts the direct path segment. Hence for the remainder of this report we assume that

$$\alpha_{\mathcal{D}}(r,t,f) \simeq \begin{cases} \alpha_{\mathcal{D},N}(f) \text{ for} & (t_{SS} + \delta) < t < (t_{SR} - \delta) \\ \alpha_{\mathcal{D},D}(f) & (t_{SR} + \delta) < t < (t_{SS} - \delta) \end{cases} \tag{10}$$

and

$$(c/v_{ph}(r,t,f))_{\mathscr{D}} \simeq \begin{cases} (c/v_{ph}(f))_{\mathscr{D},N} \\ (c/v_{ph}(f))_{\mathscr{D},D} \end{cases} \tag{11}$$

where t_{SR} and t_{SS} are the appropriately chosen* ionospheric sunrise and sunset times and 2δ is an appropriate transition time interval. D and N refer to daytime and nighttime conditions.

It must be emphasized that the conditions expressed in equations 10 and 11 are very strong hypotheses that at present we are forced to make. The reason is that for estimation purposes one needs an integrated signal to noise ratio (S/N_I) of at least + 20 dB if we are to determine a good estimate of $(H_\varphi)_T$. However at a typical receiver site the S/N ratio (as measured in a 1 Hz bandwidth) is usually about -25 dB. Hence one must integrate for a few hours to achieve a sufficient value of S/N_I for the purpose of estimating $(H_\varphi)_T$ with a reasonable set of error bounds. In order to deduce useful estimates of $\alpha_{\mathscr{D}}(f)$ from the $(\hat{H}_\varphi)_T$ estimates one needs the error bounds on $(\hat{H}_\varphi)_T$ that would result from integrating over tens of hours. It is, of course, necessary that the signal amplitude and phase are nearly constant over this long integration time. To approximate this long integration time we take a few equispaced samples per day (or night), collect samples over a few days and incoherently average the results. It must be emphasized that this technique presupposes that $\alpha_{\mathscr{D},N(D)}(f)$ and $(c/v_{ph}(f))_{\mathscr{D},N(D)}$ are essentially constant from day to day (particularly for the same GMT time intervals). The bulk of our experimental data supports this last assumption (again within

---

*See schedule for method of selecting t_{SS} and t_{SR} (Appendix H).

the limitations of the generally low S/N ratios).

We have noted that the measurements performed in this experiment yield $|\widehat{H_\varphi(d)}|_T$ and not $|\widehat{H_\varphi(d)}|_\mathfrak{D}$. (Only the magnitude is measured and not its relative phase.) Normally $|H_\varphi(d)|_T$ is measured at a few receiver sites all on the same great-circle path with the transmitter. Since we do not know the magnitude of $(H_\varphi(d))_\mathfrak{R}$ or its phase relative to $(H_\varphi(d))_\mathfrak{D}$ one cannot directly deduce $(H_\varphi(d))_\mathfrak{D}$ from $(H_\varphi(d))_T$. However, for all the receiver sites where we have been or plan on operating it is true that $|H_\varphi(d)|_\mathfrak{D} >> |H_\varphi(d)|_\mathfrak{R}$. Hence for the range $(1 < d \leq 10$ Mm) the *total field* standing wave pattern appears as a sinusoidal pattern with an amplitude which increases with d superimposed on the direct field (see Fig. 2). Then, *if* the relative phase between $(H_\varphi)_\mathfrak{D}$ and $(H_\varphi)_\mathfrak{R}$ at a particular site were random from measurement to measurement it seems obvious that an appropriate average of a series of $|\widehat{(H_\varphi)_T}|$ measurements would give a value very close to the magnitude $|(H_\varphi)_\mathfrak{D}|$.* If this were done at two receiver sites on the same great circle path (see Section IV for details) one could then compute a value for $\alpha_\mathfrak{D}(f)$ which is relatively free of errors due to the standing wave pattern. The problem reduces to providing relative phase shifts between $(H_\varphi)_\mathfrak{D}$ and $(H_\varphi)_\mathfrak{R}$ for a large enough set of measurements. A simple way to change phase is to change frequency slightly (one must assume that the attenuation rate does not change significantly over this same small frequency shift). By

---

*The probability distribution function for the relative phase between $(H_\varphi)_\mathfrak{D}$ and $(H_\varphi)_\mathfrak{R}$ must however be reasonably uniform from 0 to 2π.

selecting a number of slightly different frequencies a proper set of phase shifts can be obtained and hence averaging the total fields will give a result close to the direct field alone. (The theoretical justification for this procedure is detailed in Appendix G.)

III. DESCRIPTION OF EXPERIMENTAL APPARATUS AND METHOD OF ANALYSIS

Figures 4 and 5 are simplified block diagrams showing the field site recording equipment and the laboratory playback facility. A detailed description of the field site recording equipment is presented in Appendix A. This section provides a brief discussion of how the receiver processes the received signal and permits a simple calibration procedure.

An injected calibration signal (whose frequency is 1 Hz removed from the transmitted frequency) is used to provide a continuous gain calibration of the receiver. A frequency synthesizer provides the calibration signal as well as the phase reference signals which are used in the quadrature correlation receivers. The calibration procedure is discussed more fully in Appendices E and A. Note from Fig. 4 that both a narrowband and a wideband channel are provided. All of the processing reported here is on the narrowband channel data. All the data were recorded on magnetic tape and processed at the laboratory playback facility.

The magnetic tapes are played back (see Fig. 5) with a speedup factor of 32 so as to reduce processing time from about 12 hours per tape to about 23 minutes. Each of the channels consists of a pair of correlators in quadrature followed by squarers and a summer. The outputs are recorded on a chart recorder. (A Hewlett-Packard 2 pen X-Y recorder provides good resolution.) The units marked PAR (Princeton Applied Research Model 120) consist basically of a multiplier followed by a single pole low pass filter

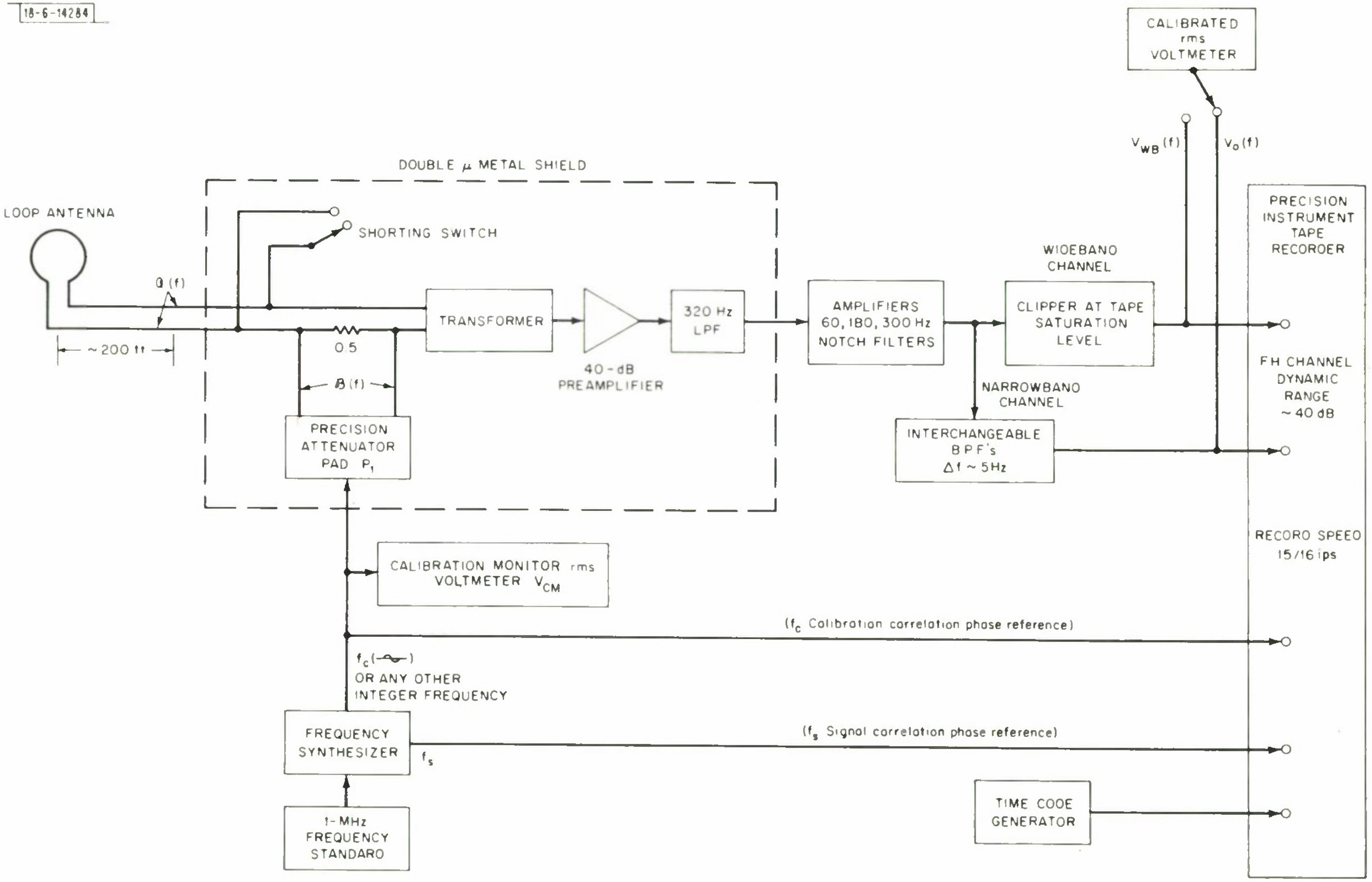

Fig. 4. Field site recording equipment.

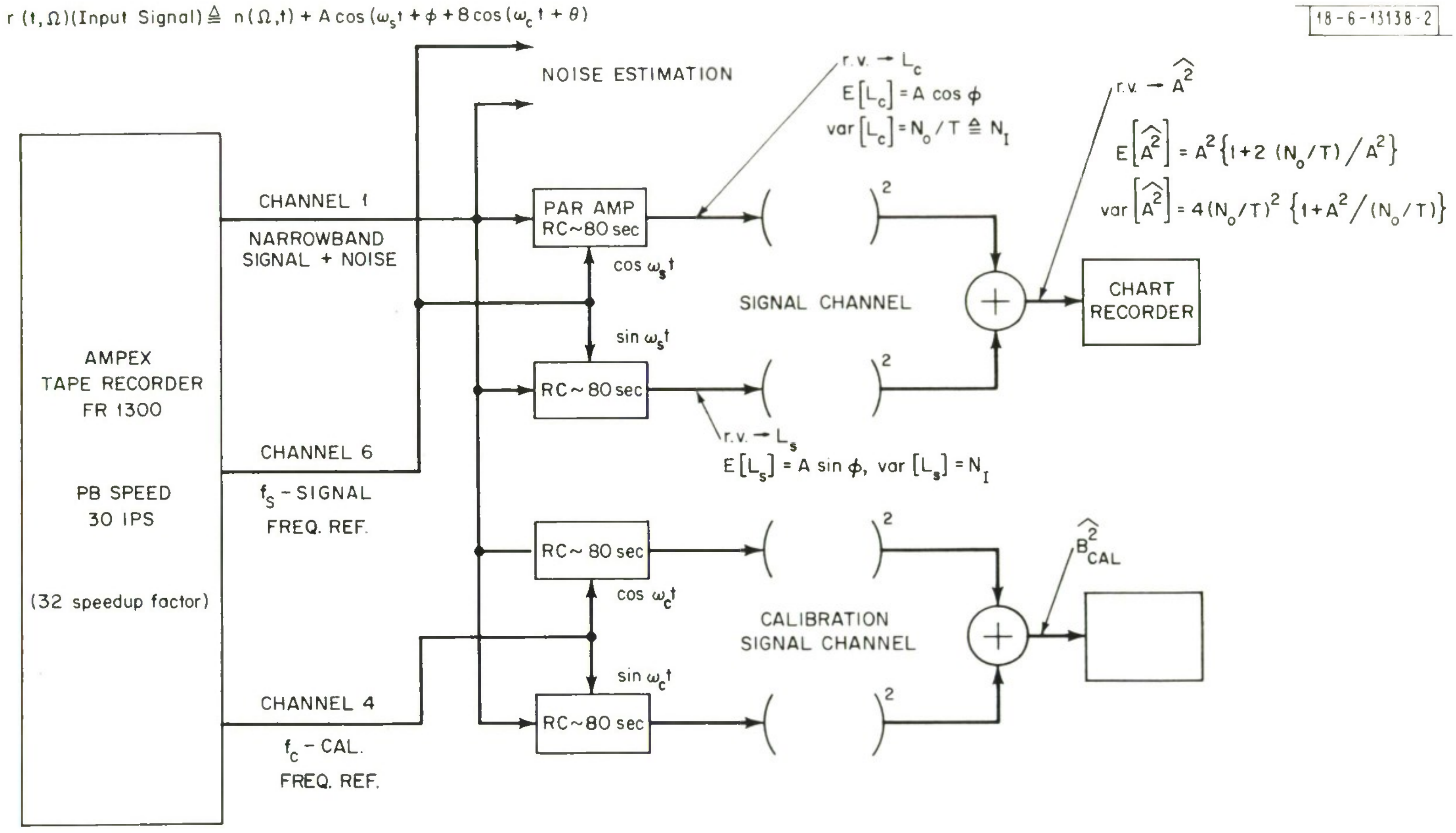

Fig. 5. Playback facility block diagram.

(see Fig. E-1). It can be shown that the equivalent integration time is $T = 2(32)RC$ where RC is the time constant of the low pass filter. For most of our processing RC = 80 sec was used which corresponds to $T \sim 1.42$ hours. Even with this long integration time the signal to noise ratio at Hawaii was typically only 10-20 dB. This low value of S/N_I (low for purposes of <u>accurate estimation</u> of the signal level) necessitates a very careful study of the noise. As noted in Appendix A the noise of interest is distinctly non-Gaussian atmospheric noise which completely dominates the receiving system noise. The input signal to the quadrature correlator receivers can be represented by

$$r(t,\Omega) \overset{\Delta}{=} n(t,\Omega) + A\cos(2\pi f_S t + \varphi) + B\cos(2\pi f_C t + \theta) \qquad (12)$$

where (A,φ) and (B,θ) are the amplitude and phase angles associated with the transmitted and calibration signals respectively. $n(t,.)$ is a non-Gaussian noise process with zero mean. Let us consider the transmitted signal channel only since the results for the calibration signal are the same with (B,θ) replacing (A,φ). Let the outputs of the PARs at time T be denoted by the random variables L_c and L_s. It is an easy matter to show that

$$E[L_c] = E[\tfrac{2}{T}\int_0^T (\cos\omega_s t)\, r(t,\Omega)dt] = A\cos\varphi$$

$$E[L_s] = E[\tfrac{2}{T}\int_0^T (\sin\omega_s t)\, r(t,\Omega)dt] = A\sin\varphi$$

$$\mathrm{var}[L_c] = \mathrm{var}[L_s] = N_o/T \overset{\Delta}{=} N_I \qquad (13)$$

where $n(t,.)$ was assumed to be a white noise process with the spectral density given by

$$S_n(f) = \frac{N_o}{2}, \qquad -\infty < f < +\infty . \tag{14}$$

Lincoln Laboratory wideband ELF noise studies [11] have shown the noise to be nearly 'white' over the bandwidths used in this set of measurements. N_I is termed the integrated noise. After L_s and L_c are individually squared and then summed, the result is another random variable (denoted by $\widehat{A_b^2}$) which has the properties

$$E[\widehat{A_b^2}] = A^2 \{1 + 2N_I/A^2\} \tag{15}$$

and

$$\mathrm{var}\,[\widehat{A_b^2}] = 4(N_I)^2 \{1 + A^2/N_I\} . \tag{16}$$

It is seen that the estimator $\widehat{A_b^2}$ is a biased estimator of A^2 with the bias term being $(2N_I)$. After the determination of N_I the bias term can be subtracted off to give the unbiased estimator of A^2 which we denote by $\widehat{A_u^2}$ to differentiate it from the biased estimate $\widehat{A_b^2}$ (i.e., $\widehat{A_u^2} = \widehat{A_b^2} - 2N_I$). Note that this is one of the reasons why N_I must be calculated. See Appendix B for an explanation on how N_I is calculated.

We will now outline the steps one must take in order to obtain a single unbiased estimate of input field strength.

1) At a specified sample time, t_i, values of $\widehat{A_b^2}(t_i)$ and $\widehat{B^2}(t_i)$ are read off the calibrated X-Y chart recorder graph.

2) Using these two values plus the calibration constants measured in the field the biased estimator of $|H_\omega^2|_b$ is computed with the use of equation (e-8) (Appendix E).

3) The equivalent integrated input noise $(H_N^2(t_i))_I$, is computed.

First $H_N^2(t_i)$ is determined as shown in Appendix B. The variance σ_x^2 computed from the Varian 620i program is related to the equivalent input H_φ noise (H_N^2 dBH/$\sqrt{\text{Hz}}$) by equation b-19. The noise typically is analyzed for a period of an hour centered about the sampling time, t_i, of the estimator $\widehat{A_b^2}(t_i)$. The equivalent integration time T (= 2(32)RC) is determined by the quality of the data one is analyzing. For this set of experiments we have chosen RC = 80 sec which sets T = 1.42 hours. Then

$$(H_N^2)_I \stackrel{\Delta}{=} ((H_N^2)/T \ . \tag{17}$$

4) The unbiased estimator for the input field strength is then given by

$$[\widehat{H_\varphi^2}(f_S)]_u = [\widehat{H_\varphi^2}(f_S)]_b - 2H_N^2(f_S)/T \ . \tag{18}$$

Figures 8 to 15 show typical X-Y recordings from Utah and Hawaii. The traces are $\hat{A}_b^2$ and $\hat{B}^2$ versus time of day. The samples are separated far enough in time that they are independent samples.

The question of 'error bars' on the sample estimates is particularly relevant since it is important to be able to differentiate between level changes due to changes in signal amplitude or phase and variations due to the normal noise behavior. This is particularly important since we have made the assumption that the received signal level is approximately constant over the recording period and yet we commonly see changes in $\hat{A}_b^2$ over this period. It is important to determine whether the changes in $\hat{A}_b^2$ over the recording period are entirely consistent with the integrated signal to noise ratio alone.

For each estimate of signal strength and integrated noise one can compute a sample S/N ratio

$$\frac{S}{N_I} = \frac{(\widehat{A^2}(t_i, f_S))_b}{N_o(t_i, f_S)/T} = \frac{|\widehat{H^2_\varphi}(t_i, f_S)|_{b,T}}{H^2_N\,(t_i, f_S)/T} \quad . \tag{19}$$

The quantities $(\widehat{A^2}(t_i, f_S))_b$ and $N_o(t_i, f_S)/T$ refer to the output of the receiver whereas $(\widehat{H^2_\varphi}(t_i, f_S))_{b,T}$ and $H^2_N(t_i, f_S)/T$ refer to equivalent magnetic field strengths at the antenna inputs. Throughout the text we often use the first pair of quantities since they are obtained first in the analysis. This particular sample S/N_I ratio then uniquely specifies a confidence interval (for a specified confidence level ϵ). Since the uncertainty in N_I is negligible compared to the uncertainties in S/N_I due to noise, we assume that N_I is in fact a known quantity as far as determining the confidence interval. Appendix C describes in detail the means of determining the confidence interval $(A^2_L(\epsilon), A^2_U(\epsilon))$ for each field strength sample. The interpretation is that the confidence interval (itself a random interval) includes the true value of A^2 with a probability $(1 - \epsilon) \times 100\%$.

The integrated signal to noise ratio obtained for a single sample may be satisfactory for an estimate of $|H_\varphi|_T$. However, it is difficult to employ simple H_φ estimates from two stations to measure an effective attenuation rate α_{eff}. Let us assume as an example two stations separated by 4 Mm with the stations having S/N ratios of 20 dB and 30 dB. (These numbers are greater than those exhibited in Utah and Hawaii.) The 80% confidence limits are computed to be (20 + 1.0 dB, 20 - 1.25 dB) and

(30 ± .35 dB) respectively. Thus the noise in itself leads to a spread in α_{eff} estimates of about ± .35dB/Mm. The obvious step then is to incoherently average successive samples where approximately the same ionospheric conditions occur and if this is not enough one can then average from day to day. It seems obvious that one should also weight more heavily those data where the noise is low. One appropriate weighting would be to weight each sample inversely by its measured noise sample. At the frequency f_j the average is then

$$\overline{(A^2(f_j))} = \frac{\sum\limits_{i=1}^{M} \frac{\widehat{(A_i^2(f_j))_u}}{N_{I,i}}}{\sum\limits_{i=1}^{M} \frac{1}{N_{I,i}}} \tag{20}$$

or the equivalent in terms of H_φ

$$\overline{|H_\varphi^2(f_j)|_{u,T}} = \frac{\sum\limits_{i=1}^{M} \frac{\widehat{|H_\varphi^2(f_j)|_{u,i,T}}}{(H_N^2)_{I,i}}}{\sum\limits_{i=1}^{M} \frac{1}{(H_N^2)_{I,i}}} \tag{21}$$

where i denotes the ith sample out of the M total samples taken at frequency f_j. The average $\overline{(A^2(f_j))}$ is a random variable and Appendix D outlines how to specify confidence limits for this random variable.

By the above process, at each frequency f_j, a weighted average value for the square of the total field strength is calculated. However, what is desired is not the total field (which includes the round-the-world component) but rather a good estimate of the direct component of the field. In order to average out the around-the-world signal the weighted total fields, $\overline{H_\varphi^2(f_j)}$ are in turn averaged over the selected frequencies to give an approximation for the direct field contribution alone at the mid-frequency, f_m. The second averaging process result in

$$\overline{\overline{|H_\varphi^2(f_m)|}}_{u,\ell} = f_m^2 \frac{1}{(2N+1)} \sum_{j=1}^{2N+1} \frac{\overline{|H_\varphi^2(f_j)|_{u,T}}}{f_j^2} \quad . \qquad (22)$$

The inverse weighting with f_j^2 is to reduce the frequency dependence (see equation 1). It must be remembered that over the band $(f_1, \ldots, f_{2N+1}), \alpha$, h and c/v_{ph} were assumed to be constant with frequency. f_m is the midpoint frequency in this band. Also explained in Appendix D is the means of calculating confidence limits on the random variable $\overline{\overline{|H_\varphi^2(f_m)|}}_{u,\ell}$.

IV. CALCULATION OF THE ATTENUATION RATE AND EXCITATION FACTOR

Let us assume that we have computed unbiased estimates for the direct field strength $\overline{\overline{|H_\varphi|}}_{\mathcal{D},u}$ at two receiver sites on a great circle which also intercepts the transmitter site. Denote the receiver site locations by x and y. The magnitude of the field strength is related to the attenuation rate by equation 1 which can be rewritten

$$\overline{\overline{|H_\varphi|}}_{\mathcal{D},u} = \frac{ILf}{2\eta}\sqrt{\frac{2\pi\mu_o}{c}}\cos\Phi\left\{\frac{1}{h\sqrt{\sigma_e(\frac{c}{v_{ph}})}}\right\}\left\{\sqrt{\frac{1/r_e}{\sin d/r_e}}\right\}e^{-\alpha'_{\mathcal{D}}d}. \tag{23}$$

Let us consider the case where the two receivers are on the same side of the transmitter. The above equation can then be used in two distinct ways. First, for estimates made for the same time period at two separated sites we have

$$\frac{\overline{\overline{|H_\varphi|}}_{\mathcal{D},u,x}}{\overline{\overline{|H_\varphi|}}_{\mathcal{D},u,y}} = \left\{\sqrt{\frac{\sin d_y/r_e}{\sin d_x/r_e}}\right\}e^{-\alpha'_{\mathcal{D}}(d_x-d_y)}.$$

Or

$$\alpha_{\mathcal{D}} = \frac{1}{d_y-d_x}\left\{10\log\frac{\sin(d_x/r_e)}{\sin(d_y/r_e)} + 20\log\frac{\overline{\overline{|H_\varphi|}}_{\mathcal{D},u,x}}{\overline{\overline{|H_\varphi|}}_{\mathcal{D},u,y}}\right\}\ \text{dB/Mm}. \tag{24}$$

It is evident from this equation that the excitation factor $\rho = 1/(h\sqrt{\sigma_e(c/v_{ph})})$ cancels out in the ratio since the estimates were taken for the same time periods for both sites. In this manner one can then determine $\alpha_{\mathcal{D},D}$ and $\alpha_{\mathcal{D},N}$ by using the pairs of estimates $\{\overline{\overline{|H_\varphi|}}_{\mathcal{D},u,x,D}, \overline{\overline{|H_\varphi|}}_{\mathcal{D},u,y,D}\}$ and $\{\overline{\overline{|H_\varphi|}}_{\mathcal{D},u,x,N}, \overline{\overline{|H_\varphi|}}_{\mathcal{D},u,y,N}\}$. The restrictions on $\alpha_{\mathcal{D}}$ are those referred to in the text associated with equation 10. After α_ℓ has been determined the excitation factor ($\varepsilon = 1/(h\sqrt{\sigma_e(c/v_{ph})})$ can be determined from equation 23 since all the other terms are known.

As a result of the high accuracy to which $\overline{\overline{|H_\varphi|}}_\ell$ must be known there may be a residual bias error in calibration which, although slight, is significant in light of the high accuracies we require in the $\widehat{|H_\varphi|}_T$ measurements. If either or both of the two sites has a consistent bias error in its calibrations, this error can show up as a potentially large error in the estimate of α_ℓ. (i.e. A 1 dB error in estimating a field strength is not usually considered serious whereas an error of say 0.3 dB/Mm in the estimate of α can have profound effects in sizing a global communications system.) However, we can obtain good relative information on α_ℓ and ε even when a bias error in calibration for a particular site is significant. We choose the signal estimates at two <u>different times</u> (a day estimate and a nighttime estimate) for a single station. The following ratio is then computed.

$$\frac{\overline{\overline{|H_\varphi|}}_{\ell,u,x,D}}{\overline{\overline{|H_\varphi|}}_{\ell,u,x,N}} = \frac{\{h\sqrt{c/v_{ph}}\}_N}{\{h\sqrt{c/v_{ph}}\}_D} \quad e^{-(\alpha'_{\ell,D} - \alpha'_{\ell,N})d_x}$$

$$= \frac{\varepsilon_D}{\varepsilon_N} \quad e^{-(\alpha'_{\ell,D} - \alpha'_{\ell,N})d_x} \quad . \qquad (25)$$

Note that if a calibration bias exists and is constant from day to night then this bias will cancel in the above equation. This can be rewritten as

$$20 \log \frac{\overline{\overline{|H_\varphi|}}_{\ell,u,x,D}}{\overline{\overline{|H_\varphi|}}_{\ell,u,x,N}} = 20 \log \frac{\varepsilon_D}{\varepsilon_N} - (\alpha_{\ell,D} - \alpha_{\ell,N})d_x. \qquad (26)$$

We can apply the same sort of reasoning to the receiver at location d_y and get

$$20 \log \frac{\left|\overline{\overline{H}}_{\varphi}\right|_{\wp, u, y, D}}{\left|\overline{\overline{H}}_{\varphi}\right|_{\wp, u, y, N}} = 20 \log \frac{\mathcal{E}_D}{\mathcal{E}_N} - (\alpha_{\wp, D} - \alpha_{\wp, N}) d_y . \tag{27}$$

It is evident that equations 26 and 27 are two linear equations for the two unknowns $(\alpha_{\wp, D} - \alpha_{\wp, N})$ and $20 \log \frac{\mathcal{E}_D}{\mathcal{E}_N}$. The solutions are

$$(\alpha_{\wp, D} - \alpha_{\wp, N}) = \frac{1}{d_x - d_y} \left\{ 20 \log \frac{\left|\overline{\overline{H}}_{\varphi}\right|_{\wp, u, y, D}}{\left|\overline{\overline{H}}_{\varphi}\right|_{\wp, u, y, N}} - 20 \log \frac{\left|\overline{\overline{H}}_{\varphi}\right|_{\wp, u, x, D}}{\left|\overline{\overline{H}}_{\varphi}\right|_{\wp, u, x, N}} \right\} \tag{28}$$

$$20 \log \frac{\mathcal{E}_D}{\mathcal{E}_N} = \frac{1}{d_x - d_y} \left\{ d_x \left(20 \log \frac{\left|\overline{\overline{H}}_{\varphi}\right|_{\wp, u, y, D}}{\left|\overline{\overline{H}}_{\varphi}\right|_{\wp, u, y, N}} \right) - d_y \left(20 \log \frac{\left|\overline{\overline{H}}_{\varphi}\right|_{\wp, n, x, D}}{\left|\overline{\overline{H}}_{\varphi}\right|_{\wp, u, x, N}} \right) \right\} . \tag{29}$$

Thus one can compute the difference $(\alpha_{\wp, D} - \alpha_{\wp, N})$ and the excitation ratio $\mathcal{E}_D / \mathcal{E}_N$ even if there is a consistent bias uncertainty at either or both of the sites.

It should be clear that the preceding discussion outlines a method of determining the attenuation rate $\alpha_\wp$ in any direction. Since in this series of tests two of our receivers are in Utah and Hawaii we can determine estimates of $\alpha_{EW, D}$, $\alpha_{EW, N}$, $\mathcal{E}_D$ and $\mathcal{E}_N$.

We should also like to investigate any anisotrophy in α which is caused by the earth's magnetic field $\underset{\rightarrow}{B}_o$ (i.e., the difference $\alpha_{EW} - \alpha_{WE}$). This can be investigated by spacing two receivers equidistant from the transmitter and on opposite sides of the same great circle path ($d_x = d_y = d$). Moreover, estimates are made when both receivers are under either day or under night conditions. Since the receivers are equidistant from the transmitter it follows that:

(1) If the attenuation coefficient is not anisotropic (direction dependent) then the total signal $(H_\varphi)_T$ at each site due to the sum of the direct and round-the-world wave will be identical; The exact position on the interference pattern is still to be determined but the pattern segment between the two receivers will be symmetric about the transmitter. If the measured signal is the same we then can say that there is no directional dependence for α even though we still have as yet not specified what α really is. (There still may be a large daytime versus nighttime attenuation rate difference.) One can make the case as an example that even if $\alpha_{EW} \neq \alpha_{WE}$, it may be that $(c/v_{ph})_{EW}$ and $(c/v_{ph})_{WE}$ are the exact values which would make the signal amplitudes at both sites equal even though the standing wave pattern is otherwise unsymmetrical about the transmitter. This objection can be countered by changing the transmitter frequency by a few Hz. Presumably the attenuation rate will not change significantly but it can be shown that the minima and maxima positions will change significantly. If the signal amplitudes at this new frequency are also the same then one must admit that there is no discernible difference in the attenuation coefficient for EW versus WE propagation.

(2) If the signals measured are truly different, then one must admit a significant directional dependence. The possibility still exists that one or both of the two receivers may have a consistent calibration bias. One can circumvent this by forming the ratios $(|\overline{\overline{H}}_{\varphi}|_{T,u,x,D}/|\overline{\overline{H}}_{\varphi}|_{T,u,x,N})$ and $(|\overline{\overline{H}}_{\varphi}|_{T,u,y,D})/(|\overline{\overline{H}}_{\varphi}|_{T,u,y,N})$ each of which should be independent of a station's calibration bias. As before if these ratios are significantly different (after the noise contributions are properly assessed) then the conclusion is that there is some directional anisotrophy. (However from these ratios alone one cannot determine whether the anisotrophy is associated with daytime conditions or with nighttime conditions.) If on the other hand the ratios are essentially the same then the conclusion is that either there is no anisotrophy or if an anisotrophy exists it is the same for both the day and night conditions. The latter conclusion seems unlikely in as much as one expects the anisotrophy, if it exists, to be more severe at night.

V. DATA PRESENTATION

The first point to be addressed is the simultaneous calibration of the three receiver systems. After the three systems were built and individually appraised as being operational, it was decided to operate (at our Plum Island, Massachusetts test site) all three systems simultaneously and compare the results before deploying these receivers to the selected sites. Unfortunately, the time allocated to this task proved insufficient. It was found that operating the three systems in the same enclosed area (a Clark Cortez van) gave rise to major interference between the three systems invalidating the results. In addition several breakdowns on the tape recorders occurred and had to be repaired. By the time most of the mutual interference was mitigated and the recorders repaired, we were forced to ship our equipment. (It should be noted that the last simultaneous measurement indicated that the Utah system gave a 1.6 dB lower reading than the other remaining system.) The intent was to perform a series of simultaneous measurements at Plum Island after the tests were finished. At the beginning of the measurement period, it was realized that the Utah signal estimates were consistently about 2 dB too low in the 40 Hz range. (It should be pointed out that the Utah antenna was fully buried, the Hawaii antenna half buried with volcanic rubble completing the cover and the Nova Scotia antenna located above the frozen ground in a specially constructed hut.) At the termination of the experiment all three systems were brought to Plum Island for a simultaneous calibration. Accordingly, we buried the Utah antenna to duplicate conditions. Unfortunately, it happened that the ground (salt) water level at the first high tide penetrated the antenna covering and destroyed the antenna. Thus we were left without a clear calibration of the Utah system.

Our response was to deduce correction factors by comparing the Utah data with the Nova Scotia data and with our previous California results (after compensating for the difference in distance). Without going into the details of this comparison we arrived at correction terms to be used in the α computation. When the raw Utah and Hawaii data are used in equation 24 the correction terms that were added to $20 \log \frac{|H_\varphi|_{Utah}}{|H_\varphi|_{Haw}}$ were 2.4 dB (40 Hz band) and 1.0 dB (70 Hz band). (It must be noted from Fig. 6 that 0.5 dB of this overall correction term is due to the difference in off-axis corrections for the Utah-Wisc. and Hawaii-Wisc. propagation paths. Hence the calibration corrections that were added to the raw Utah data are 1.9 dB (40 Hz band) and 0.5 dB (70 Hz band).) It should be recalled that the only successful simultaneous calibration at Plum Island gave the Utah system a 1.6 dB lower reading at 45 Hz. This is close to the deduced correction value of 1.9 dB. In any case, the 2.4 and 1.0 dB correction terms were the values used in the computation of the α estimates which we have orally communicated to the ELF community.

In October, 1971, during the following phase of the measurement program we decided to resolve any questions concerning our adjustment of the Utah data. Accordingly, we simultaneously calibrated all three systems at Plum Island (over a period of weeks). One of these systems was sent to the same Utah site as before and test transmissions with the EW antenna were scheduled. The results of these tests showed with high confidence the

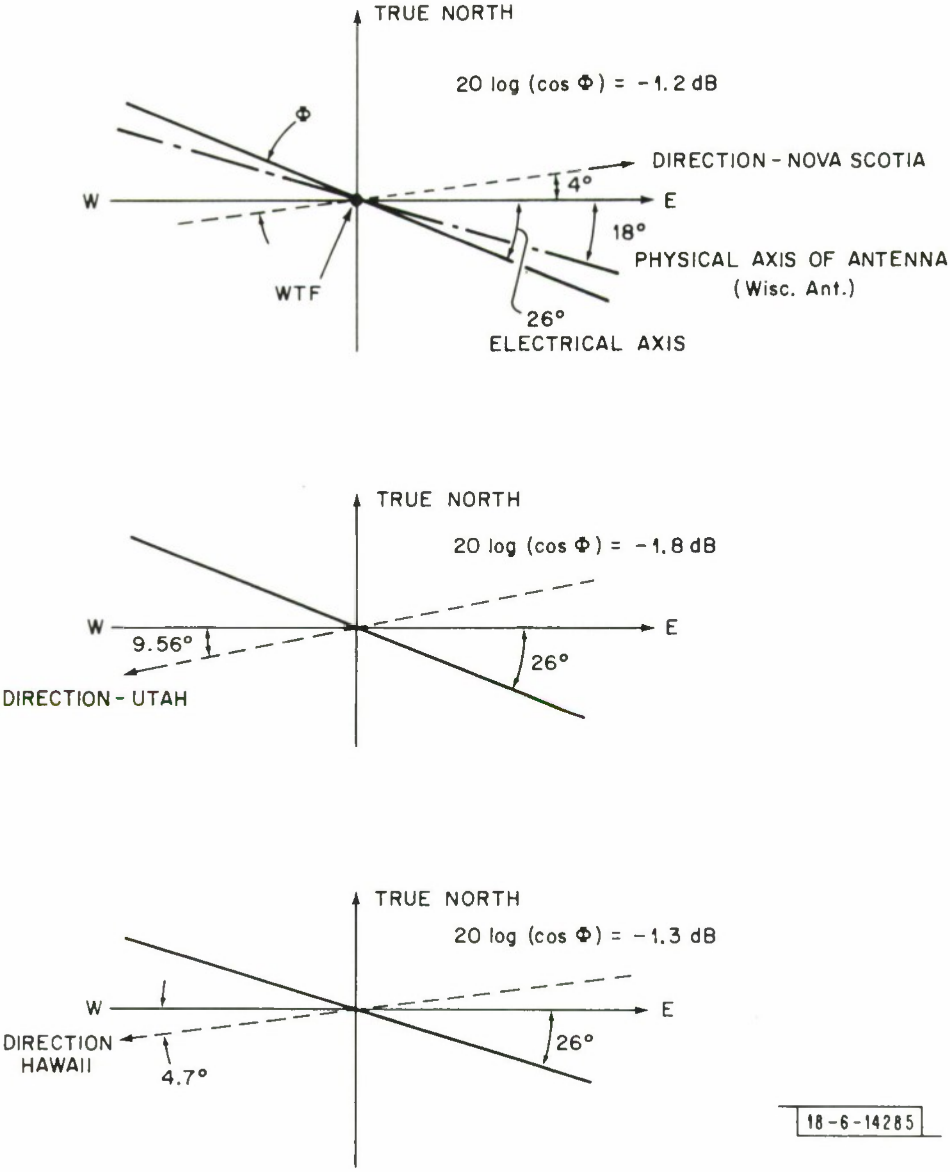

Fig. 6. 'Off axis' pointing angle corrections.

following to be true (see Fig. 7 for comparison):

(1) The results with antennas above or below ground are identical.

(2) Different Utah site selections over a 20 mile area gave the same results.

(3) The calibration correction factors to be applied to the earlier set of Utah data are 1.9 dB (40 Hz range) and 0.8 dB (70 Hz range). (This means correction terms in the α computation of 2.4 dB and 1.3 dB respectively, when the off-axis corrections are included. These numbers compare extremely well with the previously deduced values of 2.4 dB and 1.0 dB.)

It is strongly emphasized that the Utah data in this report have been corrected by 1.9 dB and 0.8 dB. Off-axis corrections will be added in only when α computations are made.

Sampling times and intervals are chosen to be the same for the Hawaii and Utah data so that one can compare the signal levels pairwise. The selection of a sampling interval depends on the signal level and noise intensity at the furthest site (Hawaii). The choice of the receiver's integration time is somewhat arbitrary. It must be short enough so that neither the amplitude nor phase of the received signal experiences significant change over the duration and long enough so that the integrated signal to noise ratio is sufficiently large so that there is a reasonable likelihood of detecting true signal amplitude variations (as opposed to those variations caused by noise alone). For our purposes, an integrated signal to noise ratio of 14 dB is a desirable lower limit (see Fig. C-2). Lower values of S/N_I reveal a rapidly

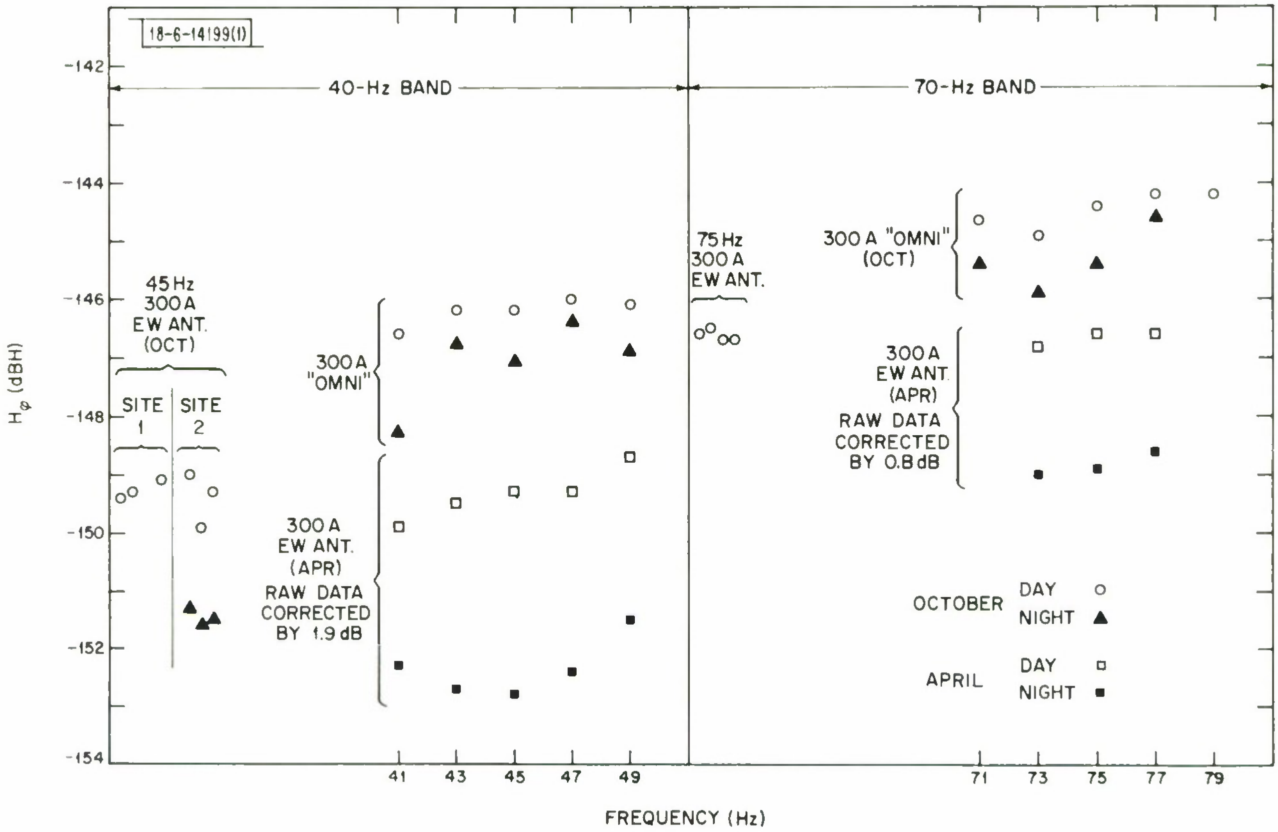

Fig. 7. Comparisons of Utah results (system calibration).

growing variation due to noise alone which would mask changes in signal level. After experimentation with several integration times, we have selected an equivalent integration time of 1.42 hours, which we have used in determining all the estimates in the following tables and figures.

The transmission schedules were selected to maximize either the number of daylight or nighttime hours over the entire Nova Scotia to Hawaii path. No attempt was made to determine the effects introduced by the day-night terminator intersecting the propagation path. One reason for this omission is that the changes associated with the transition from daytime to nighttime conditions have a duration of the same order as the integration time. Hence accurate signal estimates during this period would require a significantly shorter integration period, which, unfortunately would be offset by a low S/N_I (with large variations being introduced by the noise). A generalization that can be made, based on many recording periods taken all over New England, is that under either pure daytime or nighttime path conditions the phase change over a four to six hour period is at most several degrees. In Hawaii, the phase change associated with day to night transitions conditions is of the order of 20°. Lastly, it appears that the received signal amplitude also is nearly constant over either the daytime or nighttime conditions. There also exists a clearly recognizable amplitude change over the transition period of up to about 3 dB. All the ensuing data should be viewed for consistency with the preceeding generalization. The constancy of signal over an entirely daytime path (or nighttime path) is the foundation for all claims that we make that the average α and excitation factors derived have a real physical significance.

Figures 8 through 15 are typical representatives of the data at 45 Hz and 75 Hz at Hawaii and Utah. (The data at Nova Scotia is much the same as that in Utah.) The vertical scale for $\hat{A}^2$ (or $\hat{B}^2$) is proportional to voltage squared. We have omitted the actual voltage scale used in the computations and replaced it by a set of equivalent input field strength (H_φ) values in dBH. Note that the resulting scales are very nonlinear in dBH. The benefit of this scale is that one can easily see for example a '1 dB' variation. The sample values of $\hat{A}_b^2$ and $\hat{B}^2$ are picked off such traces and the biased estimates of H_φ^2 computed with the aid of equation e-8 (Appendix E). The traces for Utah are seen to be relatively constant over the measurement period. (This is consistent with the S/N_I being generally higher than 24 dB.) The Hawaii traces exhibit more variability. Much of this variation will be shown to be due to the noise alone; the S/N_I being typically around 12 dB for the 40 Hz range and 16 dB for the 70 Hz range. It must be noted that the noise intensity often changes by as much as 6 dB over a few hour period. This also tends to produce traces with unusually pronounced variations over a short interval.

The following table lists the sample times chosen for the two experiments.

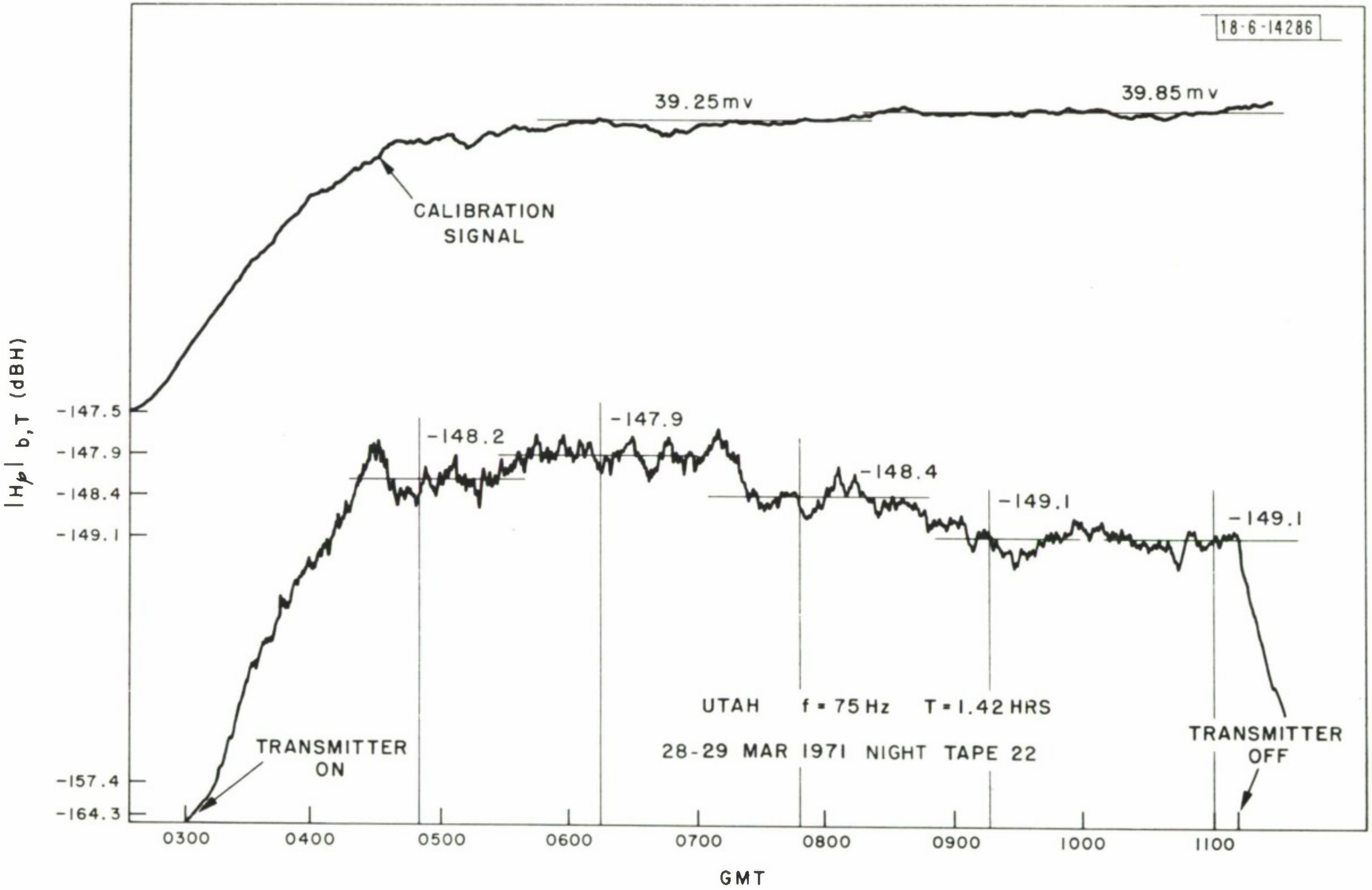

Fig. 8. Biased signal estimates $\hat{A}_b^2$ $(|\hat{H}_\varphi^2|_{b,T})$.

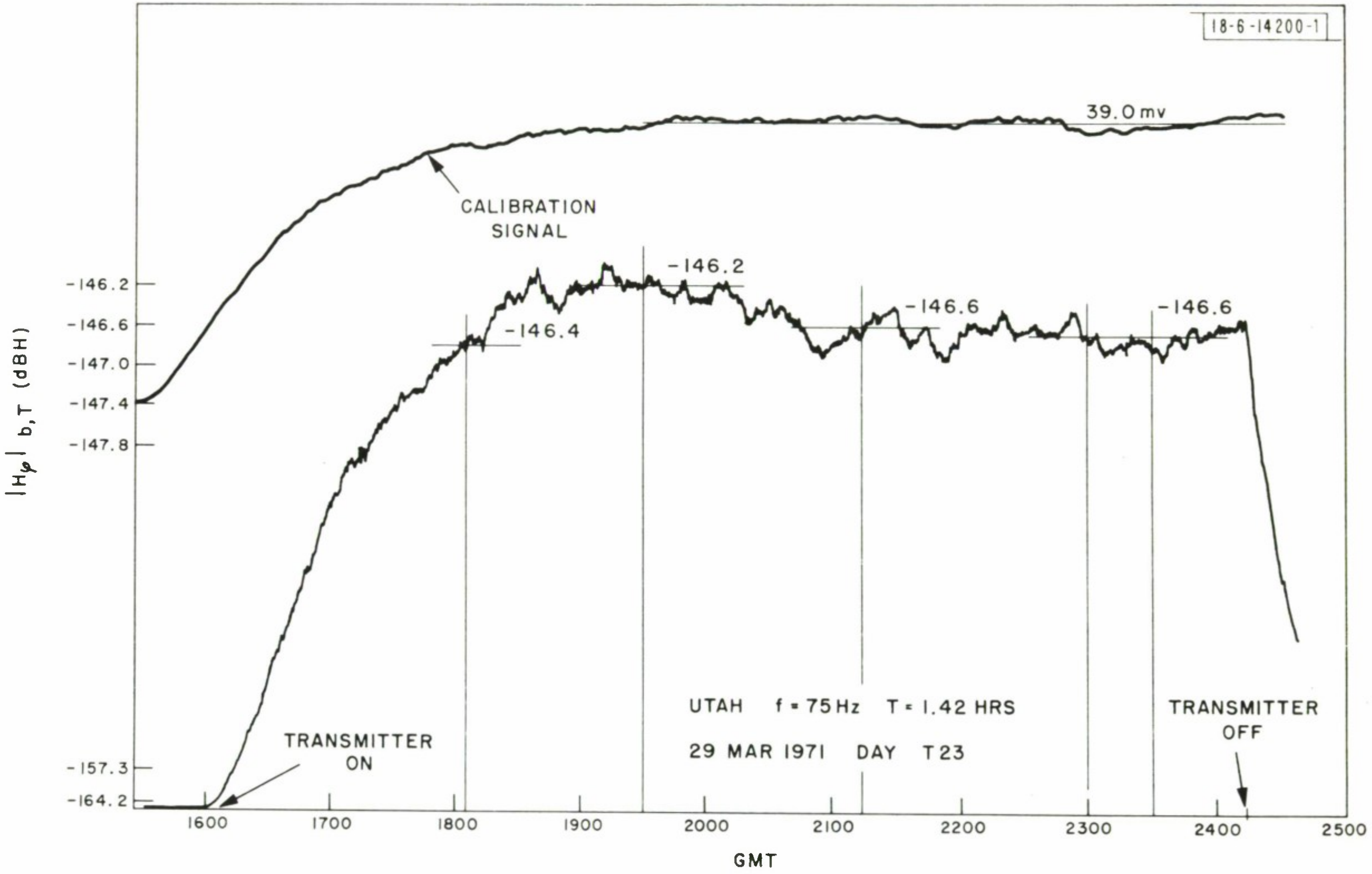

Fig. 9. Biased signal estimates $\hat{A}_b^2$ $(|\hat{H}_\varphi^2|_{b,T})$.

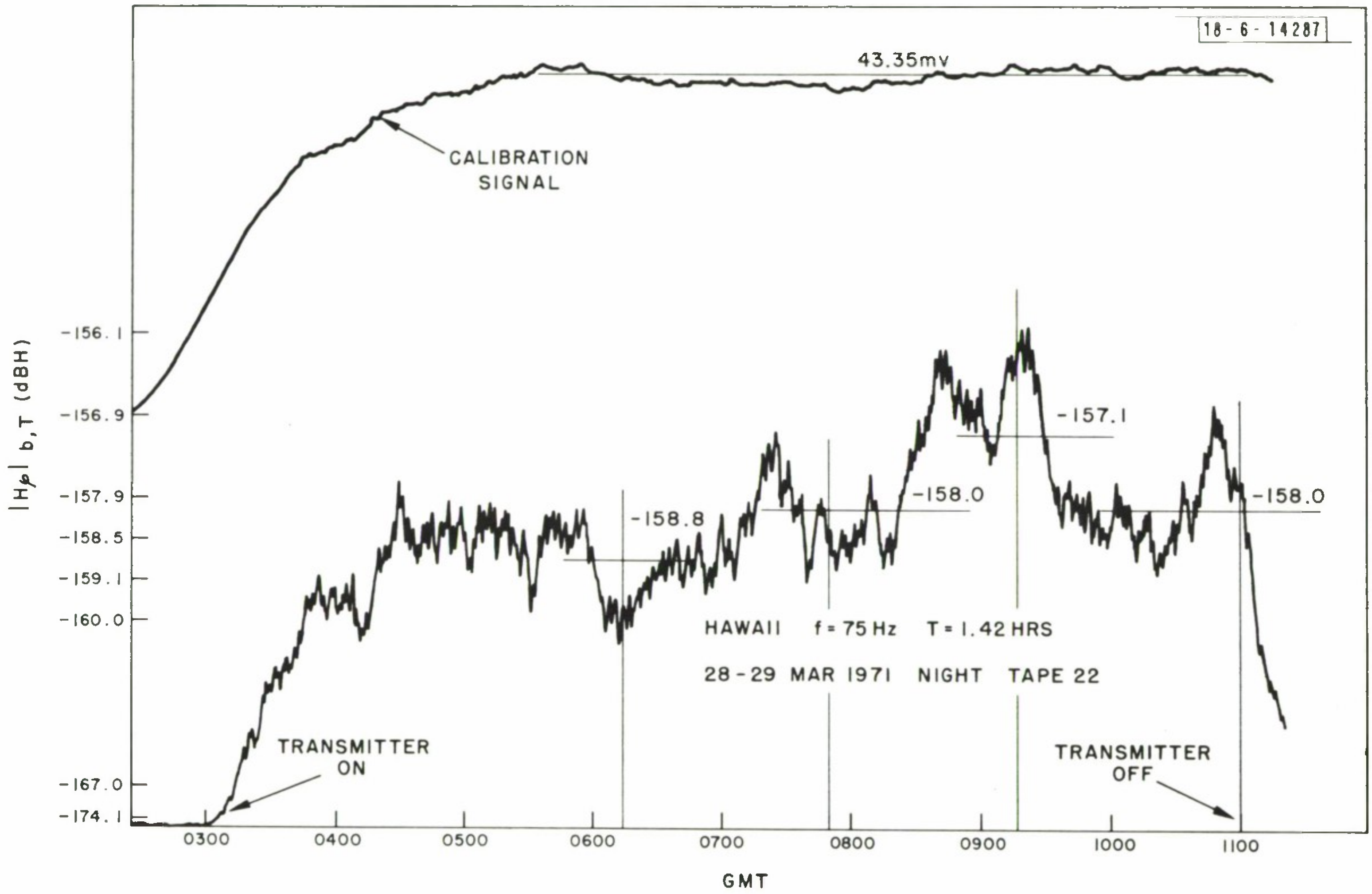

Fig. 10. Biased signal estimates $\hat{A}_b^2$ $(|\hat{H}_\varphi^2|_{b,T})$.

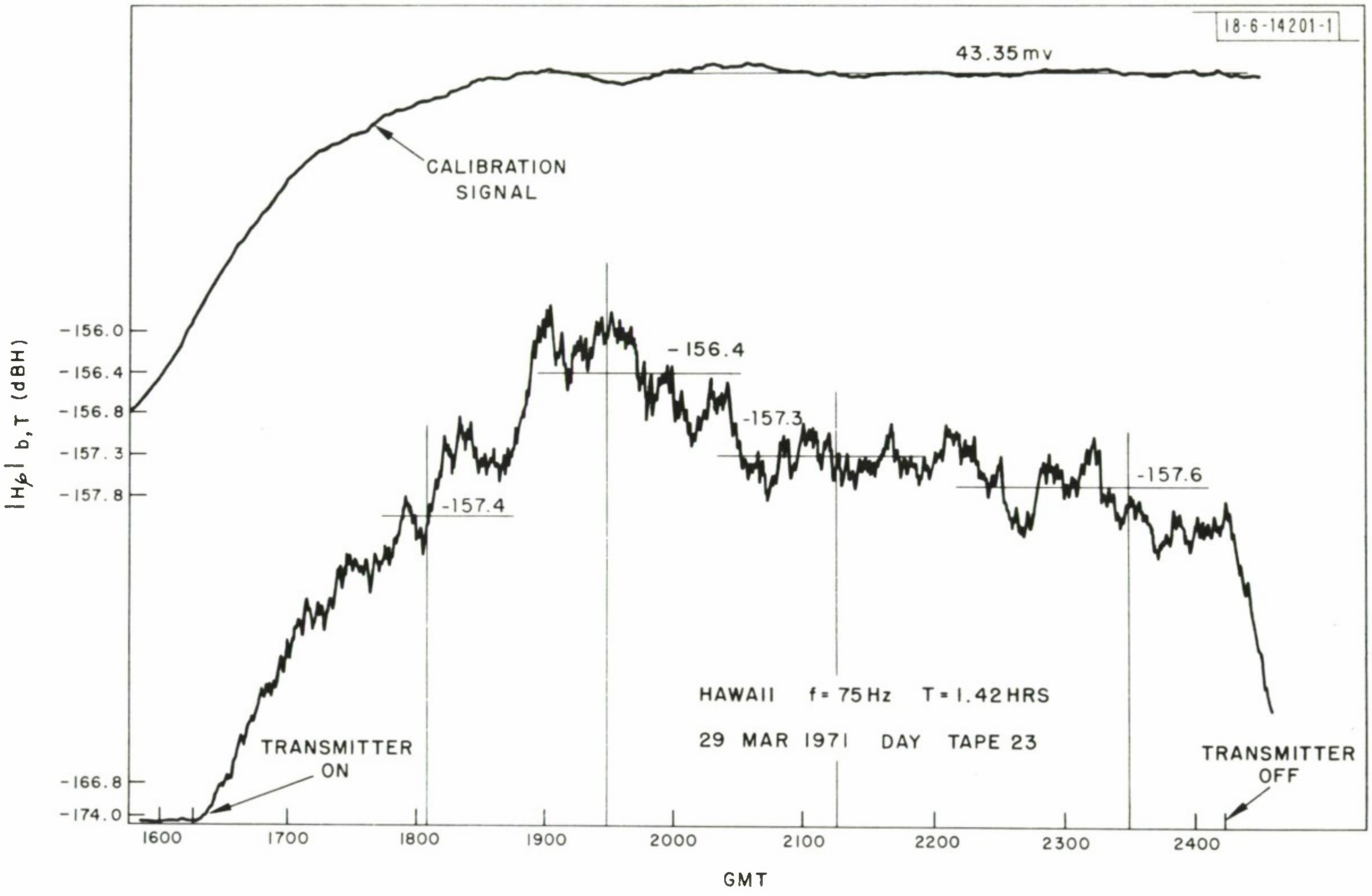

Fig. 11. Biased signal estimates $\hat{A}_b^2$ $(|\hat{H}_\varphi^2|_{b,\,T})$.

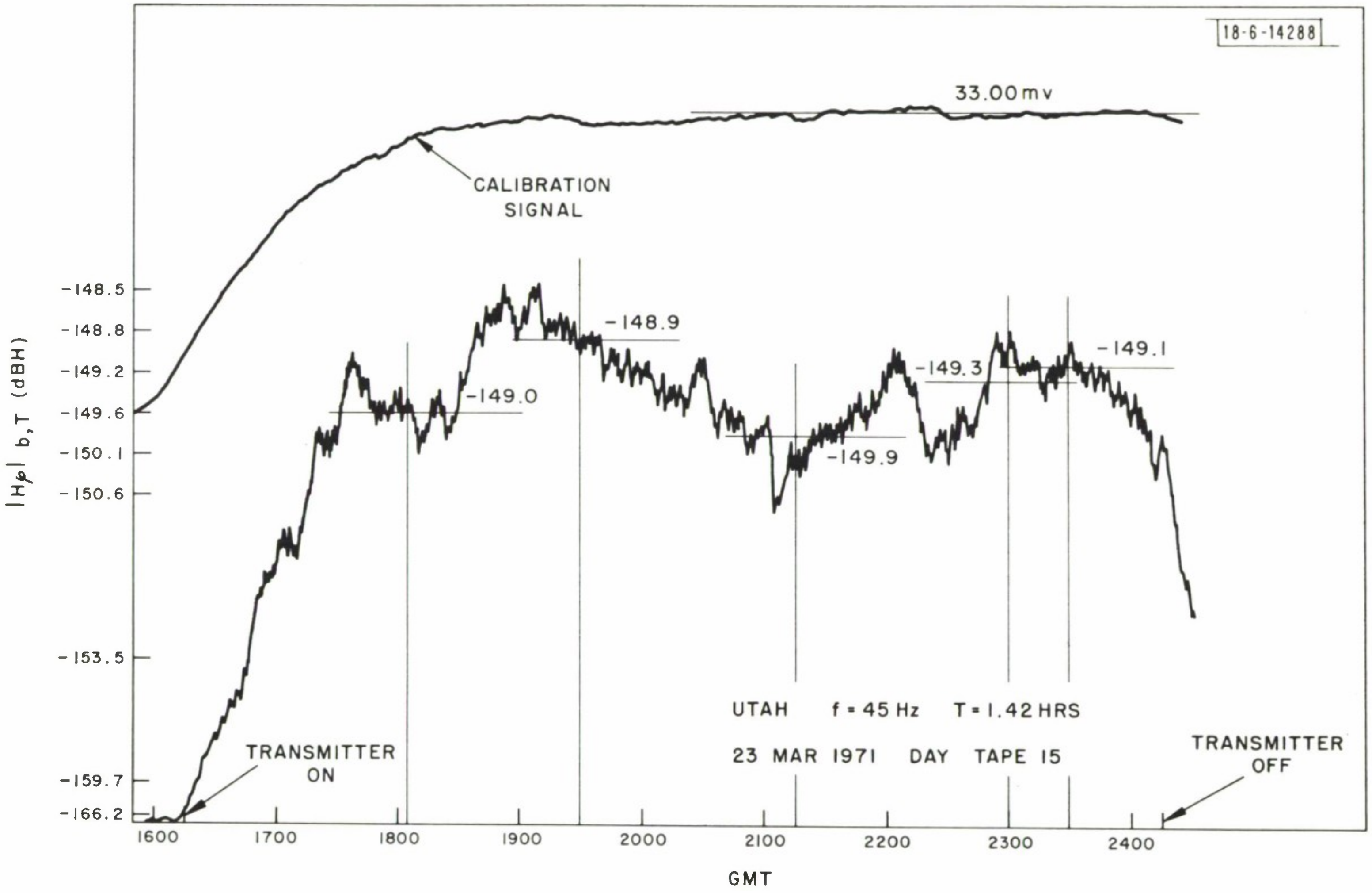

Fig. 12. Biased signal estimates $\hat{A}_b^2$ $(|\hat{H}_\varphi^2|_{b,T})$.

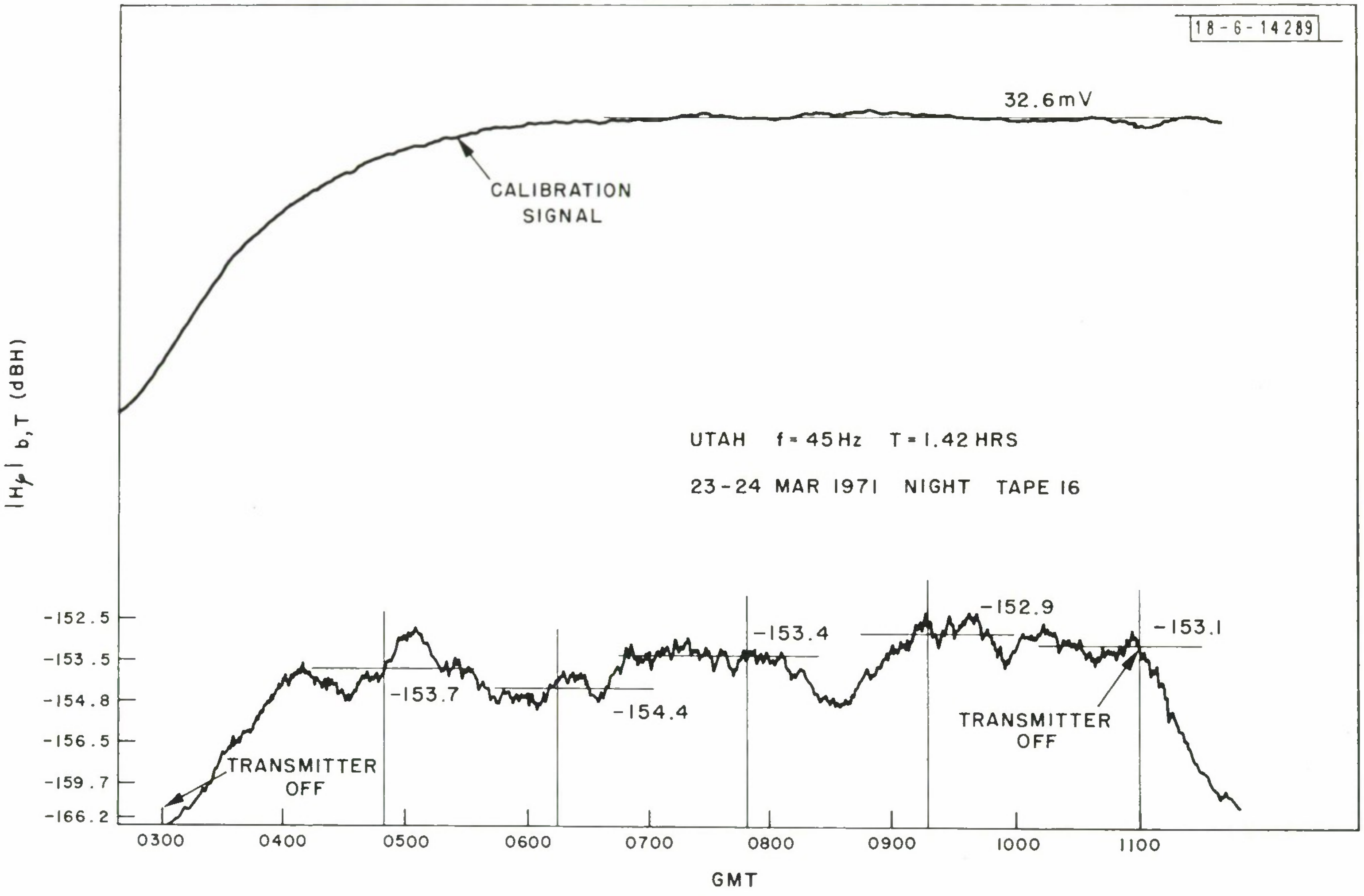

Fig. 13. Biased signal estimates $\hat{A}_b^2\,(|\hat{H}_\varphi^2|_{b,\,T})$.

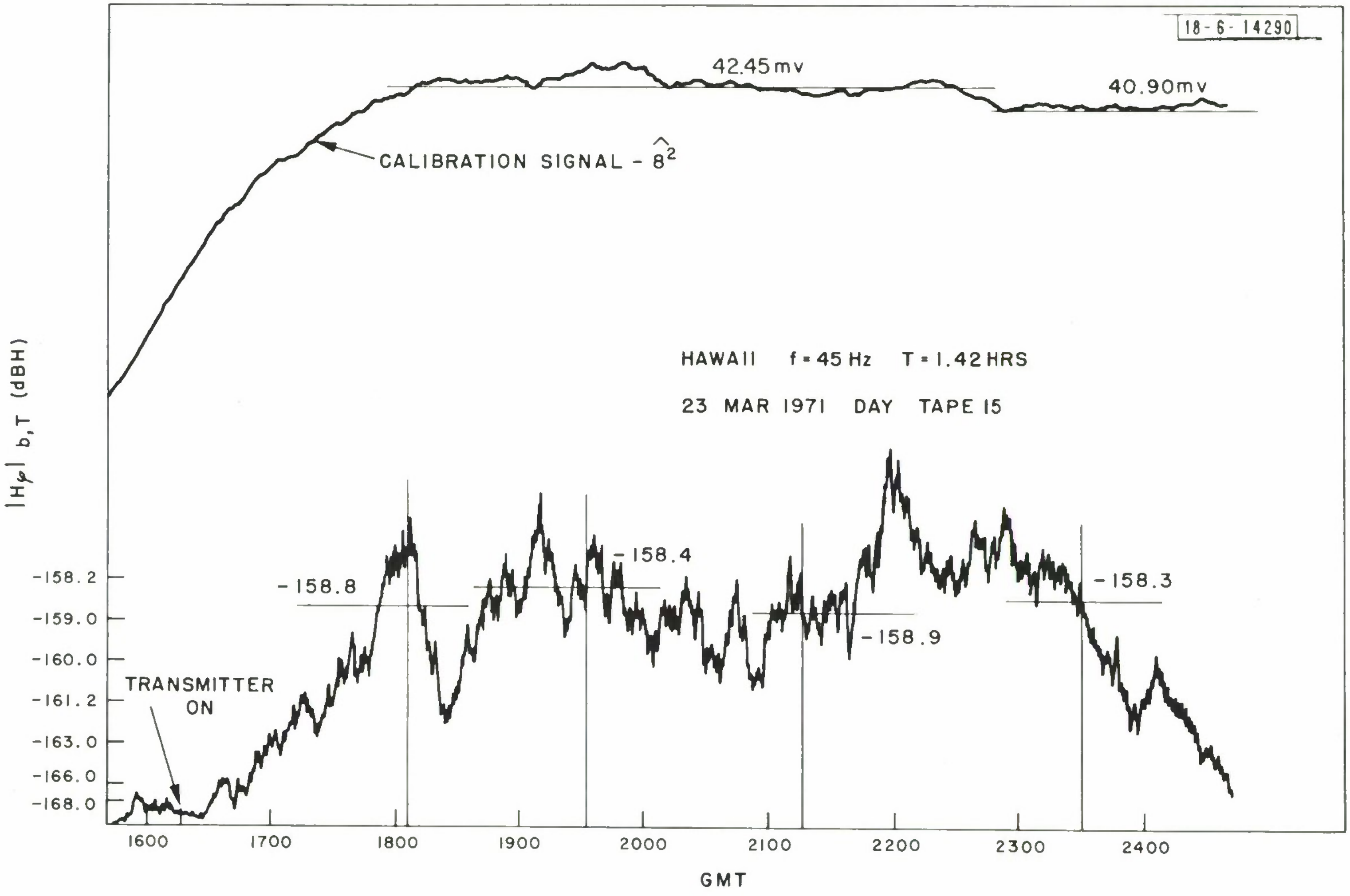

Fig. 14. Biased signal estimates $\hat{A}_b^2$ ($|\hat{H}_\varphi^2|_{b,T}$).

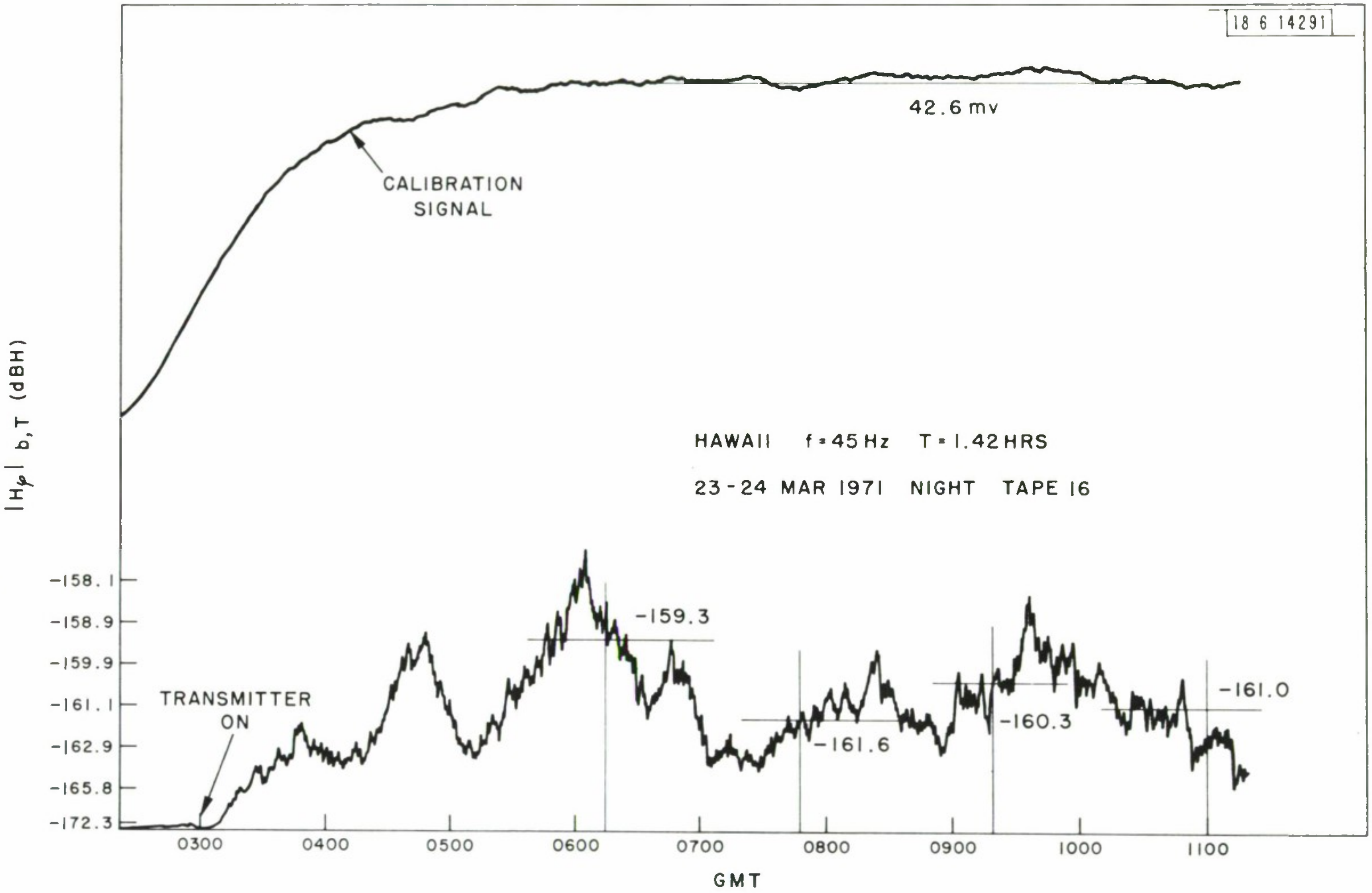

Fig. 15. Biased signal estimates $\hat{A}_b^2$ $(|\hat{H}_\varphi^2|_{b,\,T})$.

TABLE I

Sample Times (T = 1.42 hrs)

	Wisc-Utah-Hawaii path For α_{EW} computation	Utah-Wisc-Nova Scotia For α_{EW} versus α_{WE} computation
Daytime	1805 GMT 1930 2115 2330	1805 1930 2115 2300
Nighttime	0615 0748 0918 1100	0450 0615 0748 0918

These sample times were selected to avoid the effects associated with the transition period. Noise estimates (see Appendix B for details) are determined for the same sample times as the biased signal estimates, $|\widehat{H^2_\varphi}|_{b,T}$. The unbiased signal estimates, $|\widehat{H^2_\varphi}|_{u,T}$, are then computed as shown in equation 18. Typically the bias term for either the Utah or Nova Scotia data is at most 0.1 dB. The noisier Hawaii data exhibits typical bias terms between 0.3 and 1.0 dB. Figures 16-21 display the results of all the unbiased signal estimates at all the sites under either daytime or nighttime conditions. Tables II through VII tabulate the same data along with the dates of transmissions.

The major hypothesis we have made is that the received signal levels during a selected time period each day are essentially constant not only

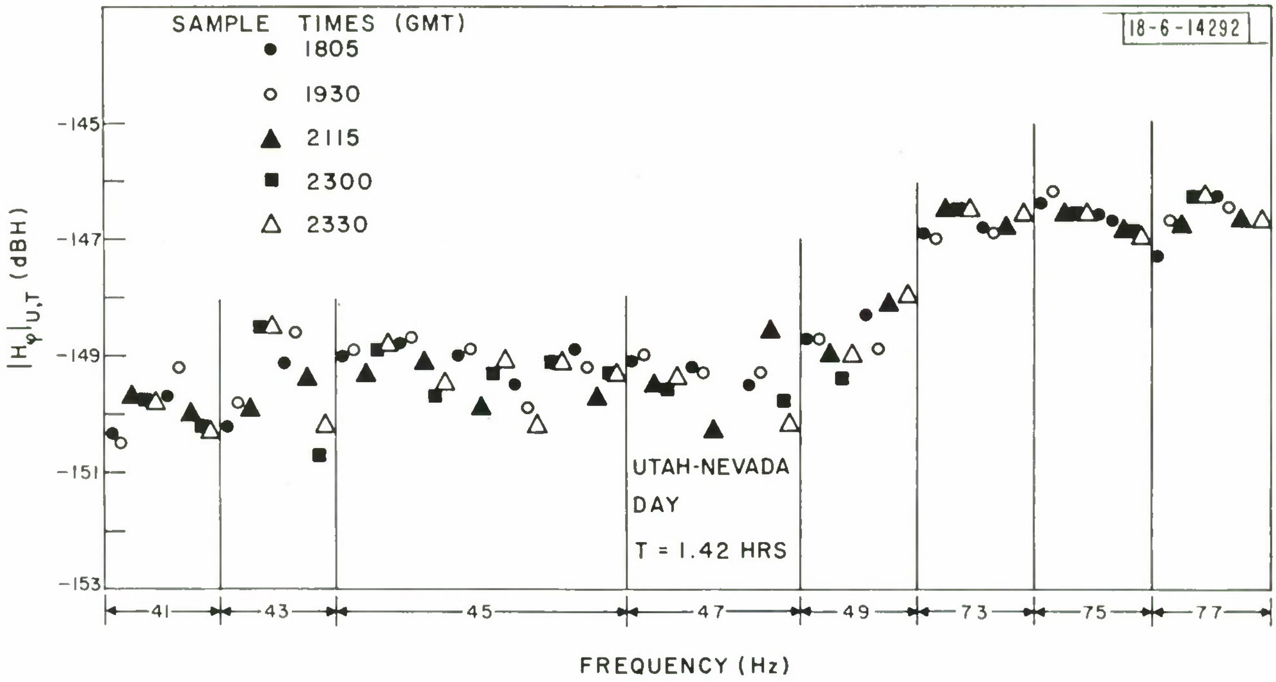

Fig. 16. Unbiased signal estimates $|\hat{H}^2_{\varphi}|_{u,\,T}$, Utah-Nev, daytime.

Table 11. Daytime Unbiased Signal Estimates H_ϕ (dbH)

UTAH – NEVADA

T = 1.42 hrs (Equiv. Integ. Time)

Tape No.	Date (1971)	Freq. (Hz)	Sample Times (GMT)							$|\bar{H}_\phi|_{\upsilon,T}$	
			1805	1930	2115	2300	2330				
8	Mar 8	41	−150.3	−150.5	−149.7	−149.8	−149.8				
37	Apr 5	41	−149.7	−149.2	−150.0	−150.2	−150.3			−149.9	
4	Mar 16	43	−150.2	−149.8	−149.9	−148.5	−148.5				
39	Apr 6	43	−149.2	−148.6	−149.4	−150.7	−150.2			−149.5	
2	Mar 15	45	−149.0	−148.9	−149.3	−148.9	−148.8				
13	22	45	−149.8	−149.7	−149.1	−149.7	−149.5				
15	23	45	−149.0	−148.9	−149.9	−149.3	−149.1				
17	24	45	−149.5	−149.9	−150.2	−149.1	−149.1				
35	Apr 4	45	−148.9	−149.2	−149.7	−149.3	−149.3			−149.3	
6	Mar 17	47	−149.1	−149.0	−149.5	−149.6	−149.4				
19	25	47	−149.2	−149.3	−150.3	—	—				
21	26	47	−149.5	−149.3	−148.6	−149.8	−150.2			−149.3	
10	Mar 19	49	−148.7	−148.7	−149.0	−149.4	−149.0				
41	Apr 7	49	−148.3	−148.9	−148.1	−148.1	−148.0			−148.7	
27	Mar 31	73	−146.9	−147.0	−146.5	−146.5	−146.5				
29	Apr 1	73	−146.8	−146.9	−146.8	−146.6	−146.6			−146.8	
23	Mar 29	75	−146.4	−146.2	−146.6	−146.6	−146.6				
25	30	75	−146.6	−146.7	−146.9	−146.9	−147.0			−146.6	
31	Apr 2	77	−147.3	−146.7	−146.8	−146.3	−146.3				
33	3	77	−146.3	−146.5	−146.7	−146.7	−146.7			−146.6	

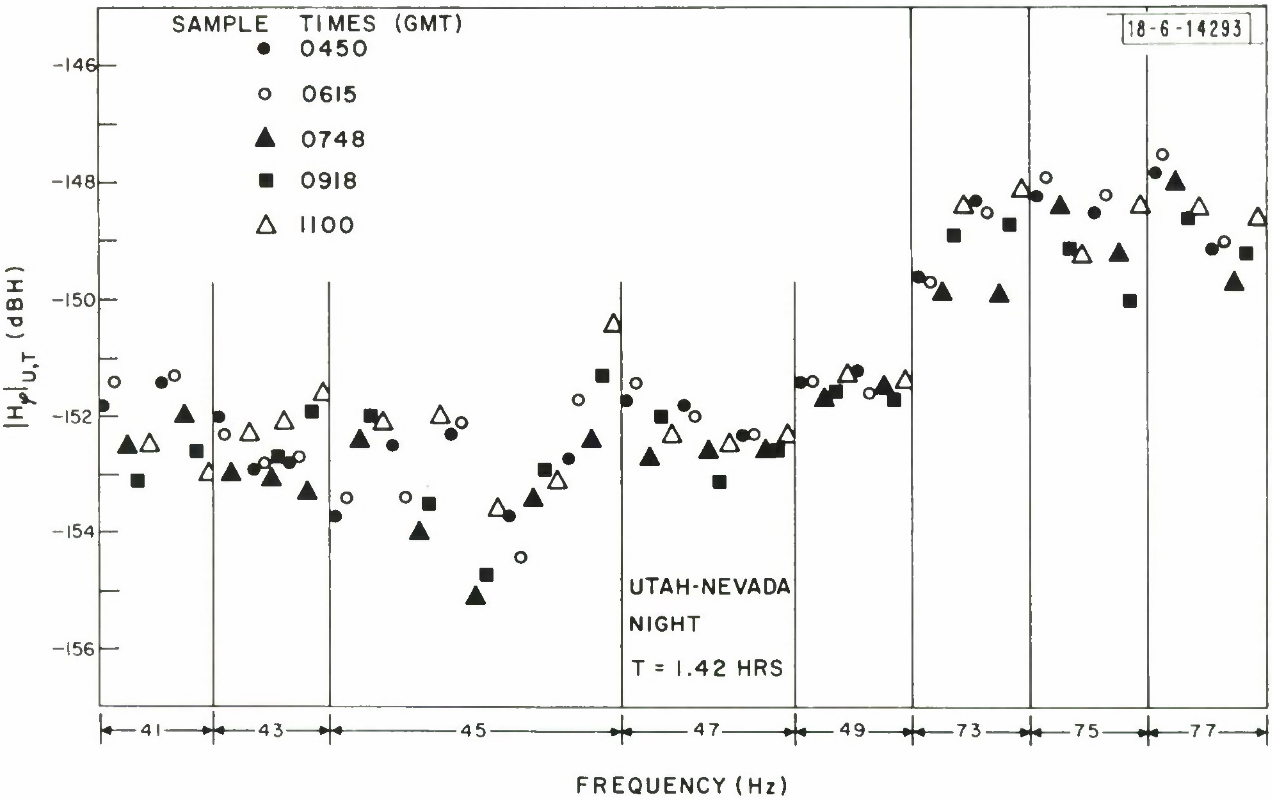

Fig. 17. Unbiased signal estimates $|\hat{H}^2_\varphi|_{u,\,T}$, Utah-Nev, nighttime.

Table III. Nighttime Unbiased Signal Estimates H_{ϕ} (dbH)

UTAH – NEVADA

T = 1.42 hrs (Equiv. Integ. Time)

Tape No.	Date (1971)	Freq. (Hz)	Sample Times (GMT)							$\overline{\lvert H_{\phi} \rvert}_{u,T}$	
			0450	0615	0748	0918	1100				
7	Mar 7-8	41	−151.8	−151.4	−152.5	−153.1	−152.5				
36	Apr 4-5	41	−151.4	−151.3	−152.0	−152.6	−153.0			−152.3 dbH	
3	Mar 15-16	43	−152.0	−152.3	−153.0	−153.0	−152.3				
11	19-20	43	−152.9	−152.8	−153.1	−152.7	−152.1				
38	Apr 5-6	43	−152.8	−154.7	−153.3	−151.9	−151.6			−152.7	
1	Mar 14-15	45	−153.7	−153.4	−152.4	−152.0	−152.1				
12	21-22	45	−152.5	−153.4	−154.0	−153.5	−152.0				
14	22-23	45	−152.3	−152.1	−155.1	−154.7	−153.6				
16	23-24	45	−153.7	−153.7	−153.4	−152.9	−153.1				
34	Apr 3-4	45	−152.7	−151.7	−152.4	−151.8	−150.4			−152.8	
5	Mar 16-17	47	−151.7	−151.4	−152.7	−152.0	−152.3				
18	24-25	47	−151.8	−152.0	−152.6	−153.1	−152.5				
20	25-26	47	−152.3	−152.3	−152.6	−152.6	−152.3			−152.4	
9	Mar 18-19	49	−151.3	−151.3	−151.7	−151.6	−151.3				
40	Apr 6-7	49	−151.2	−151.6	−151.5	−151.7	−151.4			−151.5	
26	Mar 30-31	73	−149.6	−149.7	−149.9	−148.9	−148.4				
28	Mar 31-Apr 1	73	−148.3	−148.5	−149.9	−148.7	−148.1			−149.0	
22	Mar 28-29	75	−148.2	−147.9	−148.4	−149.1	−149.2				
24	Mar 29-30	75	−148.5	−148.2	−149.2	−150.0	−148.4			−148.9	
30	Apr 1-2	77	−147.8	−147.5	−148.0	−148.6	−148.4				
32	2-3	77	−149.1	−149.0	−149.7	−149.2	−148.6			−148.6	

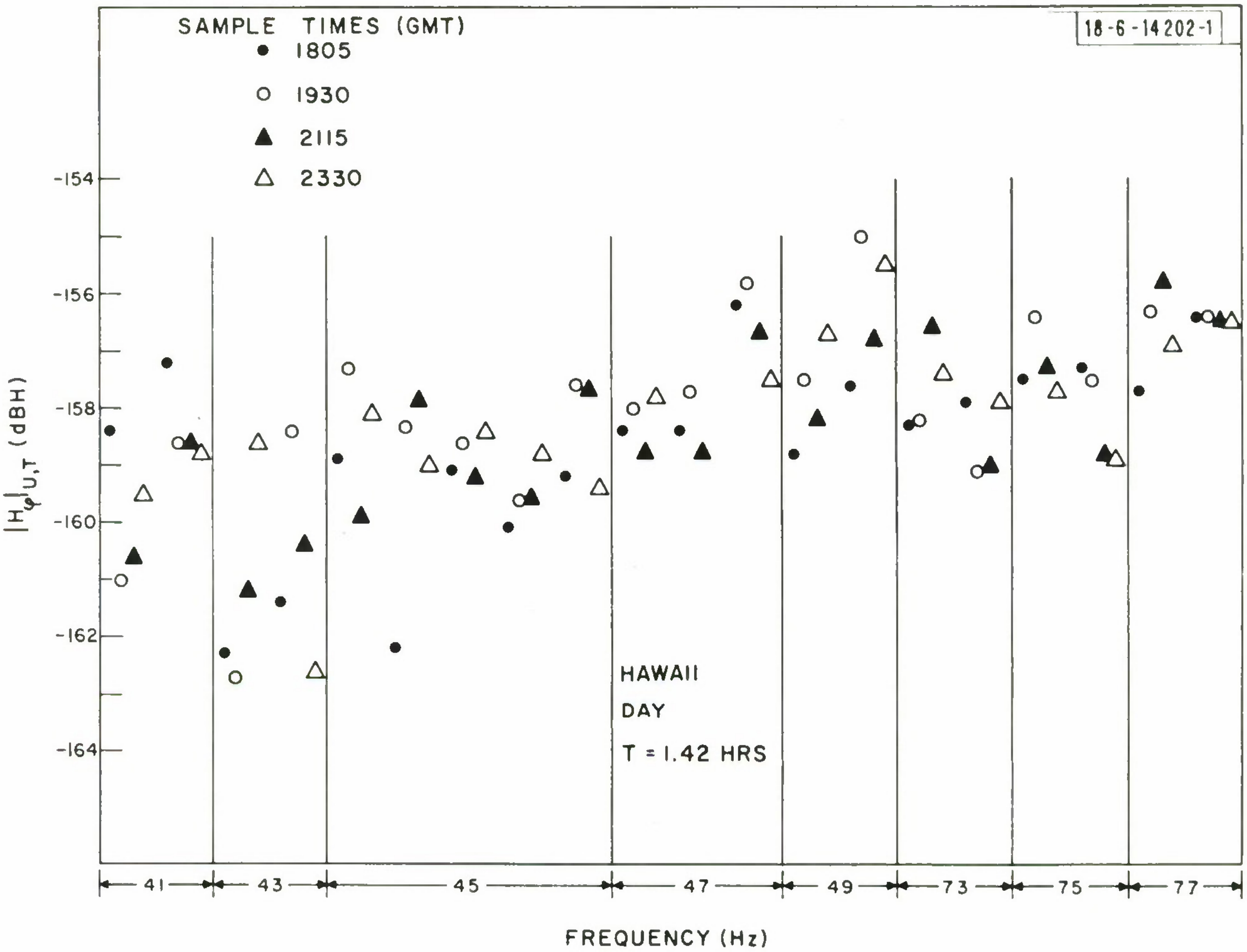

Fig. 18. Unbiased signal estimates $|\hat{H}_\varphi^2|_{u,T}$, Hawaii, daytime.

Table IV. Daytime Unbiased Signal Estimates H_ϕ (dbH)

HAWAII

$T = 1.42$ hrs (Equiv. Integ. Time)

Tape No.	Date (1971)	Freq. (Hz)	Sample Times (GMT)						$\lvert\overline{H}_\phi\rvert_{u,T}$		
			1805	1930	2115	2300	2330				
8	Mar 8	41	−158.4	−161.0	−160.6		−159.5				
37	Apr 5	41	−157.2	−158.6	−158.6		−158.8		−159.2		
4	Mar 16	43	−162.3	−162.7	−161.2		−158.6				
39	Apr 6	43	−161.4	−158.1	−160.4		−162.6		−160.5		
2	Mar 15	45	−158.9	−157.3	−159.9		−158.1				
13	22	45	−162.2	−158.3	−157.9		−159.0				
15	23	45	−159.1	−158.6	−159.2		−158.4				
17	24	45	−160.1	−159.6	−159.6		−158.8				
35	Apr 4	45	−159.2	−157.6	−157.7		−159.4		−158.8		
6	Mar 17	47	−158.4	−158.0	−158.8		−157.8				
19	25	47	−158.6	−157.7	−158.8		———				
21	26	47	−156.2	−155.8	−156.7		−157.5		−157.8		
10	Mar 19	49	−158.8	−157.5	−158.2		−156.7				
41	Apr 7	49	−157.6	−155.0	−156.8		−155.5		−157.2		
27	Mar 31	73	−158.3	−158.2	−156.6		−157.4				
29	Apr 1	73	−157.9	−159.1	−159.0		−157.9		−157.8		
23	Mar 29	75	−157.5	−156.4	−157.3		−157.7				
25	30	75	−157.3	−157.5	−158.8		−158.9		−157.6		
31	Apr 2	77	−157.7	−156.3	−155.8		−156.9				
33	3	77	−156.4	−156.4	−156.5		−156.5		−156.6		

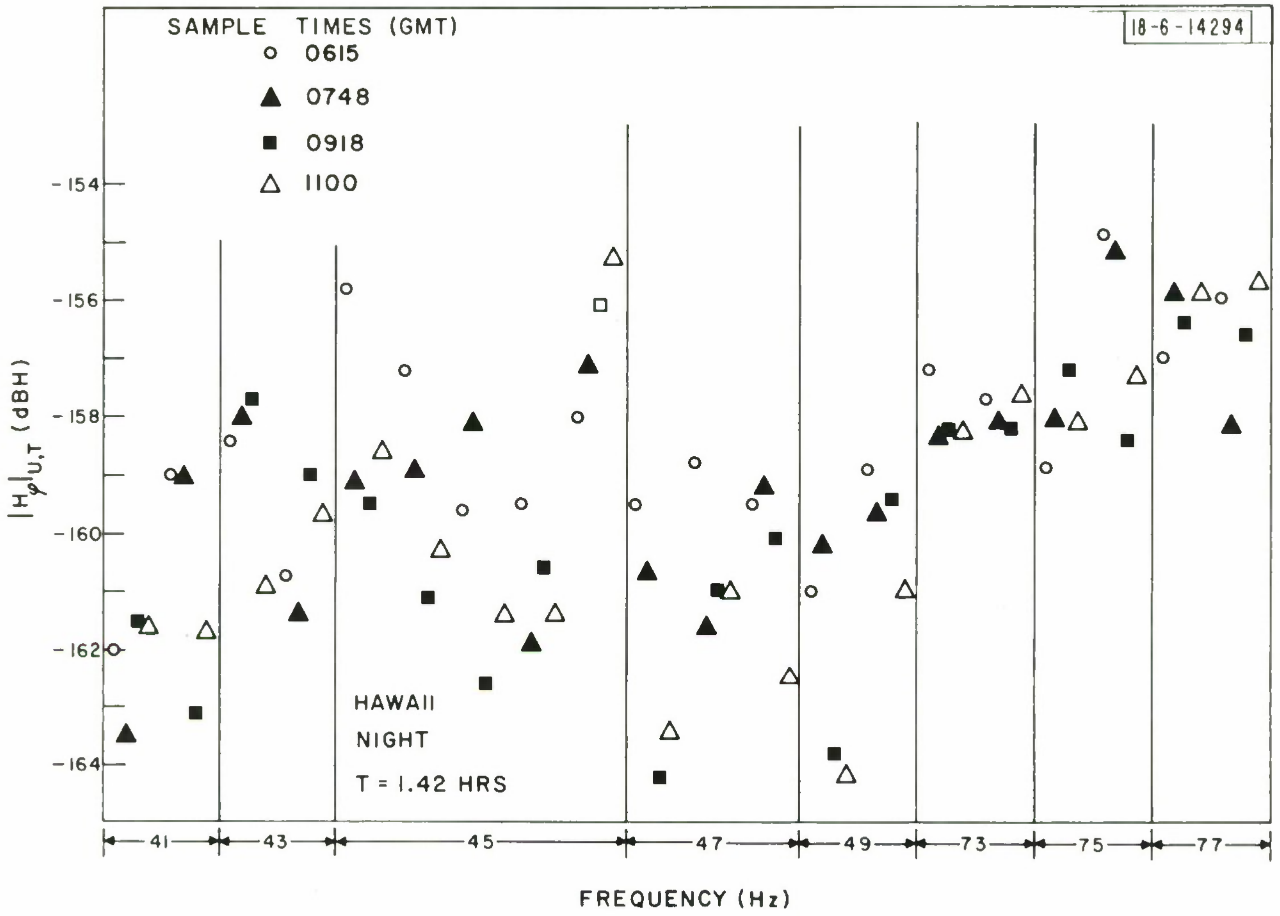

Fig. 19. Unbiased signal estimates $|\hat{H}_\varphi^2|_{u,T}$, Hawaii, nighttime.

Table V. Nighttime Unbiased Signal Estimates H_ϕ (dbH)

HAWAII

T = 1.42 hrs (Equiv. Integ. Time)

Tape No.	Date (1971)	Freq. (Hz)	Sample Times (GMT)						$|\overline{H}_\phi|_{u,T}$		
			0450	0615	0748	0918	1100				
7	Mar 7-8	41		−162.0	−163.5	−161.5	−161.6				
36	Apr 4-5	41		−159.0	−159.0	−163.1	−161.7		−161.2		
3	Mar 15-16	43									
11	19-20	43		−158.4	−158.0	−157.7	−160.9				
38	Apr 5-6	43		−160.7	−161.4	−159.0	−159.7		−159.3		
1	Mar 14-15	45		−155.8	−159.1	−159.5	−158.6				
12	21-22	45		−157.2	−158.9	−161.1	−160.3				
14	22-23	45		−159.6	−153.1	−162.6	−161.4		(−159.4)	− 16 pt ave	
16	23-24	45		−159.5	−161.9	−160.6	−161.4				
34	Apr 3-4	45		−158.0	−157.1	−156.1	−155.3		−158.7	− 20 pt ave	
5	Mar 16-17	47		−159.5	−160.7	−164.2	−163.4				
18	24-25	47		−158.8	−161.6	−161.0	−161.0				
20	25-26	47		−159.5	−160.2	−161.1	−162.5		−160.7		
9	Mar 18-19	49		−161.0	−160.2	−163.8	−164.2				
40	Apr 6-7	49		−158.9	−159.7	−159.4	−161.0		−160.8		
26	Mar 30-31	73		−157.2	−158.4	−158.3	−158.3				
28	Mar 31- Apr 1	73		−157.7	−158.1	−158.2	−157.6		−157.8		
22	Mar 28-29	75		−158.9	−158.1	−157.2	−158.1				
24	Mar 29-30	75		−154.9	−155.2	−158.4	−157.3		−157.0		
30	Apr 1-2	77		−157.0	−155.9	−156.4	−155.9				
32	2-3	77		−156.0	−158.2	−156.6	−155.7		−156.4		

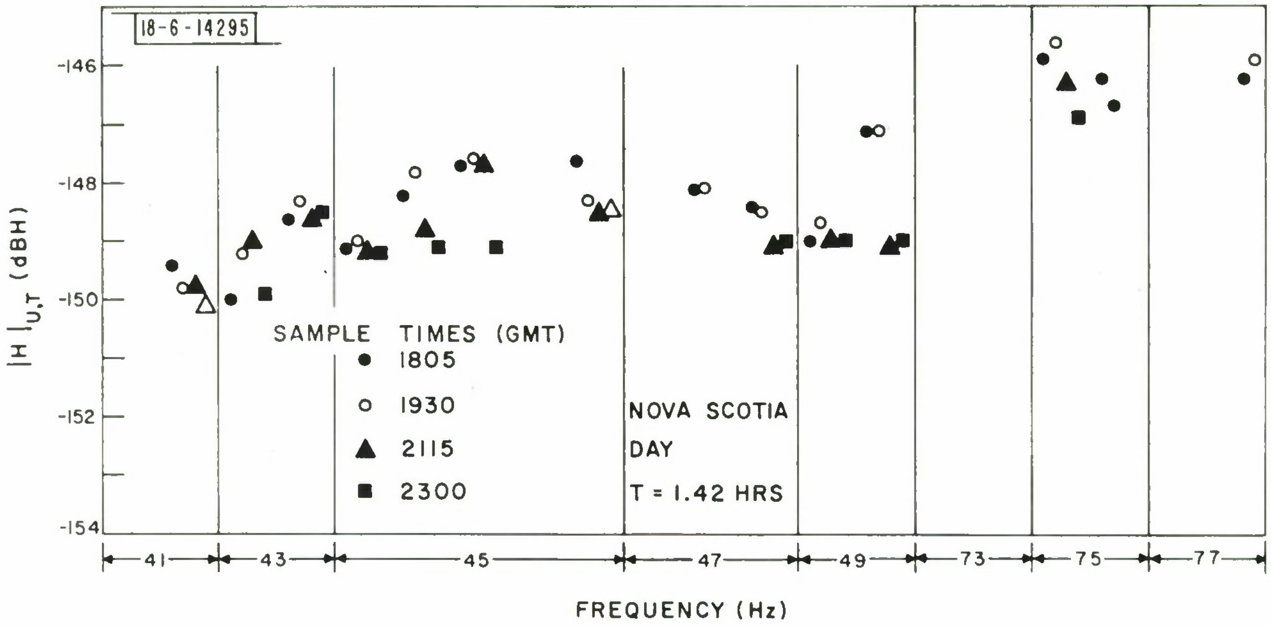

Fig. 20. Unbiased signal estimates $|\hat{H}^2_\varphi|_{u,\,T}$, Nova Scotia, daytime.

Table VI. Daytime Unbiased Signal Estimates H_ϕ (dbH)

NOVA SCOTIA

T = 1.42 hrs (Equiv. Integ. Time)

Tape No.	Date (1971)	Freq. (Hz)	Sample Times (GMT)						$\overline{\lvert H_\phi(f_i)\rvert}_{u,T}$		
			1805	1930	2115	2300	2330				
8	Mar 8	41	—	—	—	—					
27	Apr 5	41	−149.4	−149.8	−149.8	−150.1			−149.8		
4	Mar 16	43	−150.0	−149.2	−149.0	−149.9					
39	Apr 6	43	−148.6	−148.3	−148.6	−148.5			−149.0		
2	Mar 15	45	−149.1	−149.0	−149.2	−149.2					
13	22	45	−148.2*	−147.8*	−148.8	−149.1					
15	23	45	−147.7*	−147.6*	−147.7	−149.1					
17	24	45	—	—	—	—					
35	Apr 4	45	−147.6*	−148.4	−148.5	−148.5			−148.4		
6	Mar 17	47	—	—	—	—					
19	25	47	−148.1	−148.1	—	—					
21	26	47	−148.4	−148.5	−149.1	−149.0			−148.5		
10	Mar 19	49	−149.0	−148.7	−149.0	−149.0					
41	Apr 7	49	−147.1	−147.1	−147.5	−148.4			−148.2		
27	Mar 31	73	—	—	—	—†					
29	Apr 1	73	—	—	—	—†					
23	Mar 29	75	−145.9	−145.6	−146.3	−146.9					
25	30	75	−146.2	−146.7	—	—†			−146.3		
31	Apr 2	77	—	—	—	—†					
33	3	77	—	—†	−146.2	−145.9			−146.0		

* Noisy period.

† Tape recorder problems.

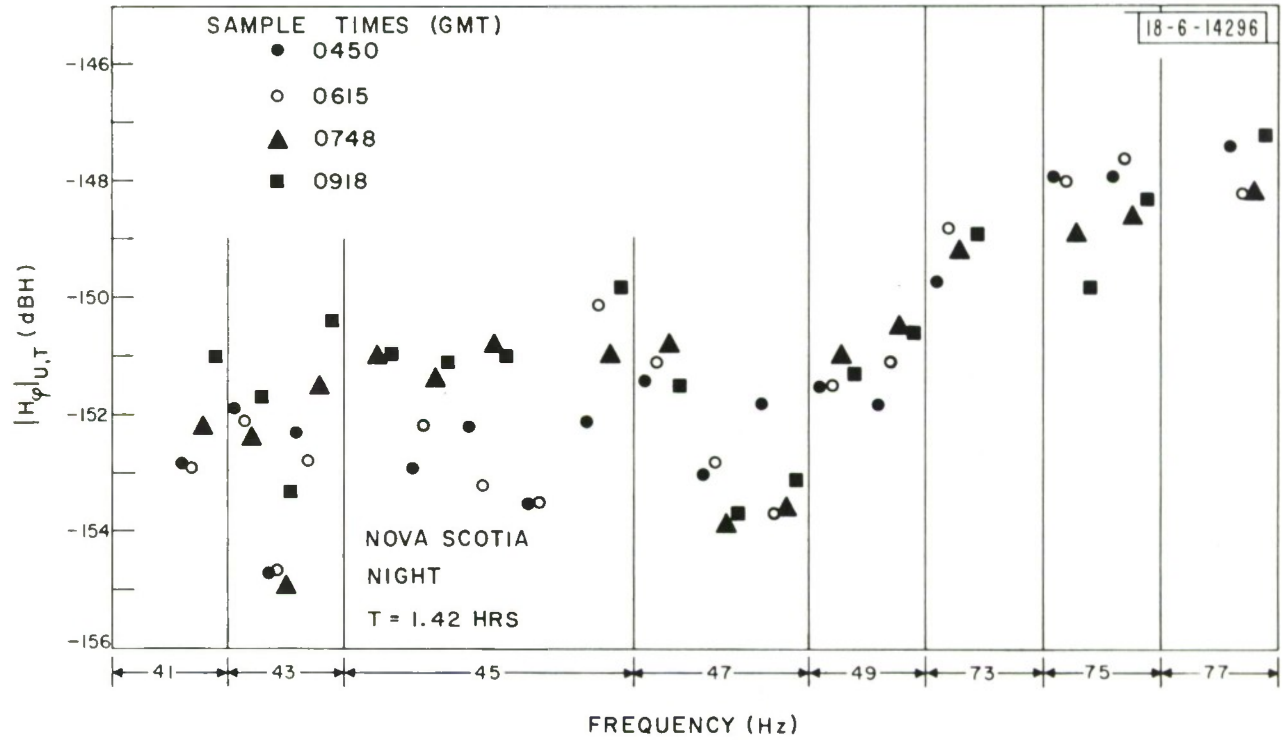

Fig. 21. Unbiased signal estimates $|\hat{H}_\varphi^2|_{u,T}$, Nova Scotia, nighttime.

Table VII. Nighttime Unbiased Signal Estimates H_ϕ (dbH)

NOVA SCOTIA

T = 1.42 hrs (Equiv. Integ. Time)

Tape No.	Date (1971)	Freq. (Hz)	Sample Times (GMT)						$\lvert\overline{H_\phi(f_i)}\rvert_{\upsilon,T}$		
			0450	0615	0748	0918	1100				
7	Mar 7-8	41	—	—	—	—					
36	Apr 4-5	41	−152.8	−152.9	−152.2	−151.0			−152.2		
3	Mar 15-16	43	−151.9	−152.1	−152.4	−151.7					
11	19-20	43	−154.7	−154.7	−154.9	−153.3					
38	Apr 5-6	43	−152.3	−152.8	−151.5	−150.4			−152.6		
1	Mar 14-15	45	—	—	−151.0	−151.0					
12	21-22	45	−152.9	−152.2	−151.4	−151.1					
14	22-23	45	−152.2	−153.2	−150.8	−151.0					
16	23-24	45	−153.5	−153.5	—	—					
34	Apr 3-4	45	−152.1	−150.1	−151.0	−149.8			−151.6		
5	Mar 16-17	47	−151.4	−151.1	−150.8	−151.5					
18	24-25	47	−153.0	−152.8	−153.9	−153.7					
20	25-26	47	−151.8	−153.7	−153.6	−153.1			−152.5		
9	Mar 18-19	49	−151.5	−151.5	−151.0	−151.3					
40	Apr 6-7	49	−151.8	−151.1	−150.5	−150.6			−151.2		
26	Mar 30-31	73	−149.7	−148.8	−149.2	−148.9			−149.1		
28	Mar 31-Apr 1	73	—	—	—	—					
22	Mar 28-29	75	−147.9	−148.0	−148.9	−149.8					
24	Mar 29-30	75	−147.9	−147.6	−148.6	−148.3			−148.3		
30	Apr 1-2	77	—	—	—	—					
32	2-3	77	−147.4	−148.2	−148.2	−147.2			−147.7		

over the period but also over similar time intervals on succeeding days. If the premise is correct then the α one obtains by suitably averaging all the data has a real physical meaning. If the premise is not quite correct then these computed values of α are 'average' values for the attenuation rates. The true attenuation rate for a particular time interval could then be a few tenths of a db/Mm different. With the transmitted power levels currently available with WTF, it is clear that we will always require a large number of samples (with long integration times per sample) in order to calculate an average value for α (with reasonable error bounds). We can, however, look at the variability of received signal estimates at the more remote receiver sites. Examination of these estimates along with their individual confidence limits may provide assurance that the hypothesis made is reasonable. In order to compute the confidence limits on each signal estimate, the corresponding noise estimates are also computed at the same sample times. As explained in Appendix B, about 2400 independent samples (over a one hour period) are taken in order to compute each noise intensity value. The noise estimates are expected to be accurate within ± .15 db provided the noise is reasonably stationary over the one hour period. As typical examples, tables VIII and IX list the values of noise intensity and rms signal to integrated noise ratios for Hawaii. For each signal to integrated noise estimate ($\hat{S}/N_I = |\widehat{H^2_\varphi}|_{b,T} / (|H^2_N|/T)$) confidence intervals are constructed (see appendix C for details). Figures 22 through 25 show the unbiased signal estimates and the 80% confidence intervals for the Utah and Hawaii data at 45, 73, 75 and 77 Hz. Some important conclusions can

Table VIII. Daytime Noise Intensities and Integrated Signal to Noise Ratios HAWAII

H_N^2 dbH/$\sqrt{Hz}$ $\hat{S}_b/N_I$ $N_I = H_N^2/T$ T = 1.42 hrs

Tape No.	Date (1971)	Freq. (Hz)	Sample Times (GMT)					Sample Times (GMT)			
			1805	1930	2115	2330		1805	1930	2115	2330
8	Mar 8	41	−133.3	−133.4	−137.0	−137.3		12.3	10.0	13.7	15.1
37	Apr 5	41	−133.0	−133.0	−134.3	−134.3		13.1	11.8	13.0	12.8
4	Mar 16	43	−134.4	−134.4	−134.8	−135.2		9.7	9.3	11.1	13.9
39	Apr 6	43	−134.0	−134.0	−133.9	−133.9		10.1	13.2	11.0	9.0
2	Mar 15	45	−133.6	−133.6	−135.3	−135.3		12.1	13.6	12.7	14.5
13	22	45	−132.5	−132.5	−134.2	−135.9		8.1	11.6	13.6	14.2
15	23	45	−133.9	−133.9	−134.3	−136.5		12.2	12.6	12.5	15.3
17	24	45	−134.4	−134.4	−136.1	−138.6		11.7	12.3	13.8	17.0
35	Apr 4	45	−133.1	−133.6	−134.3	−134.3		11.3	13.3	13.9	12.3
6	Mar 17	47	−135.5	−135.5	−136.7	−136.7		14.4	14.7	15.1	16.1
19	25	47	−132.7	−132.7	−132.7	−133.2		11.5	12.1	11.8	
21	26	47	−132.0	−131.3	−132.1	−132.8		13.1	12.8	12.7	12.6
10	19	49	−136.0	−136.0	−136.5	−137.0		14.5	15.7	15.5	17.5
41	Apr 7	49	−132.0	−132.0	−131.5	−131.5		11.8	14.3	12.1	13.3
27	Mar 31	73	−138.7	−138.7	−141.5	−142.4		17.6	17.7	22.0	22.1
29	Apr 1	73	−139.1	−139.1	−140.8	−140.8		18.4	17.2	19.0	20.0
23	Mar 29	75	−139.1	−139.1	−141.8	−141.8		18.8	19.8	21.6	21.2
25	30	75	−135.5	−135.5	−137.9	−137.9		15.4	15.1	16.3	16.2
31	Apr 2	77	−136.4	−136.4	−136.2	−136.2		15.9	17.2	17.6	16.5
33	3	77	−136.4	−136.3	−139.1	−139.1		17.2	17.0	19.7	19.7

Table IX. Nighttime Noise Intensities and Integrated Signal to Noise Ratios HAWAII

H_N^2 dbH/$\sqrt{Hz}$ $\hat{S}/N_I$ $N_I = H_N^2/T$ T = 1.42 hrs

Tape No.	Date (1971)	Freq. (Hz)	Sample Times (GMT)					Sample Times (GMT)			
			0615	0748	0918	1100		0615	0748	0918	1100
7	Mar 7-8	41	−135.6	−135.6	−135.6	−134.3		11.1	9.7	11.5	10.2
36	Apr 4-5	41	−134.7	−134.7	−134.7	−134.3		13.0	13.0	9.3	10.1
3	Mar 15-16	43									
11	19-20	43	−134.4	−133.4	−134.4	−135.5		13.3	12.7	14.0	12.0
38	Apr 5-6	43	−133.6	−133.6	−133.0	−132.9		10.4	9.8	11.4	10.7
1	Mar 14-15	45	−133.1	−133.1	−134.5	−134.5		14.5	11.4	12.4	13.2
12	21-22	45	−133.6	−134.8	−136.4	−136.4		13.7	13.2	12.6	13.4
14	22-23	45	−132.9	−132.9	−133.3	−133.3		10.8	12.2	9.0	9.5
16	23-24	45	−135.6	−135.8	−134.5	−134.5		13.4	11.3	11.3	10.6
34	Apr 3-4	45	−133.4	−133.4	−134.1	−134.1		12.7	13.6	15.2	16.0
5	Mar 16-17	47	−136.6	−136.6	−135.2	−135.2		14.4	13.2	8.7	9.4
18	24-25	47	−136.7	−136.7	−136.7	−135.1		15.1	12.5	13.0	11.5
20	25-26	47	−134.0	−134.0	−133.0	−131.0		11.9	11.2	9.5	7.4
9	Mar 18-19	49	−134.8	−134.8	−135.2	−135.4		11.2	12.0	9.1	8.9
40	Apr 6-7	49	−134.6	−134.6	−134.8	−135.0		13.0	12.3	12.7	11.4
26	Mar 30-31	73	−137.0	−138.3	−138.4	−138.5		17.0	17.1	17.3	17.4
28	Mar 31- Apr 1	73	−139.0	−138.1	−138.1	−138.9		18.5	17.2	18.1	18.5
22	Mar 28-29	75	−136.4	−136.8	−136.8	−137.4		14.7	15.9	16.8	16.5
24	29-30	75	−137.3	−136.5	−136.9	−137.3		19.5	18.5	15.7	17.2
30	Apr 1-2	77	−134.0	−135.4	−136.0	−136.4		14.3	16.7	16.8	17.7
32	2-3	77	−133.9	−133.9	−134.5	−135.5		15.1	13.0	15.1	17.0

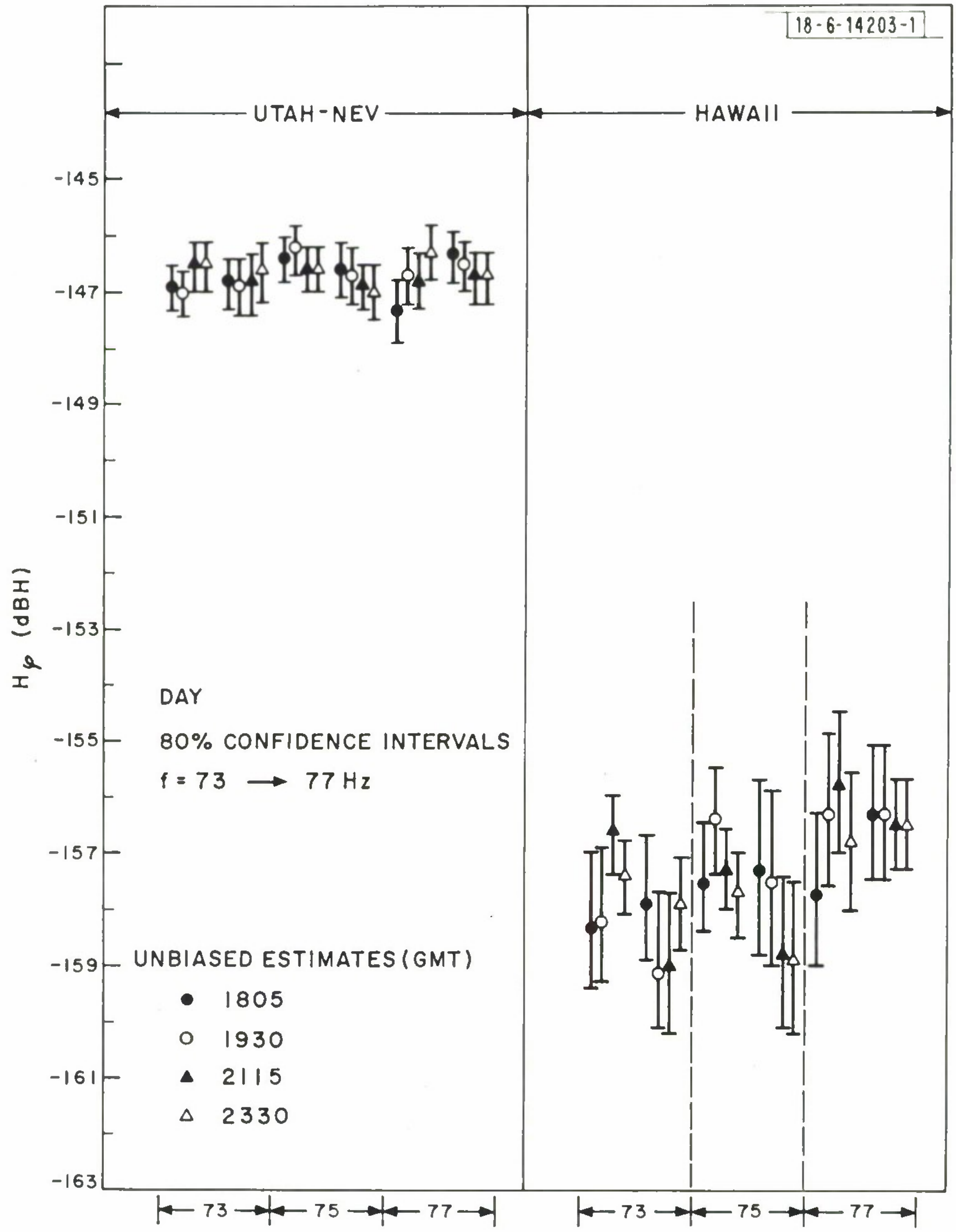

Fig. 22. Unbiased signal estimates $|\hat{H}^2_\varphi|_{u,T}$, with 80% confidence intervals, daytime.

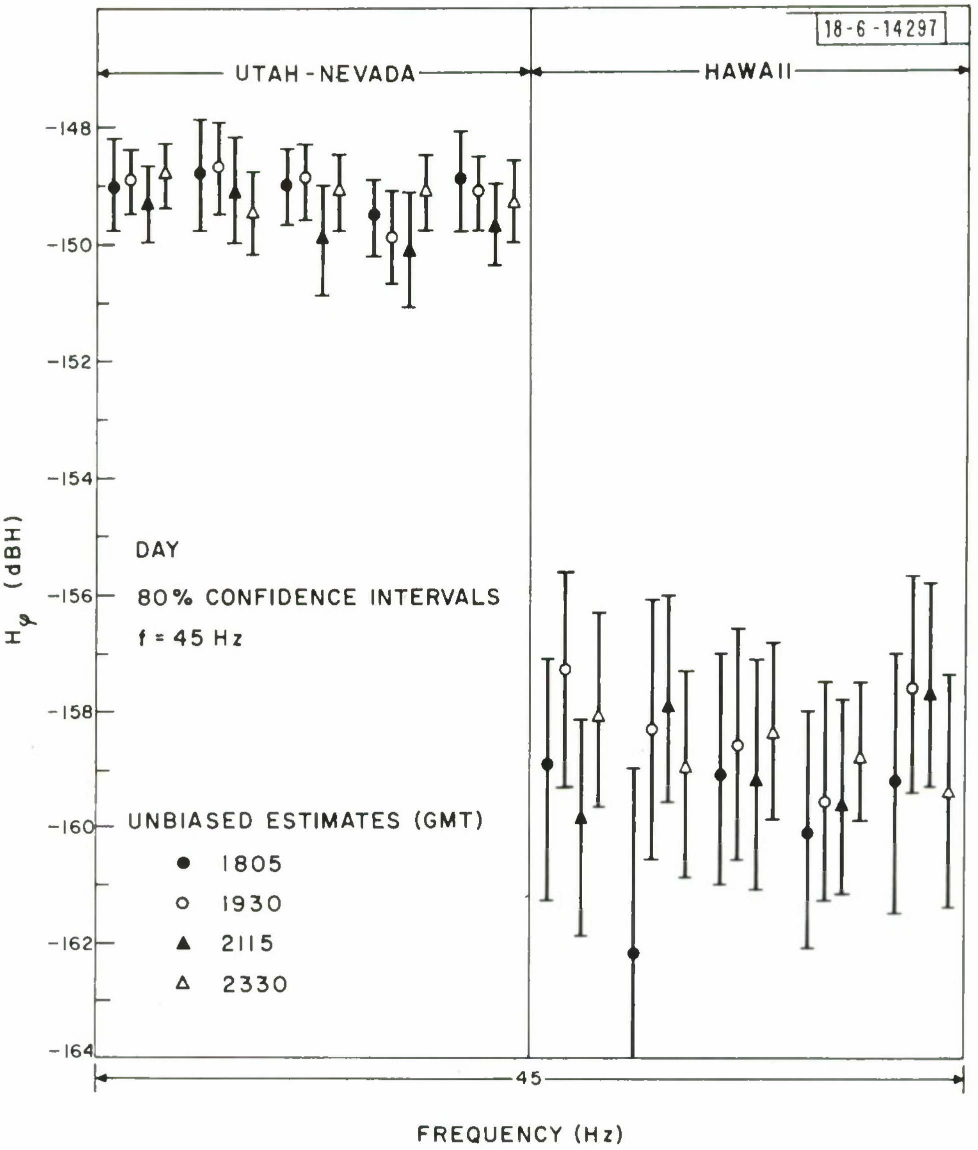

Fig. 23. Unbiased signal estimates $|\hat{H}^2_{\varphi}|_{u,\,T}$, with 80% confidence intervals, daytime.

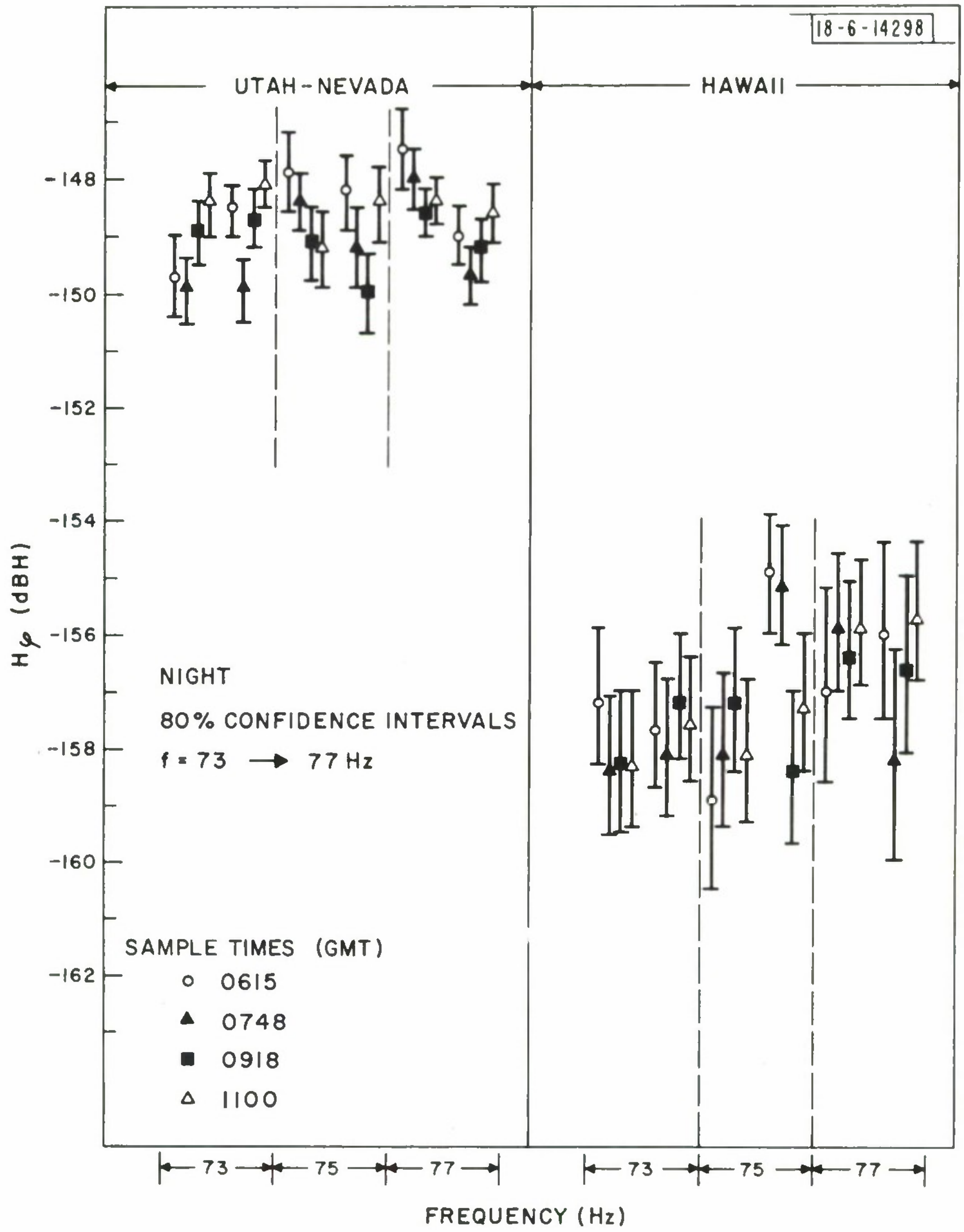

Fig. 24. Unbiased signal estimates $|\hat{H}_{\varphi}^{2}|_{u,T}$, with 80% confidence intervals, nighttime.

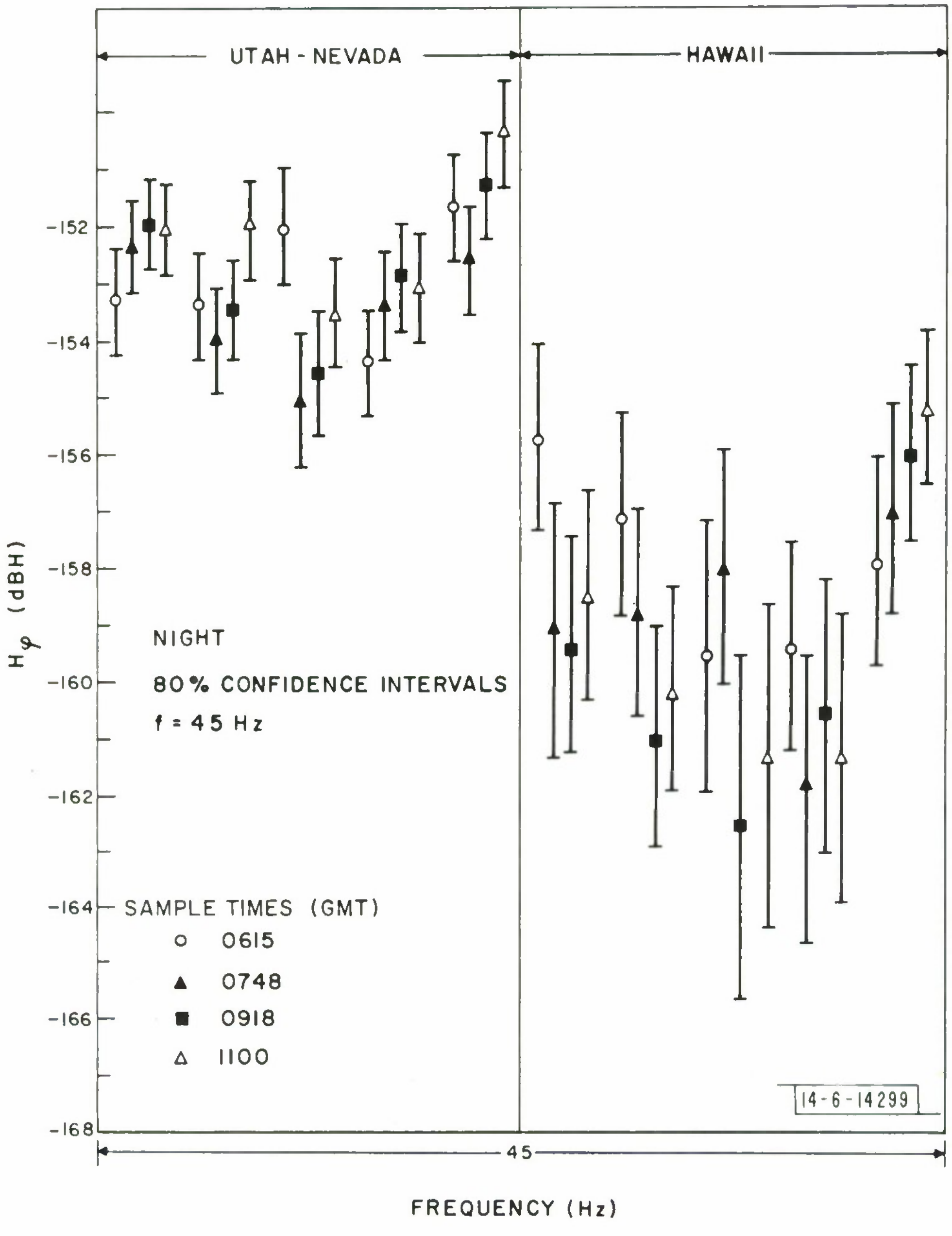

Fig. 25. Unbiased signal estimates $|\hat{H}_\varphi^2|_{u,T}$, with 80% confidence intervals, nighttime.

be drawn from these results. For the daytime data (figures 22 and 23) the confidence intervals for the Utah and Hawaii data have a significantly large common overlap interval. This fact very strongly suggests that the daytime signal strengths from sample to sample (and from day to day) are nearly constant. Implicit in this statement is that both the attenuation rate and excitation factor (in both the 40 Hz and 70 Hz ranges) are to a high degree constant quantities. It is then felt that the averaging process to be undertaken will give us average attenuation rates and excitation factors close to the true values. The nighttime data (figures 24 and 25) exhibit significantly more variability even though the integrated signal to noise ratios are not that different. It would be difficult here to argue that the signal level is in fact a constant. We maintain however that the signal level changes are due primarily to changes in the excitation factor. This is quite clearly seen in examination of figure 25. It is noted that the signal variations between Utah and Hawaii are highly correlated. This is consistent with an excitation factor change since such a change effects both sites equally and this appears to be the case. Extremely large changes in α would be required to fit the data at Utah if one attributed signal level variations as being due primarily to α changes. Moreover, this would be reflected in even larger signal variations in Hawaii. This appears not to be true. Our position then is that the signal variations at night are mostly attributable to variations in the excitation factor. Since the excitation factor cancels out when we combine the data for the two sites, the average nighttime attenuation rate computed is a reasonable approximation to the actual nighttime attenuation rates.

The size of the confidence intervals in figures 22 through 25 illustrates an extremely important point. That is, any attempt to compute an instantaneous 'real' value of α from any single pair of signal estimates is going to be totally useless because of the large uncertainty introduced by noise. Moreover, in order to measure a relatively noise free instantaneous 'real' values of α (with integration times of the order of 30 minutes or less), one would need to increase the radiated power by at least 20 db. This is clearly very expensive and hence for the foreseeable future, one is going to be forced to rely on average estimates of α as well as excitation factor.

The variation in the nighttime excitation factor also indicates the absolute necessity of making multi site measurements if one wants to deduce reasonable estimates of α. Single site measurements have their value in the estimation of signal strengths for that particular locations. One could over a long period determine the statistics of the signal variation; however, relating these statistics to the propagation parameters would be exceedingly difficult.

During October 1971, Lincoln Laboratory performed another series of ELF measurements with sites in Utah, Greenland and Norway (the results of the experiment are still undergoing processing). The preliminary conclusions are essentially identical to those discussed in this report.

Figures 26 and 27 exhibit the final signal averages (and confidence intervals) as a function of site location and frequency. The method of

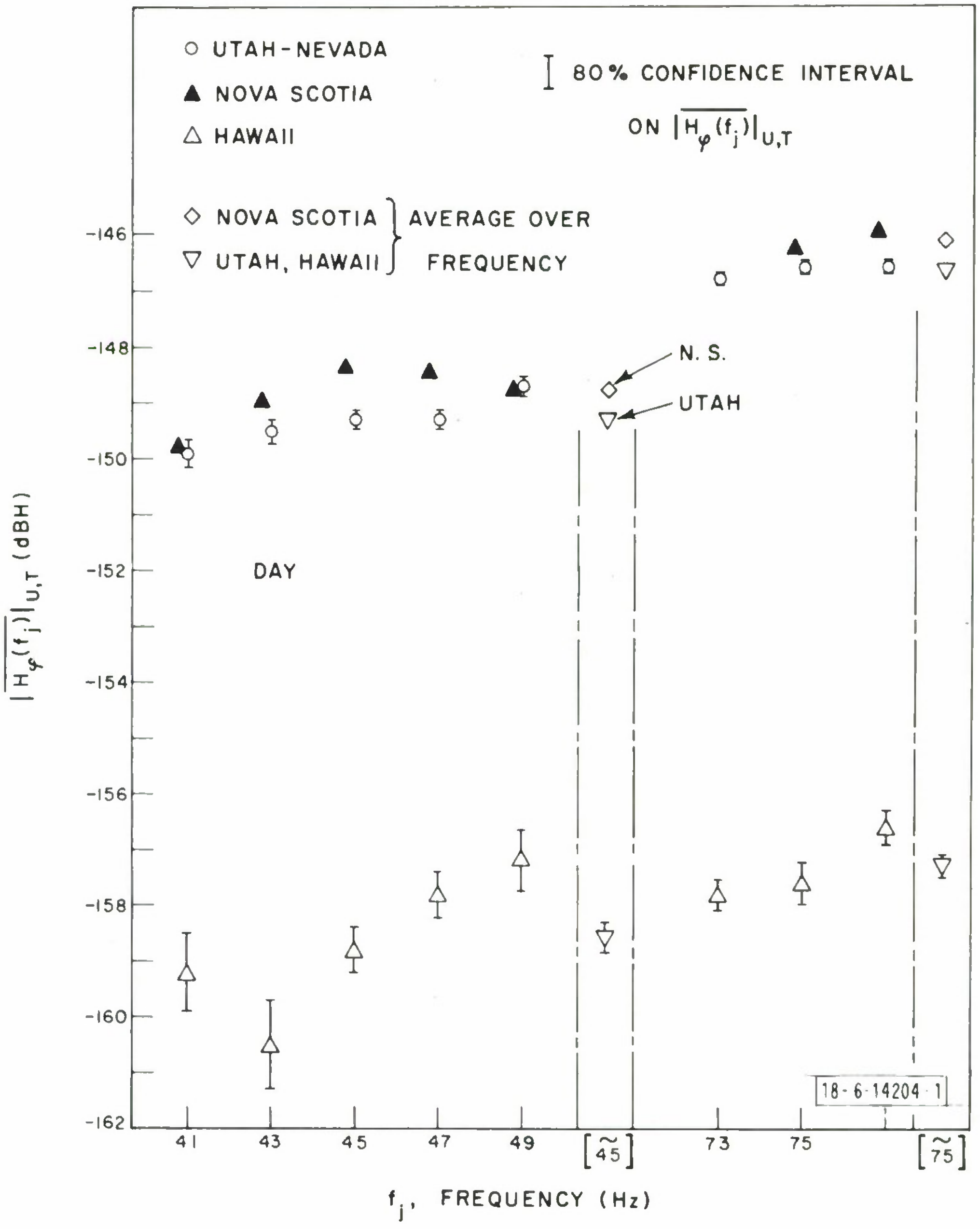

Fig. 26. Average field strengths, $\overline{|H^2_\varphi(f_j)|}$ and $\overline{\overline{|H^2_\varphi|}}$ (daytime).

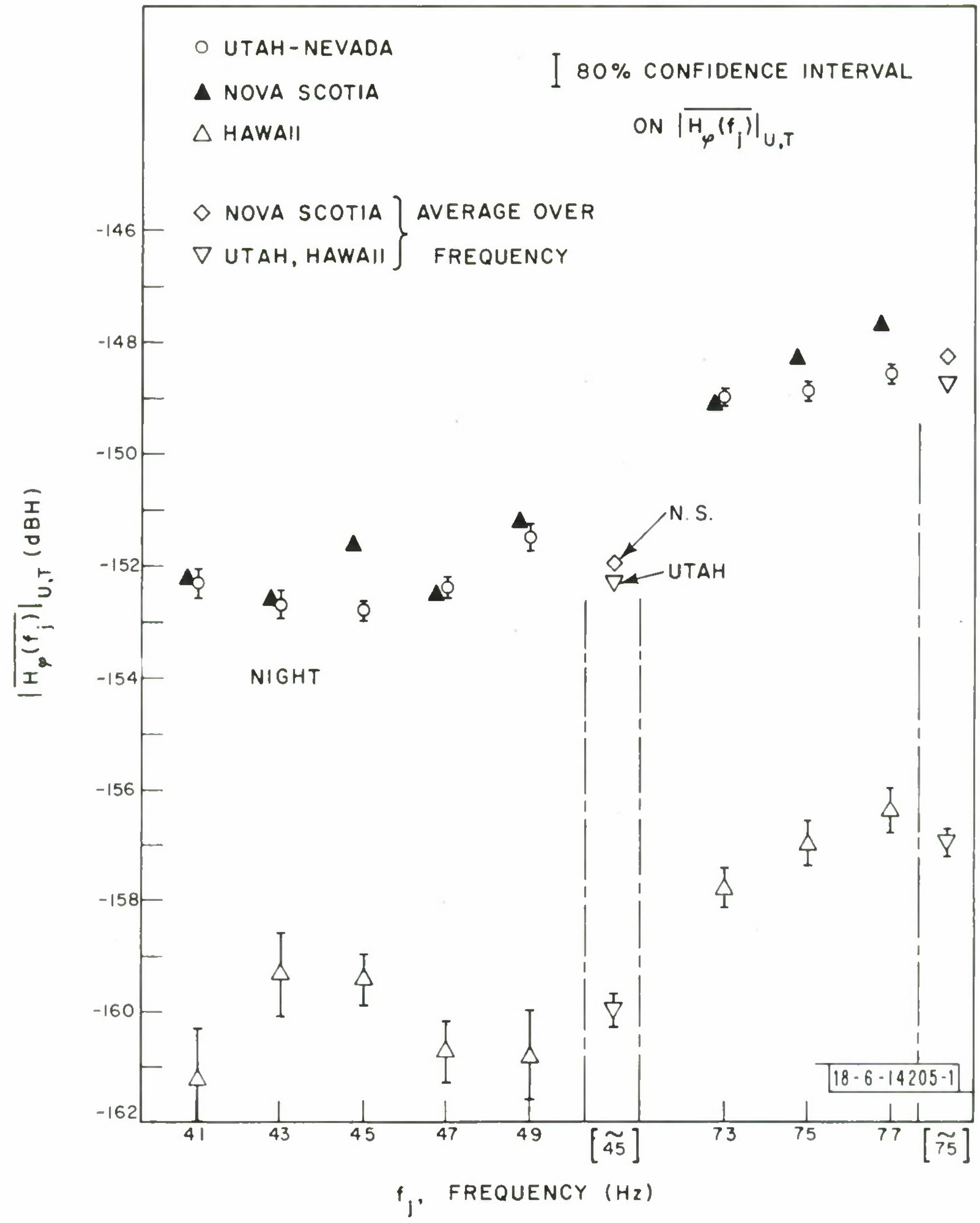

Fig. 27. Average field strengths, $\overline{|H_\varphi^2(f_j)|}$ and $\overline{\overline{|H_\varphi^2|}}$ (nighttime).

construction of confidence curves and hence the determination of confidence intervals for the averages ($\overline{|H_{\varphi}^{2}(f_j)|}_{T}$) is explained fully in appendix D. Figure D-I shows one such set of curves for the day and night averages of the Hawaii data at 45 Hz. The averages ($\overline{|H_{\varphi}^{2}(f_j)|}_{T}$) were computed from the unbiased signal estimates and noise estimates through equation 21. These averages are also tabulated in Tables II through VII.

In order to reduce the effects of the standing wave on the attenuation rate computation, it has been decided to perform a second average (over frequency) on the earlier single frequency averages $\overline{|H_{\varphi}^{2}(f_j)|}_{u,T}$. Equation 22 shows the appropriate weighting. The result $\overline{\overline{|H_{\varphi}^{2}(f_m)|}}_{u,\mathcal{B}}$ is computed for each site for both daytime and nighttime conditions.

TABLE X

$\overline{\overline{\lvert H_{\varphi}^{2}(f_m)\rvert}}_{u,\mathcal{B}}$ Estimates (dbH)				
	40 Hz Band f_m = 45 Hz		70 Hz Band f_m = 75 Hz	
	Day	Night	Day	Night
Nova Scotia	-148.8	-152.0	-146.1	-148.3
Utah	-149.3	-152.3	-146.6	-148.8
Hawaii	-158.6	-160.0	-157.3	-157.0

The 80% confidence intervals for the values of $\overline{\overline{|H_{\varphi}^{2}(f_m)|}}_{u,\mathcal{B}}$ were computed as explained in Appendix D. The confidence interval on the Utah values are less than ± 0.1 db but are not displayed since other sources of error (i.e., other than noise) would dominate. It is noteworthy that the confidence interval on the Hawaii averages is of the order of ± 0.3 db/Mm. This would imply that the values of α could be computed to less than ± 0.1 db/Mm provided the signal strengths are in fact true constant levels and provided that other sources of calibration error are not introduced.

The confidence intervals for the Nova Scotia data are approximately the same as those on Utah. However, throughout the experimental period, the tape recorder exhibited speed variations which has affected many of the signal estimates. This effect is generally small but probably of the same order as the confidence interval. We maintain that this speed control error on the Nova Scotia tape recorder accounts for some of the variation in differences in signal levels as measured in Utah and Nova Scotia. From figure 6 one observes that if α_{EW} and α_{WE} were equal, then due to the off axis correction,the Nova Scotia averages should be 0.6 db higher than those in Utah. Examination of figures 26 and 27 show that this is very likely. In any case it would be consistent with the data to state that the attenuation rate difference (i.e., $|\alpha_{WE} - \alpha_{EW}|$) is less than 0.2 db/Mm for both the 40 Hz and the 70 Hz range. (The final averages (over frequency) in figures 26 and 27 show consistent differences of about 0.5 db at both the 40 Hz and 70 Hz bands for day and night. We maintain that if differences in $|\alpha_{WE} - \alpha_{EW}|$ exist, they are so insignificant that we are unable to measure them with the transmitter power available.

Equation 1 exhibits a direct f dependence in addition to the weaker implicit dependence of f in α', c/v_{ph}, h and σ_e. Accordingly, due to the direct dependence alone, one would expect a 1.5 db ($20 \log \frac{49}{41}$) increase across the 40 Hz band and a 0.5 db increase across the 70 Hz range. Examination of figures 26 and 27 show such increases with a few exceptions. The daytime Hawaii results in the 40 Hz range would show the 1.5 db increase except for the lower than expected average at 43 Hz. Figure 18 shows the collection of unusually low values of signal strength which resulted in this average. The nighttime averaged results (Fig. 27) in the 40 Hz range are an extremely poor fit to a 1.5 dB increase over this band. Even the inclusion of the effects of round-the-world interference would not make the fit appreciably better. It can be shown using the attenuation rates listed in Table XI that the maximum variation in signal level at Hawaii would only be ± 0.3 dB. This is not enough to provide a reasonable fit to the data. It must be acknowledged simply that the nighttime signals show more variability.

VI. CONCLUSIONS

From Table X and equation 24 one can finally compute the attenuation rates. The resulting values are shown in Table XI. The significant point is that the daytime attenuation rates are higher than earlier theoretical predictions indicated. The question of error bars on the average values of α is answered in the following way. From the preceding section it was shown that the error bars (confidence intervals) on α due to the atmospheric noise alone are less than ± 0.1 dB/Mm (provided the signal level is really a constant value). The error budget due to system calibration errors (see Appendix I) shows maximum error bounds on the signal estimates of ± 0.2 dB per site. Hence the error bounds on α due to system calibration errors are again less than ± 0.1 dB/Mm. The total confidence interval for the α measurements is then about ± 0.15 dB/Mm. We maintain that the average daytime attenuation rates are in fact extremely close to the instantaneous values of α. This statement is based on the relatively constant signal levels during the day. We note that our samples come from a one month period when the solar conditions were reasonably quiet. The nighttime signal levels are noticeably more variable. A good deal of this variation is due to the changes in excitation function (that is variations in the equivalent height of the ionosphere). The variation on the instantaneous value of nighttime α is at the present not measurable. Our current speculation is that the variation is perhaps of the order of ± 0.2 dB/Mm.

The ratio of the daytime to nighttime excitation factors is computed from equation 29. The results are tabulated in Table XI. If one uses the

Table XI. Attenuation Rates, Excitation Factors, Ionospheric Heights

		α (db/Mm) (1)	$\frac{H_D}{H_N}$ (2)	(c/v_{ph}) (3)	h (km) (4)	$E = \frac{1}{h\sqrt{\sigma_e}(c/v_{ph})}$ (5)
45 Hz	Day	1.16	1.53 (3.68 db)	1.26	69.2	−58.60 db
	Night	0.81		1.07	113.0	−62.28
75 Hz	Day	1.47	1.52 (3.64 db)	1.28	65.7	−59.72
	Night	0.92		1.20	103.	−63.36

(1) From equation 24 where $\alpha_D = -.99 + \dfrac{20 \log \dfrac{|H_\phi|_U}{|H_\phi|_H} + 0.5}{4.56}$,

.5 is the off axis correction

(2) From equation 29

(3) From USC/NLL

(4) Depends on validity of σ_e and c/v_{ph} estimates

(5) From equation 23 after α determined

measured values of σ_e and some postulated values of c/v_{ph}, the values of the equivalent ionospheric heights can be determined. For the daytime in the 40 Hz band, the equivalent ionosphere is 69 km. This is consistent with the range of previous theoretical estimates for h. The slightly lower value of 65.7 km for the 70 Hz band is also reasonable (the lower value probably being due to a poor choice in c/v_{ph}). The nighttime ionospheric heights are 113 and 103 km for the 40 and 70 Hz bands respectively. A priori, one would have expected values closer to 90 km. The nighttime excitation factor is then seen to be respectively 2.0 and 1.2 dB worse than expected.

Finally, with the most accurate measurements that we are at present capable of performing, no apparent difference in $|\alpha_{EW} - \alpha_{WE}|$ is seen. Certainly this difference is less than ± .2 dB/Mm.

Table XII is constructed with the aid of the measured values of α and $\aleph_D/\aleph_N$. The totals agree well with the measured averages in Table X (there is, of course, some commonality in that Table X is used to determine α and ρ and then these are used in Table XII). However, the consistency of both tables leads one to believe that equation 1 is in fact a good formula to describe the propagation at these frequencies and distances.

Table XII. Signal Estimates

	Nava Scatia				Utah-Nev.				Hawaii			
	Day		Night		Day		Night		Day		Night	
	45 Hz	75 Hz	45	75	45	75	45	75	45	75	45	75
$[10 \log \frac{\pi\mu_o}{2c} - 20 \log \eta]$	−193.34	→										→
20 log IL $I = 300A$ (rms) $L = 22.5$ km	+136.58	→										→
20 log f	33.06	37.50	33.06	37.50	33.06	37.50	33.06	37.50	33.06	37.50	33.06	37.50
$-10 \log \sigma_e$ (1)	39.21	37.70	39.21	37.70	39.21	37.70	39.21	37.70	39.21	37.70	39.21	37.70
$20 \log (\cos \phi)$	−1.20	−1.20	−1.20	−1.20	−1.80	−1.80	−1.80	−1.80	−1.30	−1.30	−1.30	−1.30
−10 log d	−63.04	−63.04	−63.04	−63.04	−62.93	−62.93	−62.93	−62.93	−68.14	−68.14	−68.14	−68.14
$10 \log \left(\frac{d/r_e}{\sin d/r_e}\right)$	.07	.07	.07	.07	.07	.07	.07	.07	.78	.78	.78	.78
SUBTOTAL	−48.66	−45.73	−48.66	−45.73	−49.15	−46.22	−49.15	−46.22	−53.15	−50.22	−53.15	−50.22
−ad (2)	−2.34	−2.96	−1.63	−1.85	−2.28	−2.89	−1.59	−1.81	−7.57	−9.59	−5.28	−6.00
$-20 \log h \sqrt{c/v_{ph}}$ (3)	−97.81	−97.42	−101.35	−101.05	−97.81	−97.42	−101.35	−101.05	−97.81	−97.42	−101.35	−101.05
TOTAL $\lvert H_\phi \rvert_D$ (db H)	−148.8	−146.1	−151.6	−148.6	−149.3	−146.6	−152.1	−149.1	−158.5	−157.2	−159.8	−157.3

(1) $\sigma_e = 1.2 \times 10^{-4}$ (45 Hz) & 1.7×10^{-4} (75 Hz)

(2) a values from the report

(3) fram $h \sqrt{c/v_{ph}}) \sigma_e$ measurements and (1)

APPENDIX A

Equipment Design Considerations

The equipment used in the propagation experiments can logically be separated into the field recording equipment and the laboratory playback facility. What follows is a description of the field recording equipment and a discussion of the motivation behind the design.

The field equipment consists of three units: the antenna, two racks of electronic equipment, and a D. C. motor generator for prime power generation. The antenna, a 5 foot loop, is either supported vertically in a hut or buried in the ground and is separated approximately 200 feet from the electronics racks. Approximately 250 feet separate the motor generator set and the antenna. All site locations have been selected to be as far as possible from power lines, typically this distance is in the order of 3 - 5 miles. Whenever possible, the site is selected only after preliminary exploration with a "sniffer" loop to determine the extent of power line contamination. Interference at a site is influenced by the geometry of the power lines and pointing angle of the antenna as well as separation.

The pre-amplifier, filters, tape recorder and other items are mounted in two 19" racks 26 inches high. On site these racks are mounted in a panel type van. Under cold weather conditions the equipment is placed in an environmental chamber equipped with thermostatic control to maintain the temperature in the 60 - 70°F range. A 26 inch rack height limitation was selected for two reasons: (1) these racks will fit into the rear of a station wagon, if necessary, and (2) they are easily air transportable.

The D. C. motor generator is a commercially available combination which has been integrated with a larger gas tank into an environmentally protected stand alone unit.

A discussion of the field recording equipment follows.

Antenna Design

The choice of a particular antenna configuration was influenced by several considerations. Perhaps the earliest choice that had to be made was that between a "cored" antenna or an air core. It is obvious that a loop with a magnetic core can be made smaller for a given turns area product. It has been our experience, however, that the permeability of a magnetic core loop is subject to change due to various effects. Depending on the type of core material and the physical configuration sensitive antennas such as these may have their permeability altered by the earth's magnetic field. This effect can be compensated for; however, it would introduce another possible source of error. Additionally, we have observed at least one core type antenna whose NA product has changed by a factor of two over a period of two years. Whether this was due to shock while being shipped, abnormal current surges, or mechanical failure is not known, but it does re-inforce the conviction that a stable air-core loop is best suited for precision measurements.

The open circuit voltage generated in an air core loop antenna due to a magnetic field is given by:

$$v_{oc} = |H_{\varphi}| \mu_o 2\pi f N A \qquad \text{a-1}$$

H_φ - magnetic field, amp/meter

μ_o - permeability of free space, $4\pi \times 10^{-7}$ henry/meter

f - frequency of applied field assumed sinusoidal (hertz)

N - number of turns on antenna

A - area of loop $(\text{meters})^2$

From a measurement point of view the two antenna parameters which are critical to accurate field estimates are the number of turns and the area of the loop. These two parameters are often lumped together and referred to as the turns-area product (NA). The choice of a large diameter loop with fewer turns over a smaller diameter with many turns was made on the basis that the larger diameter would allow a more precise estimate of the turns-area product thus introducing less error into the measurements.

The antenna is constructed with 471 turns of no. 14 double formvar insulated copper wire wound within a loop of 5.862 cm. OD Poly Vinyl Chloride (PVC) tubing formed into a torus with inside diameter of 1.510m. The tubing is opened by cutting a section out and then winding the 471 turns of wire in the interior. After winding, the access section is replaced and the antenna sealed. A layer of 7.62 cm. wide, .013 cm. thick copper tape is wound and soldered around the antenna leaving a 1/4" air gap at one point. This copper tape provides electrostatic shielding for some of the undesirable interference. However, it is not effective at the lower ELF frequencies since a skin depth in copper is greater than the shield thickness. The shielding is effective at higher frequencies and is intended to reduce strong E field components from transmitters at VLF and above should it be necessary to locate a measurement site near transmitters. Such interference can reduce the dynamic range of the equipment by overloading the pre-amplifier.

Since the number of turns are known exactly it remains to establish the loop area, from a measurement of the mean loop diameter. For these antennas the measured mean diameter is 1.568m resulting in a turns-area-product of $909.2 m^2$. Using the parameters developed here the relationship between antenna voltage and field strength can be rewritten:

$$v_{oc} = 7.178 \times 10^{-3} \, |H_{\varphi}| f \qquad \text{a-2}$$

The measured equivalent circuit of the loop antenna is a resistor of 19.5Ω in series with an inductor of 0.8 henries. The resistance is almost entirely due to the copper loss within the antenna since radiation resistance is very small and can be neglected.

As a check on the performance of the antenna its performance was evaluated using methods described by NBS[12]. Another loop antenna consisting of one turn and a diameter of 1.000 meters was constructed and used in the calibration procedure. Agreement between the calculated and measured performance was within the experimental accuracy of the measurement apparatus.

The choice of a particular antenna configuration also involves a design decision which takes into account the desired measurements, ability to match the antenna to the pre-amplifier front end, and the noise characteristics of the pre-amplifier. Originally the selection of the 1.568 meter diameter air core antenna was based on a need to make atmospheric noise measurements. In order to maintain a 20 dB atmospheric noise to system noise ratio (1 Hz BW) at 20 Hz the present antenna was specified to realize this ratio at that frequency. Pre-amplifier noise at these frequencies is predominantly 1/f type and improved performance will therefore be certain at the higher frequencies used in the propagation tests. The point to be made here is that the present antenna is over specified for propagation measurements.

A source of noise is loop motion in the earth's magnetic field. This low frequency component associated with mechanical resonances in the loop and mount can cause severe amplifier overloading problems if left unchecked. In most cases, the antenna has been mounted in a hut to isolate it from wind motion, and on isolation pads to decouple it from earth motion due to nearby vehicular traffic. On some occasions the loops have been buried or partially buried in the ground to avoid wind motion.

A discussion of antennas is not complete without mentioning E field measurements which could be made with a whip or other type antenna. During earlier measurements of atmospheric noise whip antennas were employed. A great deal of difficulty was experienced in calibration of these antennas. Basically the problem can be traced to the high impedance levels, which are present when employing practical antenna lengths. A source impedance of 10^7 - 10^8 ohms is possible. At these high impedance levels an accumulation of moisture from antenna to ground through guy cables, base insulators, or the amplifier input terminals can seriously alter the system calibration. It was found, for example, that afternoon rain in

Florida and salt spray in Malta rendered the whip antenna virtually useless for dependable day in and day out operation in these areas. Clouds at high site elevations were also a source of error. Good results have been reported with electric field sensors from desert areas. In view of the fact that propagation measurements were planned world wide at site locations other than those dictated by weather it was felt that the whip antenna would not produce the required reliability.

Calibration Signal Injection Methods

As shown in Fig. 4 the loop antenna output is applied to a step-up transformer, pre-amplifier and other filters and amplifiers in the recording system. The following is a description of means by which the overall system gain is calibrated and monitored.

A calibration signal is continuously injected in series with the antenna at a known level and frequency. The frequency is displaced 1 Hz from the received signal frequency. In view of the long recording periods (12 hrs.) which were planned it was necessary to have available a continuous record of the system performance. A frequency separation of 1 Hz was chosen as a reasonable separation which would not interfere with the received signal analysis and yet would reveal possible changes in system gain near the frequency of interest.

Referring again to Fig. 4 a calibration signal 1 Hz removed from the received signal is generated in the synthesizer and applied through a precision pad terminated in a 0.500Ω resistor in series with the antenna. A more detailed schematic of the attenuator is shown in (Fig. A-1). A measurement

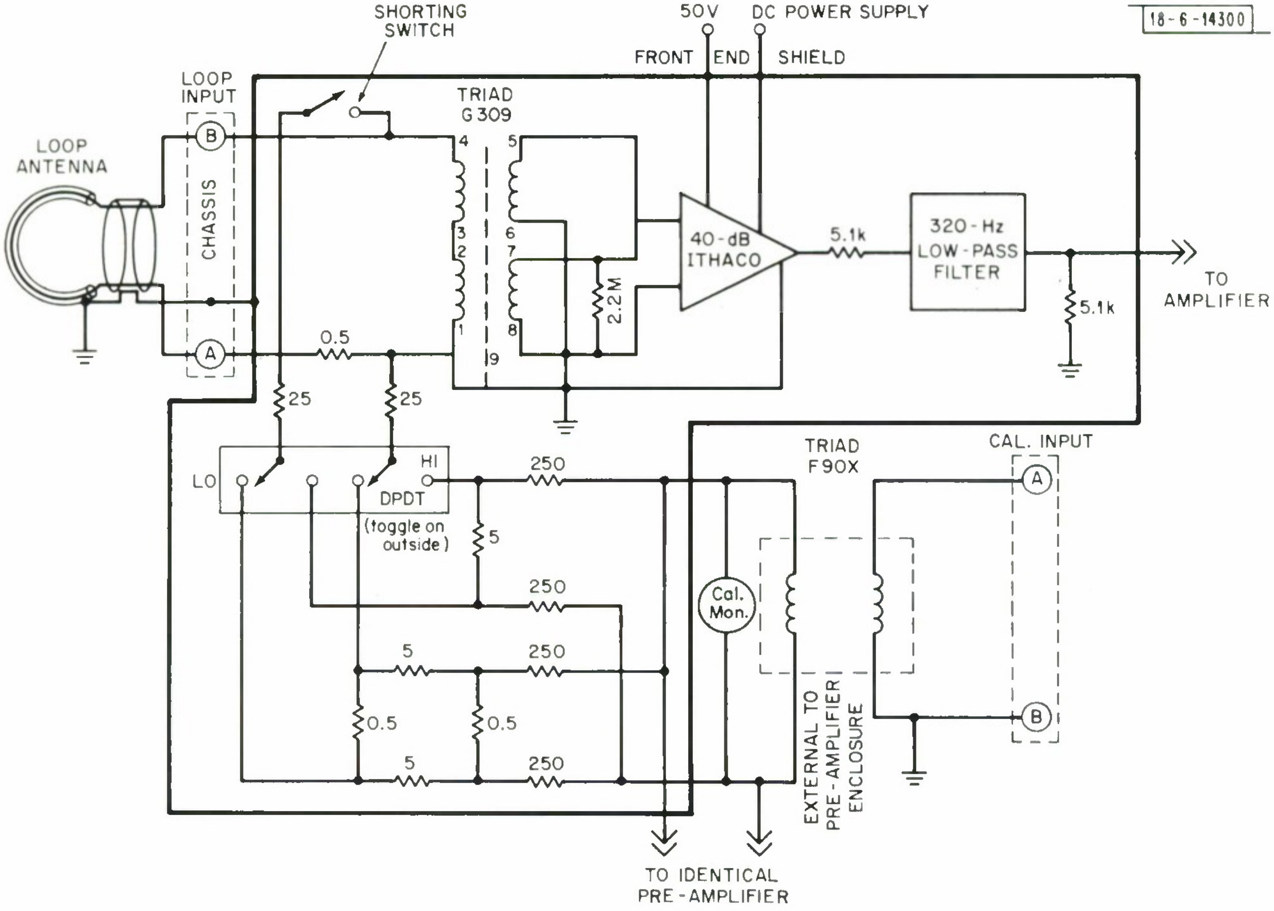

Fig. A-1. Receiver front end schematic.

of the calibration voltage at the input of the attenuator pad is made at "Cal. Mon." and knowing the attenuation ratio the voltage in series with the antenna may be calculated. The injected calibration signal amplitude is chosen to be sufficiently large so that it can be accurately measured at the output of the receiver. A ratio of the detected calibration signal on playback to injected signal at the antenna gives the gain of the system at the calibration frequency.

It will be noticed that the attenuator pad is of the "balanced H" type. It is made up of .05% and .01% resistors and has a calculated attenuation of 4.4959×10^{-7}. The attenuation of this pad has been measured in the laboratory and agrees within experimental error with the calculated value. Since the accuracy of the test equipment used in this measurement is less than the combined accuracy of the resistors the calculated value of attenuation has been utilized throughout. Although the attenuator pad itself is balanced it is employed in an unbalanced circuit since one side of the pad is grounded along with pins 1, 8 and 9 of the input transformer. A short discussion of the reasons behind this arrangement follows.

Initial attempts to employ a balanced input revealed a common mode voltage (with respect to ground) on the balanced pad. This signal was introduced by the capacitive coupling between windings on the calibration input transformers. This unwanted signal was capacitively coupled across the input transformer windings to the unbalanced input of the 40 dB Ithaco preamplifier. As such, it added vectorially with the desired injected signal which was coupled through the transformer, and gave an erroneous measure of the system gain. (Note that the relatively high impedance levels in the circuits make it relatively easy for "stray" capacitances to inject unwanted signals.) Various configurations of balanced and unbalanced inputs were tried with the method shown giving the best results. Measurements show that the common-mode signal is 30 - 40 dB below the desired signal with this arrangement.

A calibration correction factor is computed which compensated for differential system gain at the calibration and signal frequencies. Differences do exist due to ripple in band pass filters, mis-tuning of filters, and drift of component values with time and temperature. In order to mitigate this problem the system gain is measured with a shorted antenna at the two frequencies of interest before and after a recording session. This information is entered into the log and later used as a correction factor in the signal estimate. It has been found from experience that the gain at the two frequencies is nearly the same and does not change materially over a measurement session (3 - 4 weeks). Of course, it is possible to experience a system gain change over several hours but this will be noticeable in the calibration level on playback and is correctable.

The input to the attenuator pad is measured with a Ballantine model 323 True RMS Voltmeter. It has a rated accuracy of 2% at all points on scale. Before each measurement period all meters used in the experiment are compared with a laboratory secondary standard at the level where they will be used (110 - 125 mv). From this it is felt that the meters are accurate to within 0.1% absolutely and have negligible error differentially. The largest source of error in the field is probably due to meter reading.

Front End Considerations

Perhaps the most important design problems are encountered in the front end. A good design will integrate antenna characteristics with the pre-amplifier to realize a low noise front end. Originally the front end design was based on a need to measure wide-band atmospheric noise with high fidelity. As an interest in both propagation and atmospheric measurements developed the front end design was reevaluated and found to satisfy both requirements.

A great deal of early effort was expended in identifying a low-noise amplifier suitable for use at the frequencies and impedance levels which were present. Source impedances would be of the order of 1 megohm or greater and the range of frequencies extended from 20 - 300 Hz. Under these conditions the Field Effect Transistor (FET) is well suited for amplifier use. Figure A-2 shows the equivalent noise sources, both voltage and current generators, which are useful in characterizing the noise performance of the amplifier. A recent tutorial article [13] describes the uses of this equivalent circuit, and follows the design procedure employed. A major result of this analysis is the relationship for the optimum source impedance for low noise operation. Optimum source impedance is given by:

$$Z_{opt} = \frac{e_n}{i_n} \quad .$$

Since e_n and i_n are both functions of frequency the optimum source impedance varies across the band of interest and is difficult to match over a wide band.

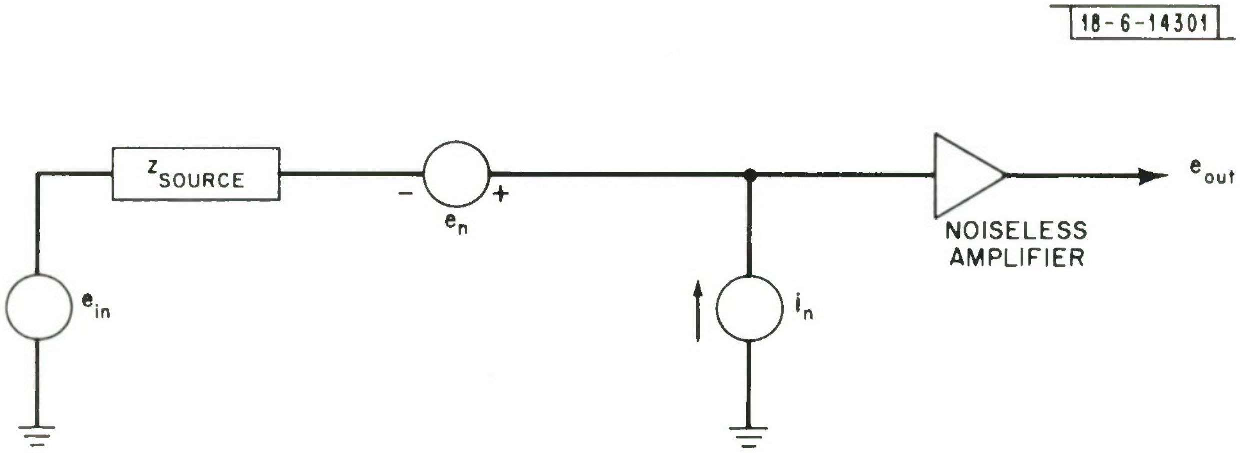

Fig. A-2. Equivalent circuit.

Several commercial FET amplifiers were investigated in the preliminary design. In addition a laboratory designed amplifier was evaluated. As a result of these investigations it was concluded that all reasonably competent amplifier designs resulted in performance characteristics which were very similar. It was also concluded that single-ended input amplifiers resulted in lowest noise operation. Parenthetically it might be noted that a selection process is employed for the crucial input transistor and each supplier had his own proprietary circuit and method. The amplifier that was selected as a result of this investigation was the Ithaco Model 144. This amplifier meets all of the requirements for the system and has the most detailed specifications of all of the units examined.

Referring to the Ithaco specification sheet the equivalent noise current in a 1 Hz bandwidth is typically .01 picoampere in the 10 to 100 Hz range. Shorted source equivalent noise voltage in the same bandwidth is 2.5×10^{-8} volts at 50 Hz. Utilizing these two pieces of information the optimum source resistance at 50 Hz is calculated as:

$$Z_{opt} = \frac{e_n}{i_n} = \frac{2.5 \times 10^{-8}}{10^{-4}} = 2.5 \times 10^{6}\Omega.$$

Note that due to the 1/f behavior of the equivalent voltage noise source, the optimum source impedance will decrease with frequency.

In order to obtain a match between the antenna and the amplifier to effect low noise performance a 50:1 step-up transformer is employed between the antenna and the pre-amplifier. At 100 Hz the antenna impedance is given by:

$$Z_{ant} = 19.5 + j502\Omega \; \underline{N} \; j502\Omega$$

Neglecting transformer primary winding resistance and secondary winding capacitance the antenna equivalent impedance reflected to the secondary is:

$$Z_{source} \approx (50)^2 \, (j502) = j1.25 \times 10^6 \Omega .$$

A $2.2 \times 10^6 \Omega$ resistor is placed across the transformer winding to flatten the frequency response of the front end. Including this resistance the magnitude of source impedance is

$$|Z_{source}| = 1.1 \times 10^6 \Omega .$$

It is observed that the optimum source impedance is not achieved at this frequency; however, the degradation due to this will be small. Due to the inductive nature of the antenna its contribution to the source impedance will increase with frequency whereas the optimum impedance should fall off. In the frequency band 40 - 300 Hz front end noise is at least 30 dB below median atmospheric noise with this arrangement.

In the equipments employed for atmospheric noise measurements the front end was located adjacent to the antenna and power was supplied from a separate battery supply. After some amplification the received signal was transferred via a balanced output line driver over a twisted pair to the rest of the recording equipment. This arrangement meant that the front end would be exposed to the extremes of temperatures and humidity. In fact, oscillations did develop with some equipments in the presence of high humidity. Excessive moisture formed feedback paths to the pre-amplifier input via the printed circuit boards that were employed. The present equipments utilize a front end located in a rack with the remainder of the equipments. Coupling to the antenna is accomplished via No. 22 shielded twisted pair. Twisting avoids incidental magnetic pick-up and the shielding reduces the effects of electric fields. The antenna is located approximately 200' from the recording equipment and 300' from the DC motor generator to avoid magnetically generated interference.

Several other precautions have been taken to avoid interference from other parts of the system and these will be described briefly here. The front end including transformer, amplifier and low-pass filter are enclosed in a 50 mil high nickel steel alloy box to avoid magnetic coupling from other components. Such shielding is effective against local power line interference and possible coupling with the locally generated reference. This shielding is in addition to that supplied by the transformer. Another important consideration is the ground system. All grounds are made with heavy copper braid and are common at one point. Ground return currents which might induce unwanted voltages at the amplifier input are avoided. Although the Ithaco amplifier exhibits 55 dB of power supply isolation great care is taken to de-couple the power supply voltage which feeds the amplifier. If suitable de-coupling is not employed, the amplifier noise performance may be degraded, or more seriously, components of the locally generated reference may be coupled into the front end. Finally, the front end and all other components of the recording system are subject to environmental control.

Notch Filters

Notch or band reject filters are included in the signal path to reduce unwanted pick-up from power lines. Several card slot positions are allocated for this purpose in order that the most effective combination of filters may be synthesized to combat the problems at the particular site. A normal complement of filters in CONUS would include on each of 60, 180 and 300 Hz rejects. Overseas operation at sites like Norway or Malta would utilize 50 Hz and higher order harmonic rejection. Experience has shown that the fundamental and odd order harmonics cause the severest problem. In fact, the Malta site has had the dubious distinction of having a larger component at 150 Hz than 50 Hz.

Another problem that is sometimes encountered is that of frequency wander in the local power system. Frequency variations of ± 0.5 Hz have been observed in Malta. It has been profitable in this situation to stagger tune three notch filters to 49.5, 50 and 50.5 Hz to establish band rejection from 49.5 to 50.5 Hz.

Individual notch filters have been designed using methods described in a Lincoln Laboratory Technical Note [14]. Typically the notch filters exhibit 40 dB of rejection at their center frequency. Quality factor ("Q") is adjusted to be in the range from 8 to 10. All components are measured within 0.1% before assembly, and final adjustments are made on each filter using a precise frequency source. Where several filters are cascaded to obtain a wider rejection range, the individual filters are adjusted in frequency and "Q" to obtain the desired response. Insertion loss, out of band, is typically 6 dB.

Band Pass Filters

Band pass filters, sometimes referred to as narrow band filters, are employed in the signal channel to establish a narrow band channel centered on the receiver frequency. Narrowing the bandwidth prior to recording eliminates problems associated with the large dynamic range of wide band atmospheric noise as opposed to the limited dynamic range of the tape recorder (40 dB). All signal estimates are made from the narrow-band channel using linear processing. Individual filters are plugged in as operations demand, each filter covers three or more possible transmitter frequencies.

The narrow band filters consist of two single pole stagger tuned band pass filters mounted on a single card. Typical bandwidths in the 40 - 50 Hz range are 3 Hz, (and 4 Hz in the 70 - 80 Hz range). Both "Q" and center frequency of the individual filters are adjusted to obtain desired response. Insertion gain varies from 24 - 28 dB depending on center frequency. Design procedures are the same as those employed for the notch filters [14].

Required Frequency Stability

In view of the long integration periods (1 - 2 hours) used to estimate the received signal it is necessary to examine the required frequency accuracy to avoid degradation of the estimate. The model shown in Fig. A-3 is representative of the measurement process and will be used to derive the required frequency stability.

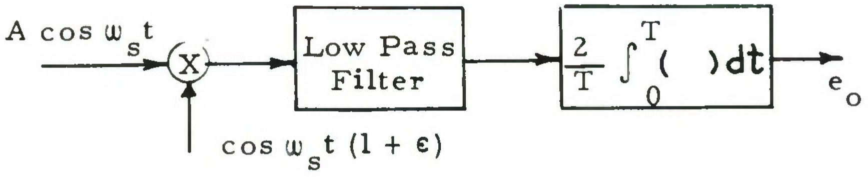

Figure A-3

The imperfect local reference can be written as:

$$\cos\omega_s t\cos\omega_s \epsilon t - \sin\omega_s t\ \ \sin\omega_s \epsilon t$$

The output of the multiplier is given by:

$$A\ (\cos^2\omega_s t\cos\omega_s\epsilon t\ -\ \sin\omega_s t\ \ \cos\omega_s t\ \ \sin\omega_s\epsilon t)$$

$$= \frac{A}{2}\ \{[\cos 2\omega_s t + 1]\ \cos\omega_s\epsilon t\ -\ [\sin 2\omega_s t]\ \sin\omega_s\epsilon t\}.$$

After removal of double frequency terms with the low pass filter the integrator output is:

$$e_o = \frac{A}{T}\int_0^T \cos\omega_s\epsilon t\ dt = \frac{A}{T}\ \frac{\sin\omega_s\epsilon T}{\omega_s\epsilon}$$

where T is the integration period.

Now expanding sin $\omega_s\epsilon T$ into a series and keeping the first two terms yields,

$$e_o = \frac{A}{\omega_s\epsilon T}\ \left[\omega_s\epsilon T - \frac{(\omega_s\epsilon T)^3}{3!}\right].$$

when the second term is much smaller than the first then $e_o = A$ as desired. The frequency stability for a 1% error (.1 dB) is then computed from

$$\frac{(\omega_s\epsilon T)^2}{3!} = .01$$

solving for ϵ

$$\epsilon = \frac{.245}{(\omega_s T)} .$$

Using worst case parameters,

$$T = 2 \text{ hrs} = 7.2 \times 10^{-3} \text{ seconds}$$

$$f_S = 80 \text{ Hz}$$

$$\epsilon = \frac{.245}{(2\Pi \times 80 \times 7.2 \times 10^3)} = 6.75 \times 10^{-8} .$$

That is, a frequency difference between transmitter and receiver of 6.75 parts in 10^8 will cause a 0.1 dB degradation in signal estimation over a 2 hour integration period.

A short discussion of possible frequency errors is now in order. Prior to deployment in the field the receiver frequency standards are compared to a Lincoln Laboratory Cesium Beam Standard which is itself tied to NBS. The transmitter's frequency standard is also continuously compared to NBS (WWVL) and maintained to within 1 part in 10^{10}. Initially, the receiver frequency standards are set to within 2 parts in 10^{10} initially, and typically exhibit a worst case monotonical change in frequency of 2 parts in 10^{10} per day. Approximately 320 days would have to elapse before a discrepancy of 6.75 parts in 10^8 was reached. From this it can be seen that errors due to frequency drift have been negligible.

Frequency Generation

Two precise frequencies are generated and recorded at each site. These two frequencies have been entitled the "Calibration" and "Signal" reference frequencies. The calibration signal is 1 Hz removed from the received signal and is recorded as a sine wave at high level on channel 7. An attenuated version of this signal is inserted in series with the antenna and is employed on playback to ascertain system gain. The Signal reference is a square wave at the received signal frequency, and is recorded at a low to intermediate level on channel 6. Both a frequency standard and a synthesizer are required to generate the required frequencies.

The frequency standard is a Frequency Electronics Model 1000-A with a frequency stability of 1 - 2 parts in 10^{10} per day. A battery pack is provided to allow 8 - 24 hours operation in the event of primary power loss. Power for the frequency standard when operating in the system is supplied at +30 VDC.

Prior to conducting measurements at field sites all frequency standards are compared with a Cesium Beam Standard located at the laboratory. Over a several day period all standards are brought into agreement ($\approx$ 2 parts in 10^{11}) with the Cesium Beam Standard and their behavior monitored. All standards are under power continuously and travel with site personnel to and from the sites. If a transit time of more than 8 hours is required an additional battery pack is "floated" across the internal supply to assure continuous operation. Whenever possible the frequency accuracy of the standards is compared against other systems in the field. For this purpose comparisons with WWVL (60 kHz) using the HP model 117A VLF Comparator and comparisons with LORAN (100 kHz) using the Beukers Model 112 Frequency Reference have been used. Upon completion of the experiment the standards are returned under power to the laboratory and their frequency again compared to the Cesium Standard. A back-up standard is available at each site in the form of the 1 mHz crystal oscillator in the Time Code Generator (TCG). Standard operating procedure is to compare the FEL standard with the TCG on site and adjust as closely as possible the TCG oscillator so that it agrees with the standard. If the standard should fail it is then possible to continue with the back-up oscillator for a limited time.

The synthesizer accepts the 1.0 mHz output from the Frequency Standard and generates the two required frequencies using two independently controlled sub-synthesizers with identical logic. Output of the synthesizer consists of two independent frequencies selectable in 1.0 Hz steps from 1 to 127 Hz. Ordinarily frequencies between 40 to 50 Hz and 70 to 80 Hz are employed since this corresponds to the present transmitter capability. The philosophy behind the synthesizer's operation can be explained briefly as:

1. A high repetition rate pulse train (average frequency 960 kHz) is fed into a six stage counter. A non-overlapping transition from each stage plus the input is used to generate a narrow pulse thus establishing seven pulse trains related in frequency by powers of 2.

2. Combinations of these pulse trains are selected by front panel switches and combined in an "OR" gate.

3. Additional countdown circuits cause the output to appear in the frequency range of interest.

4. The calibration frequency reference is applied to a low pass filter and appears as a sine wave. The signal frequency reference is

employed as a square wave.

Notice that this method makes use of the average repetition rate of the higher frequency pulse train, the consequence of which is a waveform with jitter. After further division by a large number this jitter is reduced proportionally and is typically 10 μsec at the output.

Circuitry to detect phase jumps in the signal reference frequency has been incorporated in the synthesizer. The purpose of this circuitry is to detect possible phase jumps due to faulty operation either of the logic or external causes. If such a jump is detected a light is activated which may only be extinguished manually. Since the equipment is required to operate for 12 hour intervals in an unattended condition it was felt that brief interruptions of the reference could occur and go unnoticed unless some precaution was taken. External influences such as nearly mobile radios, and starting of vehicles has caused phase jumps in the past. Nearby thunderstorms such as those experienced in Florida could also be expected to trigger the logic occasionally.

Tape Recorder

Recording at the field sites is accomplished with a Precision Instrument Model P15100 1/2" tape recorder. Tape speed is 15/16 IPS and 10 - 1/2" reels with 1. 0 mil mylar tape is utilized. This combination supplies a 12 hour record time. Seven high quality FM data channels with approximately 312 Hz bandwidth are used as the primary data channels. Two back-up lower quality edge track channels are also available, but were not employed. Power consumption is approximately 18 watts including playback monitor. Tape speed, wow and flutter are specified as ± 1% or less.

Since any analog recording system exhibits a tape speed variation with time it is necessary to record reference signals at the time of recording if long term integration is required on playback. In order to support the measurement requirements of the system, a square wave at the same frequency as the received signal is recorded on channel 6, and a high level calibration signal is recorded on channel 7. These signals are used as references on playback and serve to eliminate tape speed variations which occur on record or playback.

The tape recorders have demonstrated a degradation in performance over a three week measurement period. This degradation is evidenced by variations in tape speed of ± 5% over a 12 hour interval and increased flutter particularly towards the end of a 12 hour tape. A large portion of these troubles has been traced to a carbon disc slip clutch in the feed reel as well as improper adjustment of pinch rollers. Since the original set of measurements the tape recorders have been returned to the factory, modifications made, and improved line-up procedures developed. It is extremely important that the manual accompanying the tape recorder be used as a reference for all adjustments and maintenance, and that a complete checkup be conducted prior to field use.

Prime Power

Prime power is supplied by an Onan AK series DC motor generator set with a capacity of 750 watts. The motor-generator set is operated continuously except for oil changes, and supplies a charging current for a set of high capacity batteries (70 - 100 amp-hour) which in turn supply the required current at 28 volts to the recording system. A modification to the field winding of the generator allows the generator output to be balanced against the system demand with a net trickle current (.5a) available for the batteries. Battery capacity is sufficient to allow proper operation of the site for a period of 12 hours should the motor-generator set fail. A twelve gallon tank capacity is provided and the tank is replenished daily with regular grade gasoline.

Care is taken when setting up a site to locate the motor generator set as far away as possible from the antenna and recording gear. This arrangement tends to eliminate both electrical and mechanical coupling to the antenna. Electrical interference due to the motor-generator set has never been noticeable unless the antenna and generator were within 50 feet of each other. Mechanically coupled interference due to induced motion of the antenna in the earth's magnetic field has been observed at distances up to 250 feet in the situation where the antenna was buried and the motor-generator was resting on the ground. A simple solution to this problem was to place the motor generator on several old tire carcasses to insure mechanical de-coupling from the ground.

If the maintenance suggestions in the Onan Manual are followed the generator should give satisfactory service. The following is a short list of some of the more important precautions:

1. Use regular grade gasoline

2. Change the oil weekly using MS or MS/DS service, preferably Shell
3. Remove the panels covering M. G. set in a hot climate, and at altitudes exceeding 4000 feet
4. Re-adjust the carburetor towards the lean side when operating at high altitudes
5. Dismantle the engine and clean the carbon after 500 hours.

APPENDIX B

Noise Intensity Measurements

Accurate knowledge of the noise intensity (at the signal frequency) is necessary for the following two reasons.

1. The estimate of the signal power at the output of the receiver's summer is a biased estimator (i.e., $E[\hat{A}^2] = A^2 + 2(\frac{N_o}{T})$). The bias which is determined by the noise intensity consequently must be subtracted from the sample value $\hat{A}^2$ to give the unbiased estimate of A^2.

2. The confidence limits on each estimate $\hat{A}^2$ depend on the ratio $\frac{\hat{A}^2}{N_I}$ (where $N_I = \frac{N_o}{T}$). Accordingly a small confidence interval for $\hat{A}^2$ requires an even smaller confidence interval for N_I.

For purposes of this experiment we have set an acceptable confidence interval of ± .2 dB on N_I. It should be noted that the best way to reduce the confidence interval in estimating a signal level is to integrate over the entire data record and come up with a single value $\hat{A}^2$. On the other hand, to reduce the confidence interval in noise intensity estimation the scheme is to get as many independent samples in the data record as possible. We will defer until the end of this section, the method by which we select the number of samples needed to provide a specified confidence interval about N_I.

Figure B-1 shows the primary method by which the noise intensity was computed. The output of a single correlator (PAR) is sampled at a reasonably high rate ($f_{sample} \sim 20$/sec) and recorded on magnetic tape. The output random variable is denoted as L_x (x denotes either the cosine or sine reference channel). The sample mean $\overline{m}_x$ and sample variance $\overline{\sigma_x^2}$ are

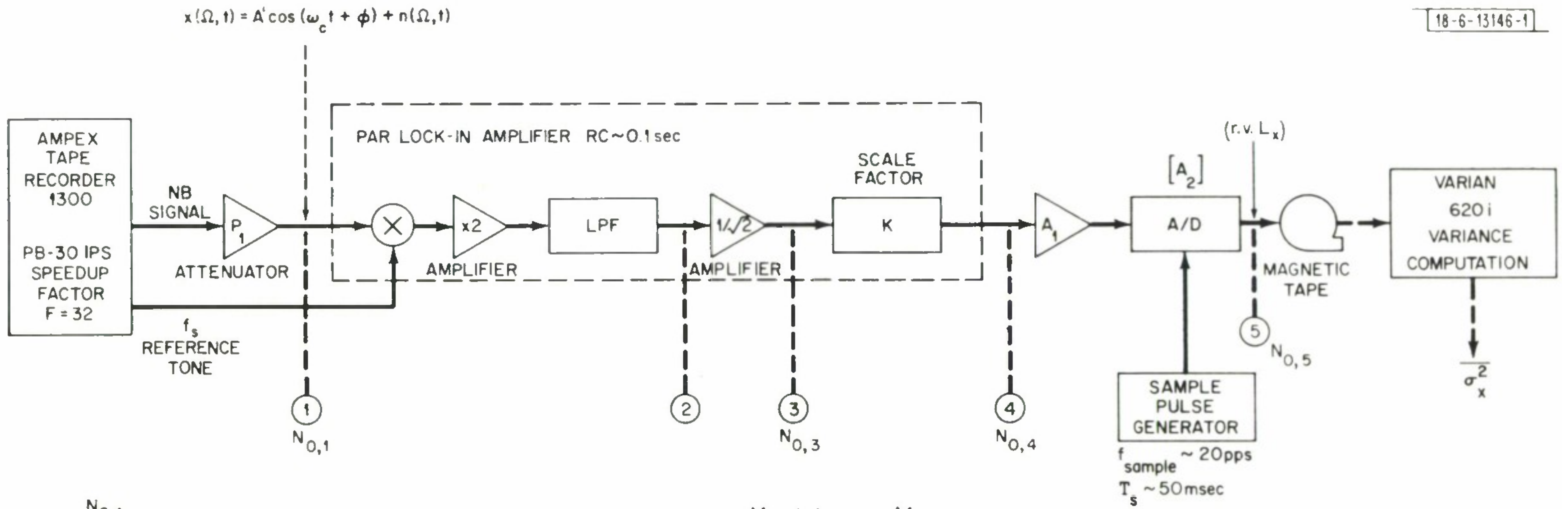

$S_o(f) = \frac{N_{0,1}}{2}$ FOR POSITIVE AND NEGATIVE VALUES OF f SUCH THAT $f_c - \frac{\Delta f}{2} < |f| < f_c + \frac{\Delta f}{2}$

Fig. B-1. Primary noise estimation method.

defined by

$$\overline{m}_x = \frac{1}{M} \sum_{i=1}^{M} (L_x)_i \tag{b-1}$$

$$\overline{\sigma_x^2} = \frac{1}{M} \sum_{i=1}^{M} \{(L_x)_i - \overline{m}_x\}^2. \tag{b-2}$$

It can be shown

$$E[\overline{m}_c] = \left(\frac{KA_1A_2}{\sqrt{2}}\right) A \cos \varphi, \quad E[\overline{m}\ ] = \left(\frac{KA_1A_2}{\sqrt{2}}\right) A \sin \varphi$$

and

$$E[\sigma_x^2] = \left(\frac{M-1}{M}\right)\left(\frac{KA_1A_2}{\sqrt{2}}\right)^2 \frac{N_o}{T} \rightarrow \left(\frac{KA_1A_2}{\sqrt{2}}\right)^2 \frac{N_o}{T} \overset{\Delta}{=} \frac{N'_{o,1}}{T} \tag{b-3}$$

for large M where $N_o = N_{o,1}$ in Fig. b-1; $N'_{o,1}$ includes the constant $(KA_1A_2/\sqrt{2})^2$ and $T = 2(32)RC$. (RC being the time constant of the LPF.) The above is true provided the random variables $(L_x)_i$ are identically distributed and statistically independent.

The important point is that the sample variance $(\overline{\sigma_x^2})$ is computed from the M independent samples taken at the output of <u>one</u> of the correlators. The routines for sample mean and variance have been implemented on a Varian 620i computer. Since the received signal levels are expressed in terms of an H field at the <u>input to the antenna</u>, we need to relate an equivalent input H_N^2 noise intensity to the Varian computed variance $\overline{\sigma_x^2}$. First the noise intensity at the antenna output [(volts)^2/Hz] is related to an equivalent magnetic field noise intensity [(amp-m)^2/hz] though equation a-2

$$H_N^2 = \frac{N_{o,ant}}{(.007178f)^2} \tag{b-4}$$

The system gain at the signal frequency from the antenna output to the tape recorder output is the product of tape recorder voltage gain G_T and the voltage gain G_S between the antenna output and tape recorder input

$$G_{sys} = G_T \cdot G_S = G_T G_C \left(\frac{G_S}{G_C}\right) = G_T \left(\frac{G_S}{G_C}\right)\left(\frac{V_o(f_c)}{\beta(f_c)}\right) \quad . \qquad \text{(b-5)}$$

The parameters in equation b-5 are fully defined in Appendix E and it is only necessary to note here that they are all quantities measured during the normal receiver calibrations. Along with the tape recorder voltage gain there is a noise bandwidth expansion due to playback speedup. The effect of speedup is to stretch the noise spectrum by the speedup factor F. Following the tape recorder we have been using an attenuator (with voltage gain $P_1 < 1$). Hence the noise intensity input into the (PAR) correlator is related to the antenna output noise intensity by

$$N_{o,1} = \frac{N_{o,ant} \cdot (G_{sys} \cdot P_1)^2}{F} \quad . \qquad \text{(b-6)}$$

The output of the PAR correlator $(N_{o,4})$ can be shown to be related to the input noise intensity $N_{o,1}$ by the relationship

$$N_{o,4} = \frac{N_{o,1}}{2RC} \cdot \left(\frac{1}{\sqrt{2}}\right)^2 \cdot \mathcal{K}^2 \quad . \qquad \text{(b-7)}$$

Finally, the voltage amplifier A_1 and the A/D voltage gain $[A_2]$ relate $N_{o,4}$ and the computed variance $\overline{\sigma_x^2}$

$$\overline{\sigma_x^2} = (A_1 A_2)^2 \, N_{o,4} \quad . \qquad \text{(b-8)}$$

Equations b-4, b-5, b-6, b-7 and b-8 are combined to yield

$$H_N^2 = \frac{1}{(.007178f)^2} \cdot \frac{F}{(G_T \cdot G_S \cdot P_1)^2} \cdot \frac{4RC}{\mathcal{K}^2} \cdot \frac{1}{(A_1 A_2)^2} \, \overline{\sigma_x^2} \cdot^{*} \qquad \text{(b-9)}$$

---

[*] For the actual analysis the following constants were used $A_1 = A_2 = 1$, RC=.01 sec, F=32 and $K = (10/(50 \times 10^{-3}))$.

H_N^2 is the equivalent antenna input noise intensity $\{(\text{amp-m})^2/\text{Hz}\}$ of noise picked up by the single loop antenna. The results of the noise measurements are listed in tables VIII and IX in Section V.

The virtue of the above noise analysis is that a number of noise estimates for each tape can be computed several minutes after the equipment has been set up and calibrated. An alternative method of computed noise intensity is used on occasion. The method consists of digitizing large segments of the wideband channel on playback. The resulting digital tape will be in the same format as was used for Lincoln's wideband noise study. One of the spectral programs produces a noise spectrum from which one can pick off the noise intensity level at 45 Hz. The primary disadvantage of this method is that it is time consuming and costly in computer time. The agreement between the noise intensity made by variance computation and that made by the spectrum estimate is extremely close (differences are seldom more than a few tenths of a dB). The advantage of the spectrum computation is that it shows clearly sources of strong interference at frequencies sufficiently close to 45 Hz (75 Hz) which may affect the signal estimate. The spectrum computations also clearly show the noise to be white over the receiver bandwidths of interest.

As a slight digression we will outline how we select the number of samples needed to satisfy a specified confidence interval about H_N(dBH). Let us first assume that the output of the correlator $(L_x)_i$ has had its mean subtracted off. Denote this new variable by ℓ_i. Previous empirical results derived from Lincoln's wideband noise studies of ELF noise have indicated that as the non-Gaussian wideband noise is subjected to successively narrower band pass filters, the output becomes more Gaussian. This is apparent for real time equivalent integration times of a few seconds for most sites where wideband noise has been collected. The probability distribution function for ℓ_i is then approximated by

$$f_{\ell_i}(\ell_i) = \frac{1}{\sqrt{2\pi}\sqrt{\frac{N'_{o,1}}{T}}} e^{\frac{-\ell_i^2}{2}\left(\frac{N'_{o,1}}{T}\right)^{-1}} . \tag{b-10}$$

The sample variance (equation b-2) can be written

$$\overline{\sigma^2} \cong \frac{1}{M} \sum_{i=1}^{M} \ell_i^2 \triangleq \frac{1}{M} \chi^2 .$$

$\overline{\sigma^2}$ itself is then a random variable with a distribution which can be shown to be a χ^2 distribution with M degrees of freedom, i.e.,

$$f_{\sigma^2}(\sigma^2) = \frac{M}{(N'_{o,1}/T)} 2^{M/2} \Gamma\left(\frac{M}{2}\right) \left\{M \frac{\sigma^2}{(N'_{o,1}/T)}\right\}^{\frac{M}{2}-1} \times e^{-\frac{M\sigma^2}{(N'_{o,1}/T)}}$$

$$\text{for } \sigma^2 \geq 0 \tag{b-11}$$

$$= 0 \text{ for } \sigma^2 < 0.$$

The mean and variance of the random variable σ^2 are most easily found by determining the moment generating function for the random variable ℓ_i^2. This can be shown to be

$$\psi_{\ell_i^2}(t) = \frac{1}{\sqrt{2\left(\frac{N'_{o,1}}{T}\right)}\sqrt{\frac{1}{2\left(\frac{N'_{o,1}}{T}\right)} - t}} .$$

Since the random variables ℓ_i are sampled at a sufficiently slow rate so as to imply independence of samples one can construct the moment generating function of the sum $Z \triangleq \sum_{i=1}^{M} \ell_i^2$ from

$$\psi_Z(t) = \psi_{\Sigma \ell_i^2}(t) = \prod_{i=1}^{M} \psi_{\ell_i^2}(t)$$

$$\psi_Z(t) = \frac{1}{\left(2\frac{N'_{o,1}}{T}\right)^{M/2} \left\{\frac{1}{2\left(\frac{N'_{o,1}}{T}\right)} - t\right\}^{M/2}} \quad . \tag{b-12}$$

Now the first two moments of the distribution of Z are found from equation b-12

$$E[\sigma^2] = \frac{1}{M} E[Z] = \frac{1}{M} \frac{\partial \psi_Z(t)}{\partial t}\Big|_{t=0} = \left(\frac{N'_{o,1}}{T}\right) \tag{b-13}$$

and

$$\text{var}[\sigma^2] = \frac{1}{M^2} \{E[Z^2] - (E[Z])^2\} = \frac{1}{M^2} \left\{\frac{\partial^2 \psi_Z}{\partial t^2}\Big|_{t=0} - \left(\frac{\partial \psi_Z}{\partial t^2}\Big|_{t=0}\right)^2\right\},$$

$$= \frac{2\left(\frac{N'_{o,1}}{T}\right)^2}{M} \quad . \tag{b-14}$$

From b-13 one sees that σ^2 is an estimator of $\frac{N'_{o,1}}{T}$ and from b-14 the variance of the estimate decreases inversely with the number of samples chosen. It is observed that $f_{\sigma^2}(.)$ is a function both of M and the true variance $\left(\frac{N'_{o,1}}{T}\right)$. The confidence limits σ_U^2 and σ_L^2 are chosen such that

$$\int_{\sigma_U^2}^{+\infty} f_{\sigma^2}\left(\sigma^2; M, \frac{N'_{o,1}}{T}\right) d\,\sigma^2 = \frac{\epsilon}{2} \tag{b-15}$$

and

$$\int_{o}^{\sigma_L^2} f_{\sigma^2}\left(\sigma^2 ; M, \frac{N'_{o,1}}{T}\right) d\,\sigma^2 = \frac{\epsilon}{2} . \qquad \text{(b-16)}$$

It should be clear that both σ_L^2 and σ_U^2 are functions of both ϵ and M. For large values of M, Holsinger [15] provides some approximate formulas for the confidence interval

$$\sigma_U^2 = \sigma^2 \left[1 - \frac{K_\epsilon}{\sqrt{2(M-1)}}\right]^{-2} \qquad \text{(b-17)}$$

$$\sigma_L^2 = \sigma^2 \left[1 + \frac{K_\epsilon}{\sqrt{2(M-1)}}\right]^{-2}$$

where K_ϵ is defined by

$$\frac{\epsilon}{2} = \frac{1}{\sqrt{2\pi}} \int_{K_\epsilon}^{\infty} e^{t^2/2} dt. \qquad \text{(b-18)}$$

Thus for a confidence level $\epsilon/2 = 10\%$ and for a ± .2 dB confidence interval, the required number of samples, M, is computed from equations b-17 and b-18 to be about 1,600. As normal practice we have chosen a sampling interval of 50 msec for 2 minutes of playback data so that approximately 2400 samples are collected for the variance computation. (It should be noted that 50 msec is equal to five time constants when RC = .01 sec. The real time bandwidth that the noise is subjected to is $\Delta f' = 100/F = 3.4$ Hz. The wide band non-Gaussian data being subjected to this 3.4 Hz filter comes out reasonably Gaussian.)

An example of the output of the noise program on the Varian 620i is shown in Fig. B-2. σ_X^2 is given as 1.265 $(\text{volt})^2$. The equivalent input noise at the antenna is given by equation b-9 which is rewritten for this particular experimental configuration

$$20 \log (H_{\varphi})_N = [-128.91 + 20 \log \frac{1}{P_1} + 20 \log (\frac{1}{f_S}) + 20 \log \frac{G_C}{G_S} + 20 \log \frac{V_{CM}}{\sqrt{B^2}} + 10 \log (\sigma_X{}^2)] \text{ dBH}/\sqrt{\text{Hz}}. \qquad \text{(b-19)}$$

For Utah tape no. 13 (at 1900 - 2000 GMT) the input noise intensity at 45 Hz is calculated to be -134.2 dBH/$\sqrt{\text{Hz}}$ ± .15 dB.

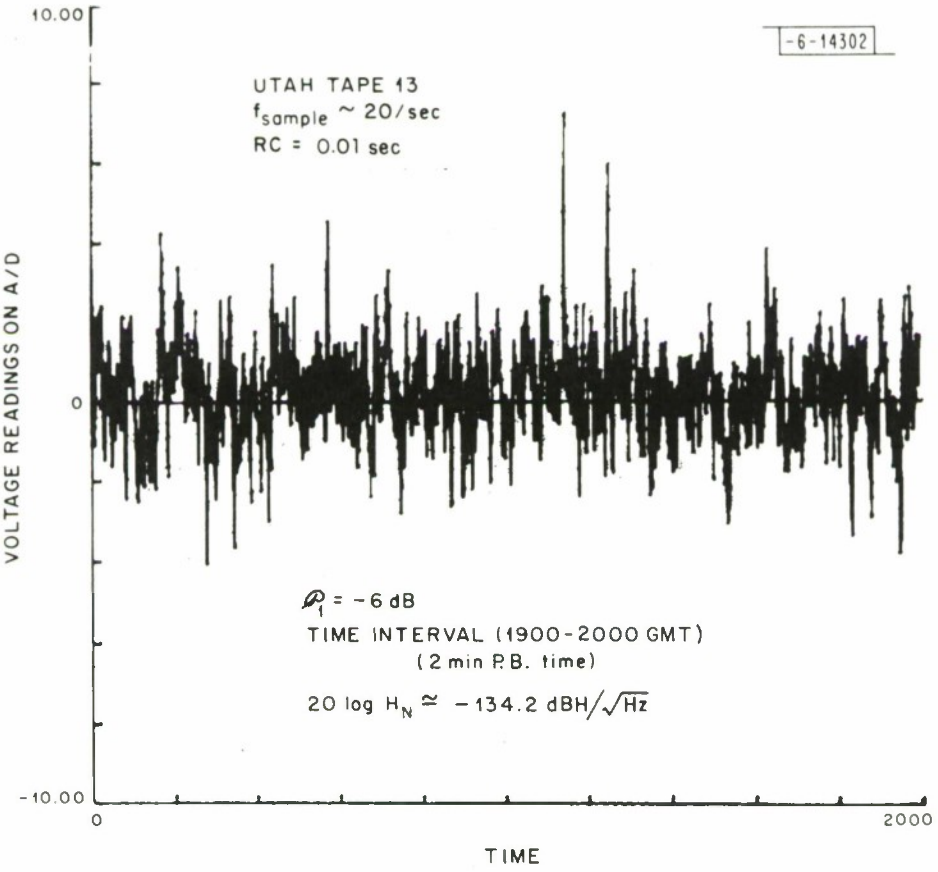

Fig. B-2. Typical noise.

APPENDIX C

Confidence Interval for Signal Estimates

The output of the typical receiver structure shown in Fig. 4 is the random variable $\hat{A}^2$ where

$$\hat{A}^2 = L_c^2 + L_s^2 . \tag{c-1}$$

The random variables $L_c(\Omega, t_i)$ or $L_s(\Omega, t_i)$ (where t_i is the sample time) appear from the data to have the following properties.

(a) At each sample interval, the computed variances of L_c and L_s are identical within experimental tolerances;

(b) Since the equivalent integration bandwidths are of the order of a few thousandths of a Hertz the variables L_c and L_s are very close to being Gaussian distributed;

(c) The means are $A \cos \varphi$ and $A \sin \varphi$ respectively.

Hence the probability functions are therefore

$$\begin{aligned} f_{L_c}(L_c) &= \frac{1}{\sqrt{2\pi N_I}} e^{-\frac{(L_c - A\cos\varphi)^2}{2N_I}} \\ f_{L_s}(L_s) &= \frac{1}{\sqrt{2\pi N_I}} e^{\frac{(L_s - A\sin\varphi)^2}{2N_I}} . \end{aligned} \tag{c-2}$$

The next assumption made is that L_c and L_s are uncorrelated. Examination of the output traces of the individual quadrature channels always show a lack of correlation. It is suggested that the extremely narrow filter bandwidth is the cause of this lack of correlation. The reasoning is as follows. It is known that most of the energy is contained in the relatively infrequent large sferics. These sferics pass through the extremely narrow filter giving rise to 'transient' sinusoid with a certain phase relation with respect to the phase of the receiver's signal reference frequency. Since the phase relationships between succeeding large sferics and the receiver's reference frequency are random; one could expect at one time that virtually all the noise energy shows up on one of the quadrature outputs whereas the energy from a succeeding sferic may show up only on the other quadrature outputs. A randomization of the phase relationship between the filtered sferic and the receiver's reference frequency clearly leads to a lack of correlation between L_c and L_s. Hence if it is assumed that L_c and L_s are uncorrelated, it is easy to show (see Van Trees[8]) that the cumulative distribution function for $\hat{A}^2$ is related to the Marcum Q function by

$$P(\hat{A}^2 \le \gamma^2) = 1 - \int_{\gamma/\sqrt{N_I}}^{\infty} \ell I_o(a\ell)\, e^{-\frac{\ell^2 + a^2}{2}}\, d\ell \qquad \text{(c-3)}$$

$$P(\hat{A}^2 \le \gamma^2) \triangleq 1 - Q\left(\frac{A}{\sqrt{N_I}}, \frac{\gamma}{\sqrt{N_I}}\right) \qquad \text{(c-4)}$$

where

$$\ell = \sqrt{\frac{\hat{A}^2}{N_I}} \quad \text{and} \quad a = \sqrt{\frac{A^2}{N_I}} \quad .$$

Let us select a <u>confidence level ϵ</u>. It is standard practice to derive the confidence curves from the relations

$$\frac{\epsilon}{2} = P(\hat{A}^2 \le \gamma^2{}_L) \qquad \text{(c-5)}$$

and

$$\frac{\epsilon}{2} = P(\hat{A}^2 \geq \gamma_H^2).$$

Figure C-1 shows Marcum's Q function with the curve parameter $\frac{A}{\sqrt{N_I}}$ converted to dB. Figure C-2 shows the confidence curves (for fixed levels of ϵ) which are derived from equations c-4 and c-5 and Fig. C-1. Using the confidence curves is particularly simple. Assume the confidence level ϵ is specified and that one measures a value $\hat{A}^2/N_I$. A horizontal line is drawn on Fig. C-2 through this value of $\hat{A}^2/N_I$. The two values of A^2/N_I [defined by the intersection of the horizontal line with the confidence curves (with parameter $\epsilon/2$] form the limits of the confidence interval. An example of how to construct a confidence interval is also shown on the figure. The confidence interval $(A_L^2/N_I, A_H^2/N_I)$ is itself a random variable. The true value of A^2/N_I is included within this interval with probability $1-\epsilon$. From these confidence curves it is easy to see that the confidence interval rapidly increases in size with decreasing values of $\hat{A}^2/N_I$.

We also use on occasion the term confidence band. To determine a confidence band one first computes a theoretical signal level and the corresponding signal to integrated noise ratio. Then a vertical line is drawn on Fig. C-2 through the value of A^2/N_I intersecting the appropriate pair of confidence curves at two points. The range of expected sample $\hat{A}^2/N_I$ values enclosed by two horizontal lines through the two intercept points will be called the confidence band. In brief the difference between the confidence band and the confidence interval is the following. If we have a theoretically calculated

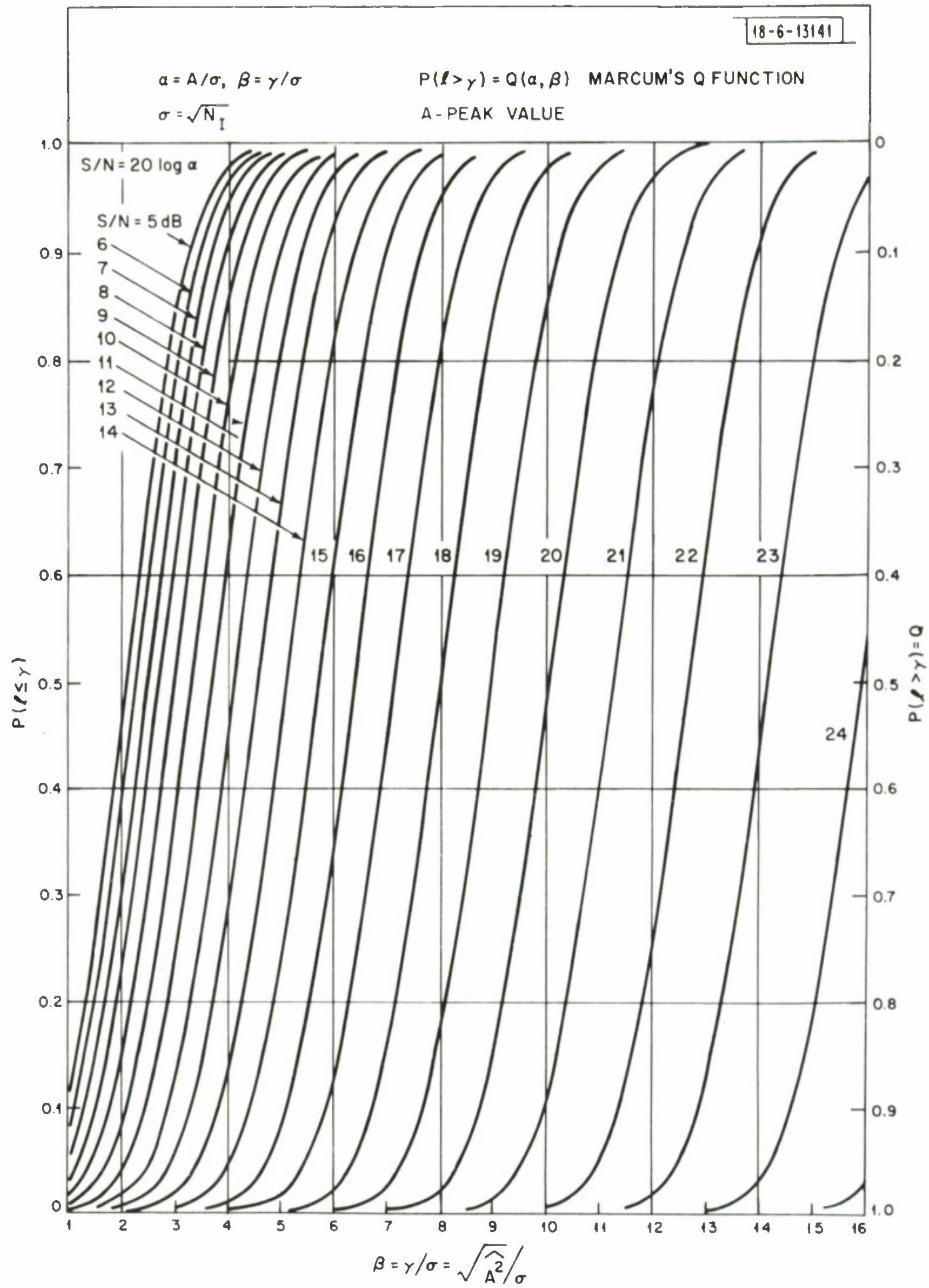

Fig. C-1. Cumulative probability distribution (Marcum's Q function).

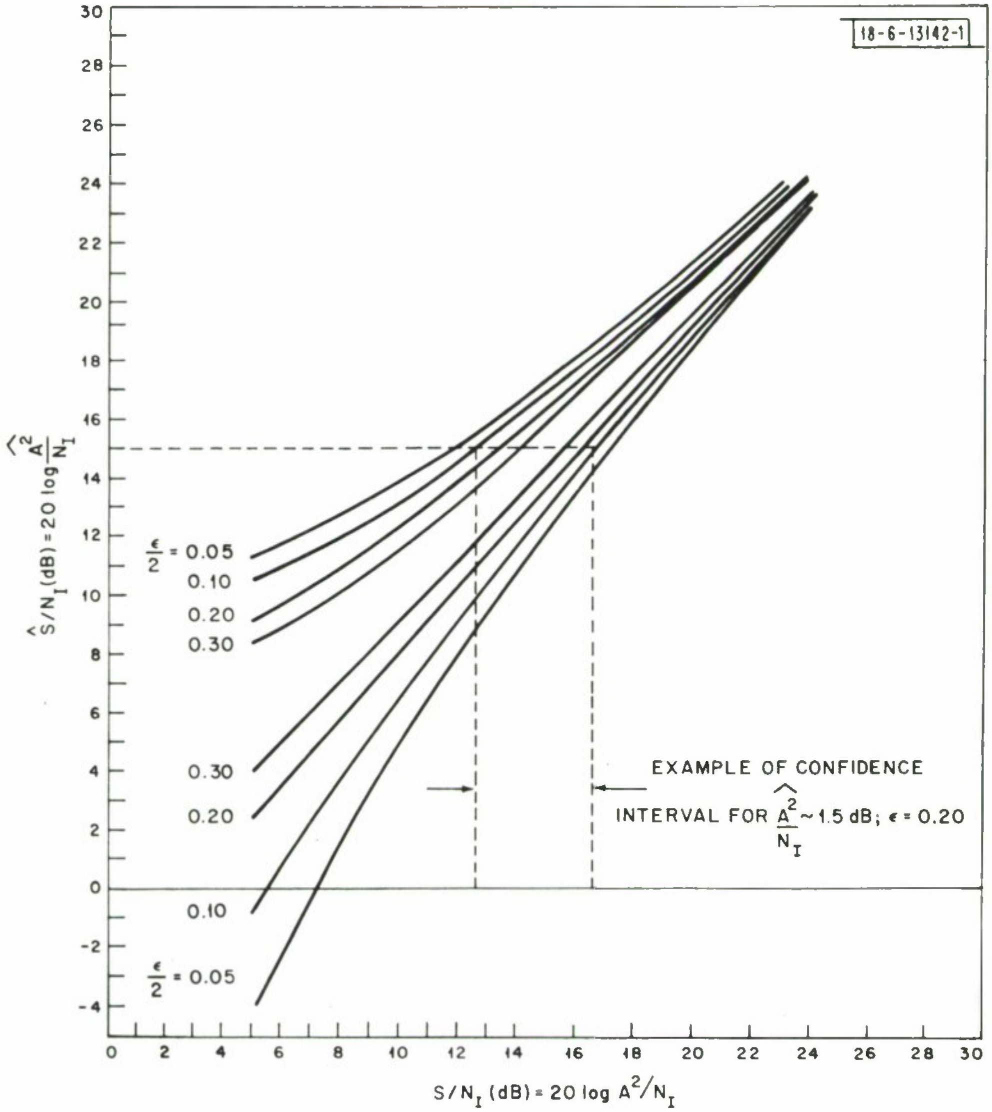

Fig. C-2. Confidence curves (for Marcum's Q function).

signal value, then the confidence band gives the range of sample biased signal levels that one might experimentally measure $\{(1-\epsilon)$ 100% of the samples would be in the band$\}$ provided that the theoretical calculated value was in fact the true value. If on the other hand we are presented with a set of experimentally measured biased signal levels, then for each of these measurements we have a unique confidence interval. The statement can then be made that with probability $(1-\epsilon)$ 100% each interval will include the true value of signal A^2/N_I.

Confidence curves (see Fig. C-2) for S/N ratios between 5 and 25 dB have been derived from the Marcum Q function tables. However, Marcum's Q function tables are not tabulated for $S/N = A^2/N_I > 25$ dB. Nevertheless, there is a simple asymptotic expression for $Q\left(\frac{A}{\sqrt{N_I}}, \frac{\gamma}{\sqrt{N_I}}\right)$ as given by Van Trees[16]

$$Q\left(\frac{A}{\sqrt{N_I}}, \frac{\gamma}{\sqrt{N_I}}\right) \simeq \frac{1}{2}\left\{1+\mathrm{erf}\left(\frac{A-\gamma}{\sqrt{2N_I}}\right)\right\} \text{ for } \gamma >> \sqrt{N_I} \text{ and } \gamma >> \gamma - A. \qquad \text{(c-6)}$$

Recalling equation c-4

$$P(\hat{A}^2 \leq \gamma) = 1 - Q\left(\frac{A}{\sqrt{N_I}}, \frac{\gamma}{\sqrt{N_I}}\right) \qquad \text{(c-7)}$$

it follows that

$$P(\hat{A}^2 \leq \gamma) = \frac{1}{2}\left\{1 - \mathrm{erf}\left(\frac{A-\gamma}{\sqrt{2N_I}}\right)\right\}. \qquad \text{(c-8)}$$

The confidence intervals can be computed from this distribution. For example assume one wants to determine the $1-\epsilon = 80\%$ confidence curves. These are determined from setting equation c-8 equal to .1 and .9 and determining the value of $\frac{A-\gamma}{\sqrt{2N_I}}$ from the error function tables. This turns out to be

$$\left(\frac{A}{\sqrt{N_I}} - \frac{\gamma}{\sqrt{N_I}}\right) = \pm\ 1.286 \quad \text{for} \quad 1 - \epsilon = 80\% .$$

In table C-1 we have tabulated typical sets of confidence curves for true S/N(= A^2/N_I) ratios between 23 and 35 dB. It is notable that the interval decreases very slowly with increasing S/N ratio.

It should be carefully noted in this section that A is a peak value and not the rms value. Therefore, since the computed values $|H^2_\varphi(t_i, f_s)|_{b,T}$ are given in terms of rms rather than peak values one must add 3 dB to equation 19 before the confidence curves can be used since these curves reflect peak rather than rms values.

Table C-1.

Confidence Curves ($1 - \epsilon = 80\%$) for S/N greater than 23 db.

A/σ (db)	A/σ		Lower Limit		Upper Limit	
			γ/σ db	$(\gamma/\sigma - A/\sigma)$ db	γ/σ db	$(\gamma/\sigma - A/\sigma)$ db
23	14.125		22.17	−.83	23.75	.75
24	15.849		23.26	−.74	24.68	.68
25	17.783		24.35	−.65	25.61	.61
26	19.953		25.42	−.58	26.54	.54
27	22.387		26.49	−.51	27.48	.48
28	25.119		27.54	−.46	28.42	.43
29	28.184		28.59	−.41	29.39	.39
30	31.623		29.64	−.36	30.35	.35
31	35.482					
32	39.812		31.71	−.29	32.28	.28
33	44.669					
34	50.120					
35	56.236		34.80	−.20	35.20	.20

A is the true value of the signal level

$(\hat{A}^2)^{1/2}$ is the sample value of the signal

$\sigma = \sqrt{N_I}$ is the square root of the integrated noise.

APPENDIX D

Derivation of Composite Confidence Limits for $\overline{A^2(f_j)}$ and $\overline{\overline{A^2}}$

In Section III we defined the unbiased composite field strength at the frequency f_j as

$$\overline{(A^2(f_j))} \triangleq \frac{\sum_{i=1}^{M} \frac{(\widehat{A^2(f_j)})_{u,i}}{N_{I,i}}}{\sum_{i=1}^{M} \left(\frac{1}{N_{I,i}}\right)} \tag{d-1}$$

where $N_{I,i}$ is the ith integrated noise sample estimate and $(\widehat{A^2(f_j)})_{u,i}$ is the corresponding ith unbiased estimate for $A^2(f_j)$. It is noted that the weighting gives greater weight to those samples which exhibit the higher S/N ratio. The $N_{I,i}$ can be determined to a very high degree of accuracy and for purposes of computing a composite confidence limit these values will be considered as known constants. The mean and variance of $\overline{A^2(f_j)}$ then are

$$E[\overline{A^2(f_j)}] = \frac{\sum_{i=1}^{M} \frac{1}{N_{I,i}} E[\widehat{A^2(f_j)}]_{u,i}}{\sum_{i=1}^{M} \frac{1}{N_{I,i}}} = \frac{\sum_{i=1}^{M} \frac{1}{N_{I,i}} A^2(f_j)}{\sum_{i=1}^{M} \frac{1}{N_{I,i}}} = A^2(f_j) \tag{d-2}$$

and

$$\text{var}(\overline{A^2(f_j)}) = \frac{\sum_{i=1}^{M} \frac{1}{(N_{I,i})^2} \text{var}\,[\widehat{A^2(f_j)}]_{u,i}}{\left(\sum_{i=1}^{M} \frac{1}{N_{I,i}}\right)^2} . \tag{d-3}$$

It is seen that $\overline{A^2(f_j)}$ is an unbiased estimator for $A^2(f_j)$. For the receiver structure shown in Fig. 4 it can be shown that

$$\text{var}\,[\widehat{A^2}(f_j)]_{u,i} = \text{var}\,[\widehat{A^2}(f_j)]_{b,i} = 4(N_{I,i}^2 + N_{I,i}\,A^2(f_j)) \;.$$

For $A^2(f_j)/N_{I,i} > 10$ we can make the approximation

$$\text{var}\,[\widehat{A^2}(f_j)]_{u,i} \simeq 4A^2(f_j)N_{I,i} \tag{d-4}$$

and hence

$$\text{var}\,(\overline{A^2(f_j)}) = \frac{\sum\limits_{i=1}^{M} \dfrac{4A^2(f_j)}{N_{I,i}}}{\left(\sum\limits_{i=1}^{M} \dfrac{1}{N_{I,i}}\right)^2} = \frac{4A^2(f_j)}{\left(\sum\limits_{i=1}^{M} \dfrac{1}{N_{I,i}}\right)} \triangleq K_j^2\,A^2(f_j) \tag{d-5}$$

where $K_j^2 = \dfrac{4}{\sum\limits_{i=1}^{M} \left(\dfrac{1}{N_{I,i}}\right)}$.

Note that the noise $N_{I,i}$ is the ith sample of integrated noise centered at the frequency f_j. The random variable $\overline{A^2(f_j)}$ can be assumed to be Gaussian distributed in the vicinity of the mean $A^2(f_j)$. In equations d-6 through d-12 we assume that the dependence on f_j is implicit so as to simplify the notation. Hence the probability density function is

$$f(\overline{A^2};A^2) = \frac{1}{\sqrt{2\pi}\;KA}\; e^{-\frac{(\overline{A^2} - A^2)^2}{2(AK)^2}} \;. \tag{d-6}$$

The confidence curves are then derived from the relationship

$$\int_{(\overline{A^2})_L = -\gamma + A^2}^{(\overline{A^2})_U = \gamma + A^2} f(\overline{A^2};A^2)\,d\overline{A^2} = 1 - \epsilon \;. \tag{d-7}$$

Let us normalize by setting $y = \dfrac{\overline{A^2} - A^2}{AK}$. Equation d-7 reduces to

$$\int_{-\gamma/AK}^{\gamma/AK} \left[\frac{1}{\sqrt{2\pi}} e^{-y^2/2}\right] dy = 1 - \epsilon \ .$$

The upper and lower bounds are both determined from the following

$$Q\left(\frac{\pm\gamma}{AK}\right) = \pm \int_{\pm\gamma/AK}^{\pm\infty} \left\{\frac{1}{\sqrt{2\pi}} e^{-y^2/2}\right\} = \epsilon/2 \ . \qquad \text{(d-8)}$$

	$\epsilon/2 = .30$	$\epsilon/2 = .10$	$\epsilon/2 = .05$	$\epsilon/2 = .025$
$\gamma/AK = \beta_\epsilon$	$\beta_\epsilon = .524$	$\beta_\epsilon = 1.28$	$\beta_\epsilon = 1.64$	$\beta_\epsilon = 1.96$

The upper and lower confidence curves are thus derived from

$$\begin{aligned} (\overline{A^2})_U &= A^2 + \beta_\epsilon (AK) \\ (\overline{A^2})_L &= A^2 - \beta_\epsilon (AK) \ . \end{aligned} \qquad \text{(d-9)}$$

Figure D-1 shows a typical composite confidence curve for the averaged daytime and nighttime unbiased signal estimates at f = 45 Hz. The corresponding confidence intervals (at $\epsilon/2 = .1$) for the composite values $(\overline{A^2(45)})_D$ and $(\overline{A^2(45)})_N$ are also shown.

The last set of confidence curves one needs to compute are those for the random variable $\overline{\overline{A^2}}$ where we have defined (f_m is the mid-point or center frequency)

$$\overline{\overline{A^2(f_m)}} = f_m^2 \left(\frac{1}{2J+1}\right) \sum_{j=1}^{2J+1} \frac{\overline{A^2(f_j)}}{f_j^2} \ .$$

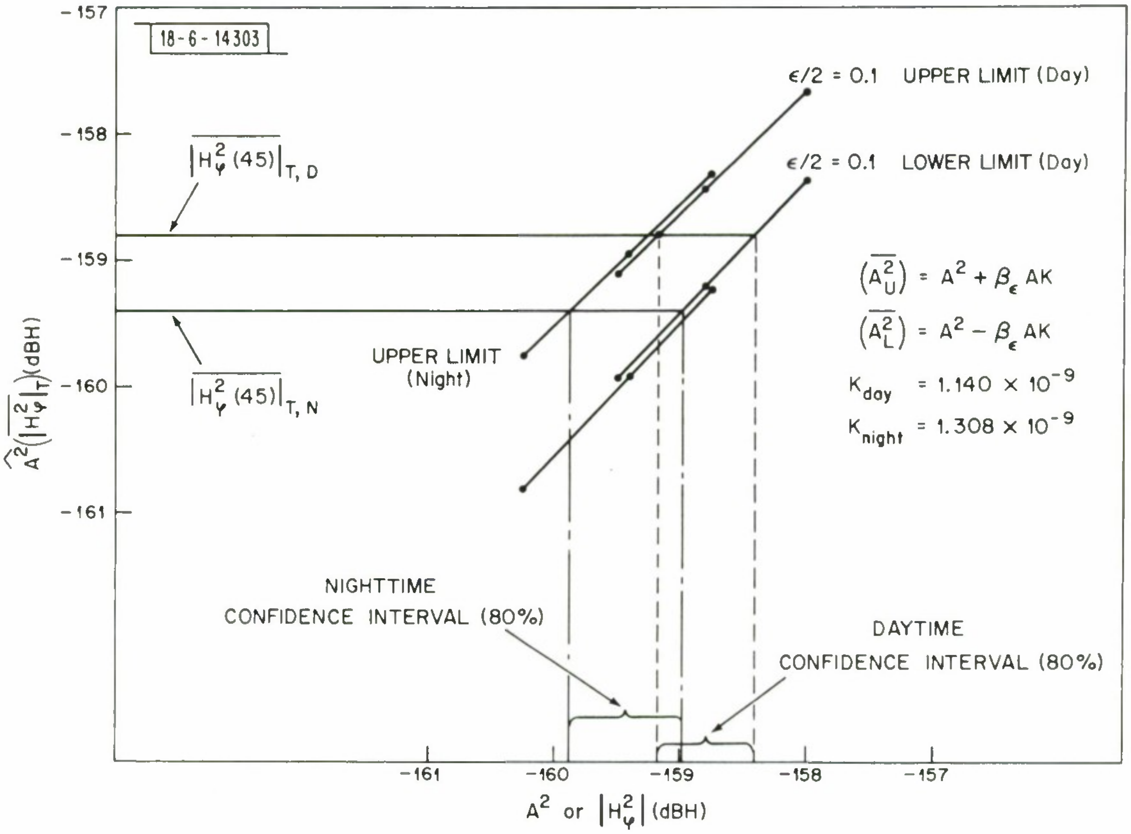

Fig. D-1. Composite confidence curve.

Now

$$E[\overline{\overline{A^2(f_m)}}] = f_m^2 \left(\frac{1}{2J+1}\right) \sum_{j=1}^{2J+1} \frac{E[\overline{A^2(f_j)}]}{f_j^2} .$$

Define

$$E[\overline{A^2(f_j)}] = A^2 + \delta A_j^2 \qquad \text{(d-10)}$$

where δA_j^2 is a small perturbation compared to A^2. A^2 is independent of the frequency f_j and related to the direct component $|H_\varphi^2(f_m)|_\mathcal{D}$. (Recall that $\overline{A^2(f_j)}$ is related to the total field component $|H_\varphi^2(f_j)|_T$ and varies with one's position with respect to the standing wave pattern.) Equation d-9 can be written as

$$E[\overline{\overline{A^2(f_m)}}] = f_m^2 \left(\frac{1}{2J+1}\right) \left\{\sum_{j=1}^{2J+1} \frac{A^2}{f_j^2} + \sum_{j=1}^{2J+1} \frac{\delta A_j^2}{f_j^2}\right\}. \qquad \text{(d-11)}$$

For the receiver locations deployed, the data show that in general, $10 \log (A^2/\delta A_j^2) >> 10$ dB. Moreover since we have designed the experiment to obtain $(2J+1)$ equispaced samples over one standing wave length one can be reasonably sure that the δA_j^2's are fairly evenly distributed about zero and that the first summation in equation d-11 swamps the second and hence

$$E[\overline{\overline{A^2(f_m)}}] \cong f_m^2 \left(\frac{1}{2J+1}\right)\left(\sum_{j=1}^{2J+1} \frac{1}{f_j^2}\right) A^2 \triangleq CA^2.$$

Since $C \simeq 1$ (i.e., $C \simeq 1.01$ for the 45 Hz band) we can set $C = 1$ and hence

$$E[\overline{\overline{A^2(f_m)}}] \simeq A^2 \text{ or equivalently} \qquad \text{(d-12)}$$

$$E[\overline{\overline{|H_\varphi^2(f_m)}}] \simeq |H_\varphi^2(f_m)|_\mathcal{D}.$$

The last equation states that $\overline{\overline{|H^2_\varphi(f_m)|}}$ is an unbiased estimator for the direct field component $|H^2_\varphi(f_m)|_{\mathcal{D}}$.

We can also compute the variance of $\overline{\overline{A^2(f_m)}}$ since

$$\overline{E(\overline{\overline{A^2}})^2} = f_m^4 \left(\frac{1}{2J+1}\right)^2 \sum_{i=1}^{2J+1} \sum_{j=1}^{2J+1} \frac{E[\overline{A^2}(f_i)\overline{A^2(f_j)}]}{f_i^2 f_j^2}$$

and

$$\mathrm{var}\,(\overline{\overline{A^2}}) = f_m^4 \left(\frac{1}{2J+1}\right)^2 \sum_{i=1}^{2J+1} \sum_{j=1}^{2J+1}$$

$$\times \left\{\frac{E[\overline{A^2}(f_i)\overline{A^2}(f_j)] - E[\overline{A^2}(f_i)]\, E[\overline{A^2}(f_j)]}{f_i^2\, f_j^2}\right\} .$$

$\overline{A^2(f_j)}$ and $\overline{A^2(f_i)}$ (where $i \neq j$) are constructed with signal estimates taken from two completely different set of days. Hence there is a lack of correlation in the noise and

$$E[\overline{A^2}(f_i)\overline{A^2}(f_j)] = E[\overline{A^2}(f_i)]\, E[\overline{A^2}(f_j)] \qquad \text{for } i \neq j.$$

This results in

$$\mathrm{var}\,(\overline{\overline{A^2}}) = f_m^4 \left(\frac{1}{2J+1}\right)^2 \sum_{j=1}^{2J+1} \frac{\mathrm{var}\,\{\overline{A^2(f_j)}\}}{f_j^4} . \tag{d-13}$$

However from equation d-5 we have

$$\mathrm{var}\,\{\overline{A^2}(f_j)\} = K_j^2\, A^2(f_j) \qquad \text{where } j \text{ refers to the jth}$$

frequency and hence in the same way as above one can make the approximation

$$\mathrm{var}(\overline{\overline{A^2}}) = f_m^4 \left(\frac{1}{2J+1}\right)^2 \sum_{j=1}^{2J+1} \frac{K_j^2\, A^2(f_j)}{f_j^4} \simeq f_m^4 \left(\frac{1}{2J+1}\right)^2 \left(\sum_{j=1}^{2J+1} \frac{K_j^2}{f_j^4}\right) A^2$$

$$\triangleq \mathcal{K}^2 A^2$$

where

$$\mathcal{K}^2 \triangleq f_m^4 \frac{1}{(2J+1)^2} \left\{ \sum_{j=1}^{2J+1} \frac{K_j^2}{f_j^4} \right\} . \tag{d-14}$$

Again, assuming that $\overline{\overline{A^2}}$ is Gaussian distributed also one can use as the distribution function equation d-6 with (A, K^2) being replaced by $(A, \mathcal{K}^2)$. Then the composite confidence limit for $\overline{\overline{A^2}}$ can be constructed in the same way as those for $\overline{A^2}(f_j)$.

APPENDIX E

Receiver Calibration

A necessary condition for accurate estimation of α is that each receiver system be well calibrated. We are looking for estimates of α accurate to within ± 0.1 dB/Mm so it is necessary that each station's receiver be calibrated to less than ± 0.3 dB. That is in the absence of noise one must be able to estimate the signal H_φ to within that accuracy. It is apparent that the errors in meter readings, in taking values from the chart recordings, in calibrating the chart recorders and PAR's, etc., when summed together cannot exceed ± 0.3 dB. This requires an extremely exacting calibration routine which is described in the remainder of this section. As noted in the text each complete receiver is composed of two parts; the field site recording equipment, and the laboratory based playback facility. The laboratory based playback facility is of course common to all the receivers. The remainder of this appendix first outlines the field site equipment calibration and then discusses the calibration of the laboratory playback facility.

Calibration of the Field Site Receiver Segment

The primary function of the calibration is to determine the *system gain* at the received signal frequency and to determine any changes in this gain over the recording duration. For this purpose a calibration signal is continuously injected in series with the antenna (refer to Figs. 4 and 5 in Section III). The calibration frequency is selected to be 1 Hz removed from the received signal frequency. Its amplitude was chosen to be sufficiently large such that its integrated signal to noise ratio exceeds 30 dB. The following notation is used; $\mathfrak{A}(f)$ is the open circuit voltage of the loop antenna, $\mathfrak{B}(f)$ is the calibration voltage impressed across the 0.5Ω resistor, A is the signal amplitude input into the quadrature correlators in the signal channel, B is the calibration amplitude input into the quadrature correlators of the calibration channel and $V_o(f)$ is the voltage output of the narrowband channel before the tape recorders. Let G represent the voltage gain from the transformer input to the output of the narrowband filter. Thus with the antenna <u>short circuited</u> and by successively injecting into the calibration pad,sinusoids of frequency f_S and f_C one can then measure the gains

$$G_C \triangleq \frac{V_o(f_C)}{\mathfrak{B}(f_C)}\bigg|_{\text{ant S. C.}} \tag{e-1}$$

$$G_S \triangleq \frac{V_o(f_S)}{\mathfrak{B}(f_S)}\bigg|_{\text{ant S. C.}} \tag{e-2}$$

where $\mathfrak{B}(f) = P_1 \cdot V_{CM}(f) = (4.4959 \times 10^{-10})(V_{CM}(f)[\text{mv. rms}])$. (e-3)

P_1 is the voltage attenuation ratio of the precision attenuator pad. Both V_{CM} and $V_o(f)$ are measured with a precision rms voltmeter. The gain of the combined record circuit of the P. I. tape recorder and the playback circuit of the Ampex tape recorder was measured and found to be independent of frequency (i. e., $G_T(f_C) = G_T(f_S) = G_T$). The system gains with the antenna <u>included</u> in the circuit are denoted by G_C' and G_S'. The overall system gain from the antenna (or attenuator) to the input to the correlator receiver is given by

$$\frac{A(f_S)}{\mathfrak{A}(f_S)} = G'_S \cdot G_T \qquad \text{(e-4)}$$

$$\frac{B(f_C)}{\mathfrak{B}(f_C)} = G'_C \cdot G_T \quad .$$

However since the antenna impedance is small compared to the transformer's input impedance

$$\frac{G'_C}{G'_S} = \frac{G_C}{G_S} \quad . \qquad \text{(e-5)}$$

Equations e-4 and e-5 are then combined to form the ratio

$$\frac{\mathfrak{A}(f_S)}{\mathfrak{B}(f_C)} = \left(\frac{A(f_S)}{B(f_C)}\right)\left(\frac{G_C}{G_S}\right) \quad . \qquad \text{(e-6)}$$

Recall from equation a-2 that the input H_φ field threading the antenna loop is related to the open circuit voltage $\mathfrak{A}(f_S)$ by

$$H_\varphi(f_S) = \frac{\mathfrak{A}(f_S)}{(.007178)f_S} \quad . \qquad \text{(e-7)}$$

With noise present, the outputs of the correlation receivers are the estimates $\hat{A}^2$ and $\hat{B}^2$. Then equations e-3, e-6 and e-7 can be combined to yield an equivalent input H_φ field estimate

$$\sqrt{H_\varphi^{\ 2}} = \frac{P_1 \cdot V_{CM}(f_C)}{(.007178)f_S} \left(\frac{G_C}{G_S}\right)\left(\sqrt{\frac{\hat{A}^2}{\hat{B}^2}}\right) \quad .$$

The following alternative form is more useful

$$10 \log \hat{H}^2 = -144.06 + 20 \log \left(\frac{G_C}{G_S}\right) - 20 \log f_S + 20 \log V_{CM}(f_C) + 10 \log \frac{\hat{A}^2}{\hat{B}^2} \qquad \text{(e-8)}$$

where V_{CM} is in mv. (rms).

In summary, the field site calibration consists of measuring G_C and G_S via equations e-1, 2 and 3 both at the beginning and at the end recording period. $V_{CM}(f_C)$ is also measured at these times. Average values $(\tilde{\ })$ of these three quantities are taken if there are small changes in value over the recording period. It is noted that $\hat{B}^2$ is continuously plotted on the chart recorder of the laboratory playback facility. This provides a continuous check of the system gain during the recording period. The four quantities $(\tilde{G}_C, \tilde{G}_S, \tilde{V}_{CM}(f_C)$ and $\hat{B}^2)$ are the calibration constants to be used in equation e-8 for the field strength.

Calibration of the Laboratory Segment of the Receiver

The main elements to be calibrated in the laboratory playback segment of the receiver are the correlation averagers (i.e., the Princeton Applied Research, Model 120 lock-in amplifiers), squarers, summers and chart recorder. The main difficulty is calibration of the PAR's and in particular maintaining each pair of PAR's in exact quadrature. One finds that if one relies on the stepped phase switch (0°, 90°, 180° and 270°) on the PAR's a possible error of the order of 1 dB in signal estimate can result. (This error is a consequence of the fact that the phase steps are not as close to 90° as advertised.) Figure E-1 shows an operational equivalent of a single PAR and Fig. E-2 shows the calibration set up for a pair of PAR's. For frequency and input scale selected the following procedure is followed

a) With the calibration oscillator set at the desired frequency and amplitude (such that the reading on the precision rms voltmeter corresponds

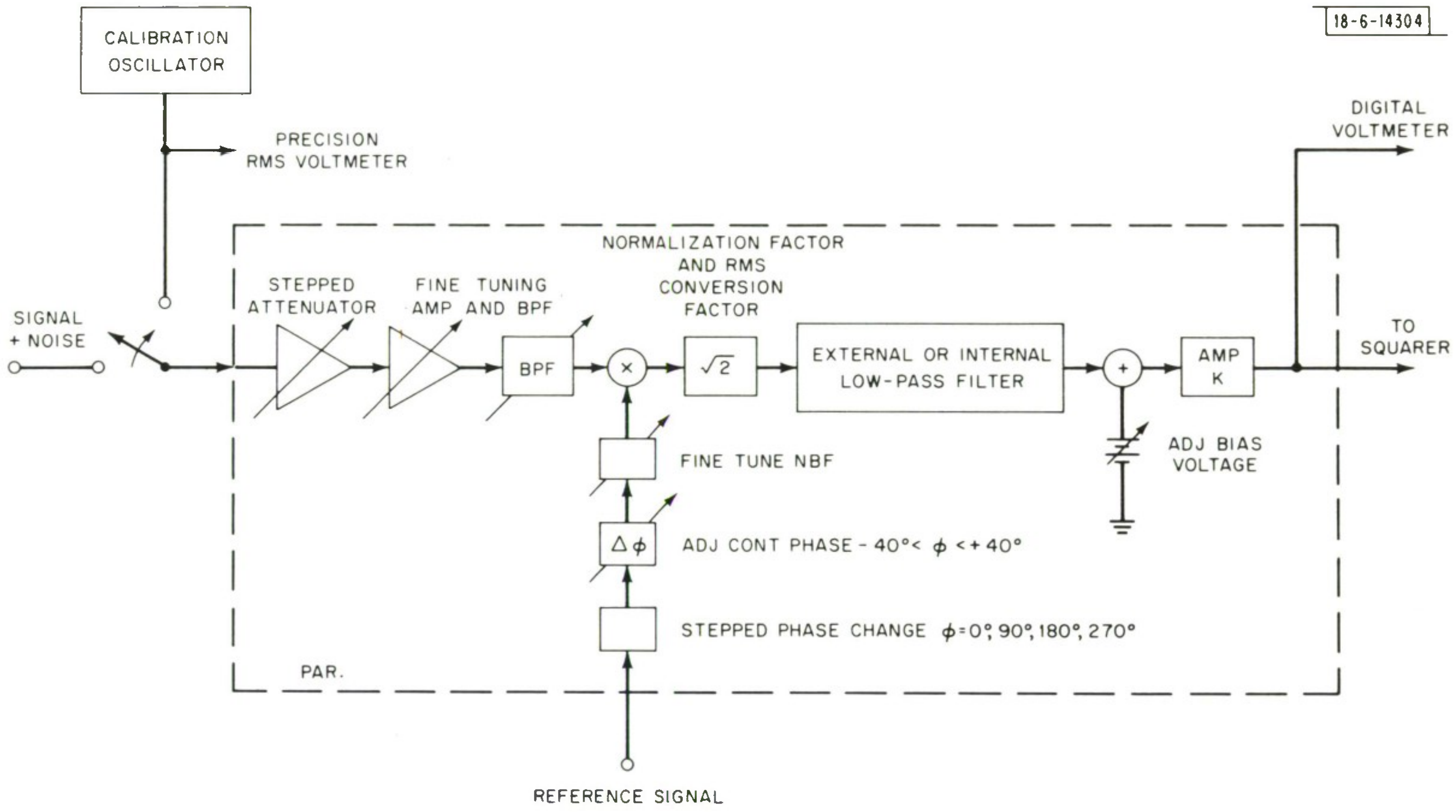

Fig. E-1. PAR representation.

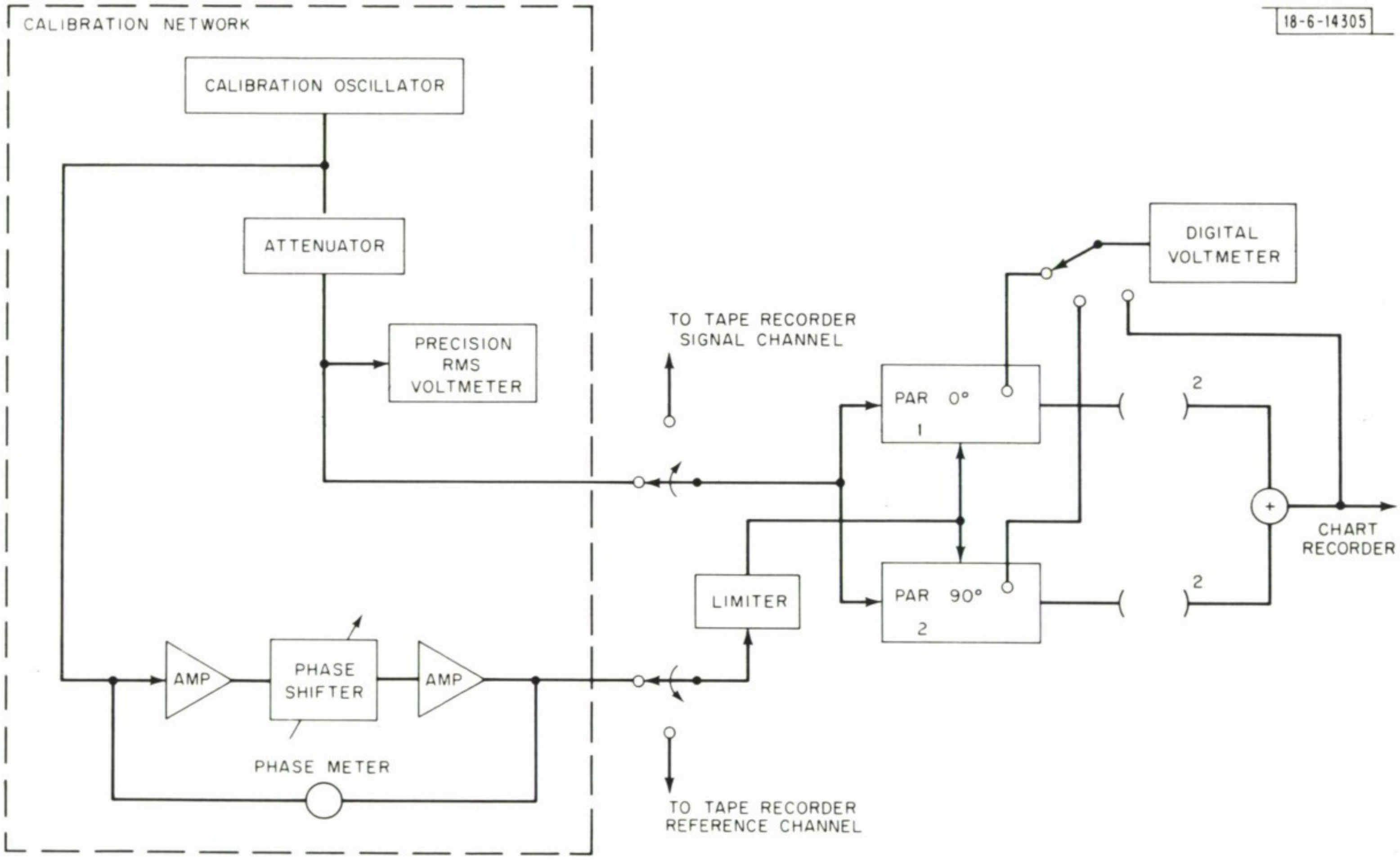

Fig. E-2. Calibration network.

to full scale input voltage) adjust the phase shifter so that the phase meter reads 0^{o}. On PAR no. 1 adjust first the frequency trim controls of the tuned amplifiers so that the output reading on the digital voltmeter (DVM) is a maximum. Then adjust the gain adjust control so that the output reads a full 10.0 volts. Ignore PAR no. 2 for the present.

b) Adjust the phase shifter so that the phase meter reads 90^{o}. On PAR no. 2 perform the same adjustments as performed on PAR no. 1 in the preceeding step. PAR no. 1 should have a reading close to 0 volts. Adjust the variable phase on PAR no. 1 a few degrees so that the output does in fact read exactly zero.

c) Adjust the phase shifter so that the phase meter again reads 0^{o}. The output of PAR no. 1 should read 10V. If not a small gain control adjustment should make it read 10V. PAR no. 2 should read close to 0 volts. Adjust the variable phase control on PAR no. 2 so that it does read 0 volts. The two PAR's now should be individually calibrated and in quadrature.

d) As a final check with the DVM connected to the output of the summer sweep the phase shifter through 360^{o} noting the output. If properly calibrated the output should not vary by more than a 0.1 dB.

The squarers and summer can be easily adjusted so that each of the segments agree with the predicted behavior to within 0.1 dB. The chart recorder is for each data run calibrated indirectly. That is after each run, with zero inputs to the PAR's, on <u>one</u> PAR a range of bias voltages (Measured with the DVM) are selected. The corresponding values then are marked on the chart recording next to the point to which the recorder pen was deflected. Hence on the chart we will have several values for the scale of the amplitude A (not the A^2 scale).

Another practical point concerns the behavior of the PAR's. Tape speed variations, if not compensated for, can yield an error in signal estimate of 1 dB or greater. This is due to the fact that the frequency responses of the tuned amplifiers in the signal PAR pair and in the calibration PAR pair are not identical. Speed variations of the order of 5% can give errors of the order of 1 to 2 dB depending on the particular band pass filters used in the tuned amplifiers. This problem has been circumvented by addition of a speed control loop which compensates within 1% for speed variations in both the recording and playback tape recorders.

APPENDIX F

Estimates of the Effects of the Round-the-World Wave

It is apparent that the earth-ionosphere cavity can have a standing wave pattern with significant nulls and peaks, wherever the direct and round-the-world signal components are comparable in magnitude. This is normally the case over a wide range of distances in the vicinity of the antipode for propagation in the lower ELF domain. Assuming a world-wide isotropic and homogeneous ionosphere of constant height, the total field is simply the sum of a direct component and an around-the-world component given by

$$(H_\varphi)_T = (H_\varphi)_{\mathscr{D}} + (H_\varphi)_{\mathfrak{R}}$$

where

$$(H_\varphi)_{\mathscr{D}} = F\, e^{-\alpha' d}\, e^{jk_o \left(\frac{c}{v_{ph}}\right) d} \qquad \text{(f-1)}$$

and

$$(H_\varphi)_{\mathfrak{R}} = -F\, e^{-\alpha'(2\pi r_e - d)}\, e^{jk_o \left(\frac{c}{v_{ph}}\right)(2\pi r_e - d)} \quad . \qquad \text{(f-2)}$$

F is given by equation 3 (Section II) and $d < \pi r_e$. Since the ionosphere is not isotropic and homogeneous, then a better approximation is to replace the exponential dependence by

$$\alpha' d \rightarrow \int_o^d \alpha'_{\mathscr{D}}(r)dr \;;\; \frac{c}{v_{ph}}\, d \rightarrow \int_o^d \frac{c}{v_{ph}}\, dr$$

$$\alpha'(2\pi r_e - d) \rightarrow \int_o^{(2\pi r_e - d)} \alpha'_{\mathfrak{R}}(r)dr \;;\; \text{etc.}$$

resulting in equations 6 and 7 in Section II. It must be mentioned that at present there is no complete mathematical justification for the simple replacement of exponential terms (although it is consistent with one's physical intuition). However, it tends to accentuate the nulls and peaks of the standing wave pattern and hence provides good bounds for the true value of total signal strength $(H_\varphi)_T$. Figure F-1 shows curves of $\left|\frac{(H_\varphi)_{\mathcal{D}}}{F}\right|$ and $\left|\frac{(H_\varphi)_{\mathcal{R}}}{F}\right|$ for various <u>constant values</u> of $\alpha_{\mathcal{D}}$ and $\alpha_{\mathcal{R}}$. In absence of phase information one can compute the maximum and minimum values of H_T from

$$\frac{|(H_\varphi)_T|_{max}}{|(H_\varphi)_{\mathcal{D}}|} = \frac{|(H_\varphi)_{\mathcal{D}}| + |(H_\varphi)|_{\mathcal{R}}}{|(H_\varphi)_{\mathcal{D}}|} \tag{f-3}$$

$$\frac{|(H_\varphi)_T|_{min}}{|(H_\varphi)_{\mathcal{D}}|} = \frac{|(H_\varphi)_{\mathcal{D}}| - |(H_\varphi)_{\mathcal{R}}|}{|(H_\varphi)_{\mathcal{D}}|} \; . \tag{f-4}$$

Figure F-2 is a graph of

$$\frac{|(H_\varphi)_T|_{min}}{|(H_\varphi)_{\mathcal{D}}|} \quad \text{and} \quad \frac{|(H_\varphi)_T|_{max}}{|(H_\varphi)_{\mathcal{D}}|} \quad \text{versus} \quad \frac{|(H_\varphi)_{\mathcal{R}}|}{|(H_\varphi)_{\mathcal{D}}|} \; .$$

We use these curves in the following ways:

(1) If the attenuation coefficients $\alpha_{\mathcal{D}}$ and $\alpha_{\mathcal{R}}$ are known constants and do not depend on location one can use curves similar to those in Fig. F-1 to determine $|(H_\varphi)_{\mathcal{D}}|/F$ and $|(H_\varphi)_{\mathcal{R}}|/F$ as well as the ratio $\frac{|(H_\varphi)_{\mathcal{R}}|}{|(H_\varphi)_{\mathcal{D}}|}$. If these are known then the maximum and minimum values of $(H_\varphi)_T$ can be found from Fig. F-2.

(2) If the attenuation coefficients $\alpha_{\mathcal{D}}$ and $\alpha_{\mathcal{R}}$ vary with direction and position then one must use the full equations 6 and 7 of Section II. Then with the use of Fig. F-2 one can compute the maximum and minimum values of $(H_\varphi)_T$.

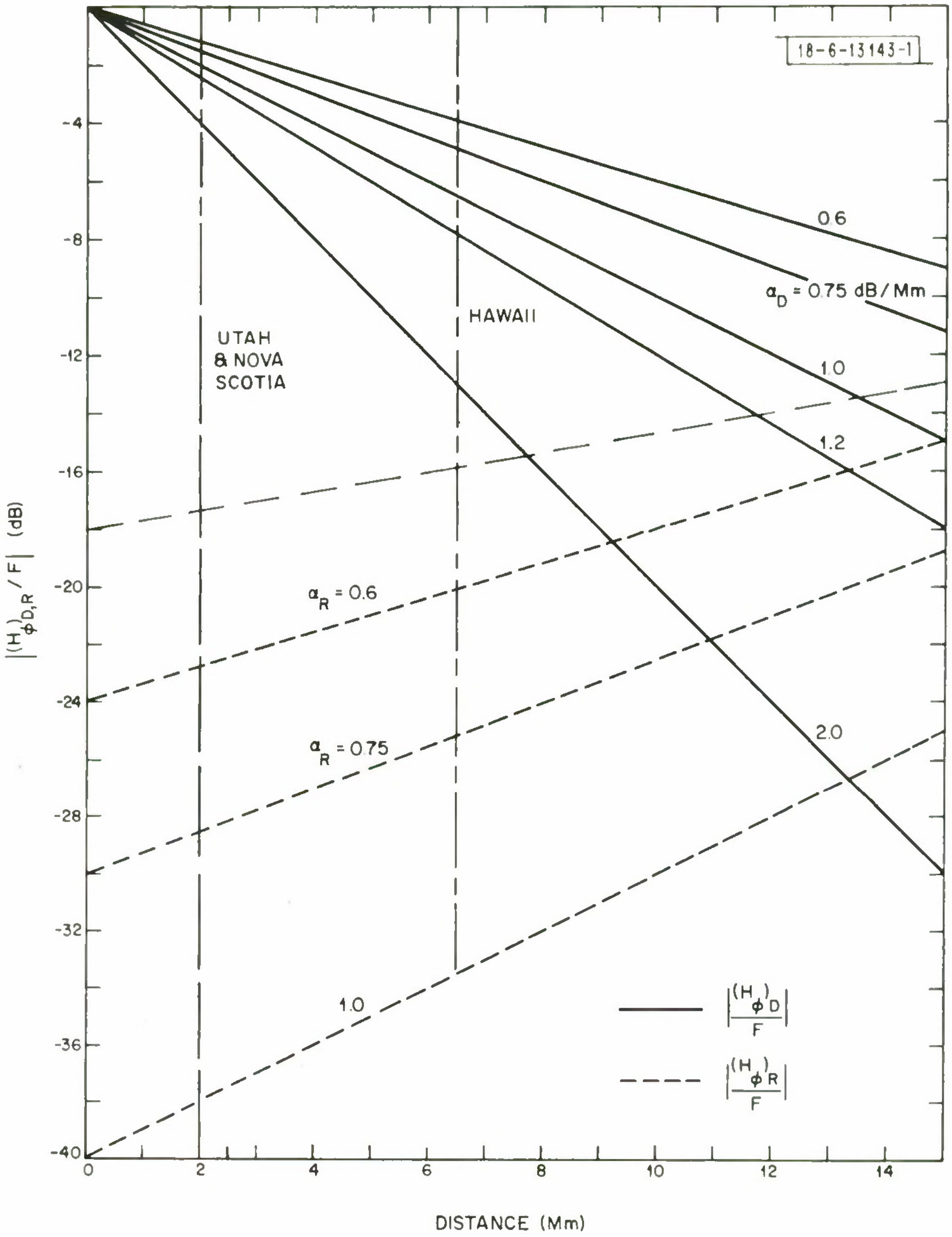

Fig. F-1. Normalized direct and round the world field strengths.

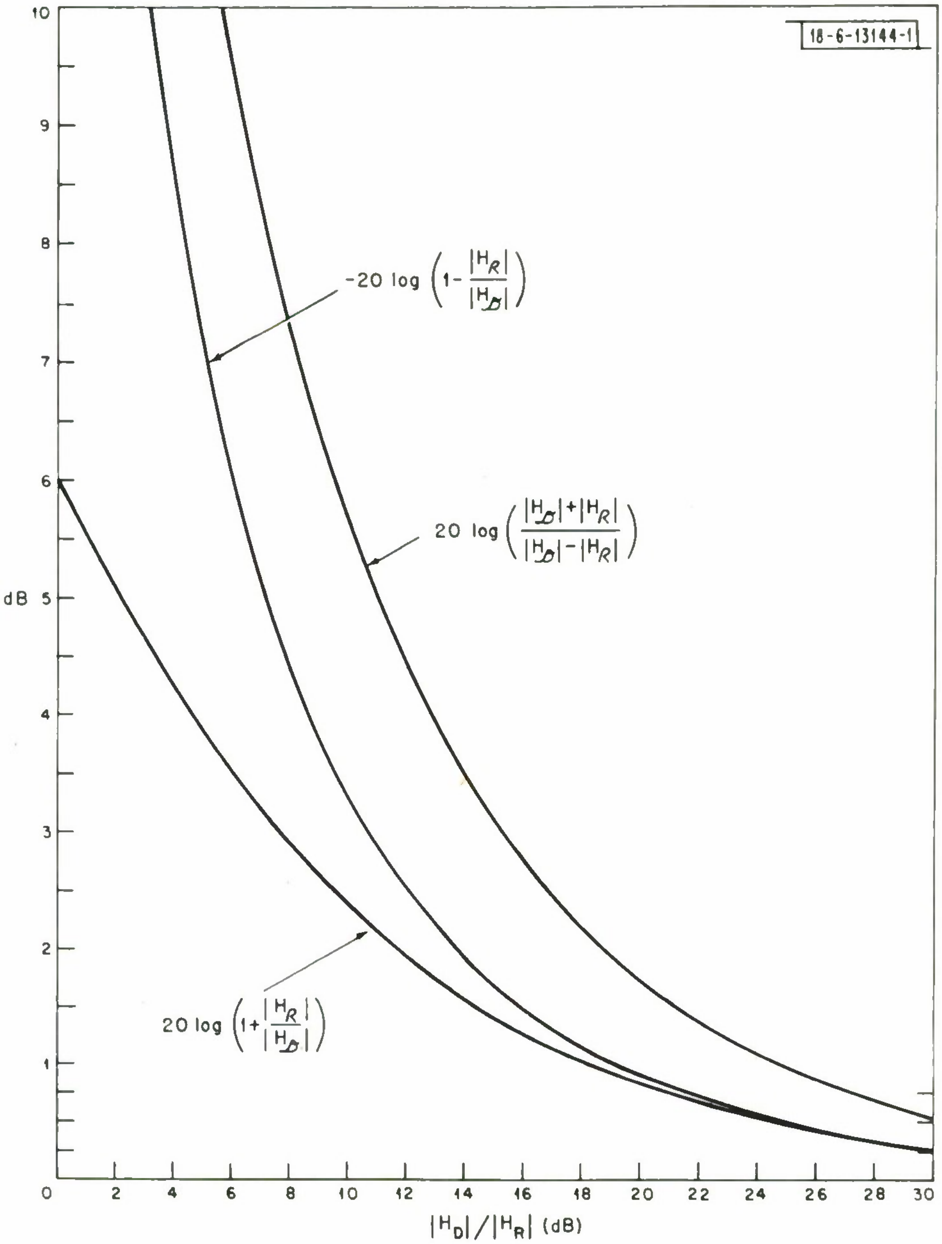

Fig. F-2. Maximum and minimum standing wave interference effects.

APPENDIX G

Location of Standing Wave Minima and Maxima and Magnitude of Standing Wavelength

Since we propose to change the position of the standing wave pattern relative to the receiver stations by changing frequency in small intervals it is necessary that we obtain reasonable assurance that the pattern shifts by about a full standing wave length over the frequency range. If this is so, the average of the total field strengths (weighted appropriately) will be a good approximation to the direct field strength at the center frequency (in this case at 45 Hz).

If one chooses as a model for the earth-ionosphere cavity the homogeneous cavity considered in the first part of Section II it can be shown that the minimums of the $|H_\varphi|_T$ standing wave pattern due to a surface dipole radiator are displaced from the antipode by a distance ρ' where

$$\rho' = \frac{(4n+3)c}{8f(c/v_{ph})} \qquad n = 0, 1, 2, \ldots$$

The standing wave length is then found from the above expression to be

$$\lambda_{sw} = \rho'_{n+1} - \rho'_n = \frac{\lambda}{2(c/v_{ph})} = \frac{c}{2f(c/v_{ph})} .$$

Now Hawaii is the station furthest away from the transmitter (d = 6.53 Mm and 13.47 M away from the antipode) and hence the station most effected by the interference. As an example let us look at the position of fourth minimum from the antipode (for $c/v_{ph} = 1.25$ and $f = 45$ Hz)

$$\rho'(45, n=4) = \frac{19(3 \times 10^8)}{8(45)1.26} = 12.56 \text{ Mm from the antipode and}$$

$$\lambda_{sw} = 2.64 \text{ Mm.}$$

Now assume we change the frequency to 46 Hz and again assume $(c/v_{ph}) = 1.26$

$$\rho'(46, n=4) = 12.27 \text{ Mm and}$$

$$\lambda_{sw} = 2.58 \text{ Mm.}$$

Thus although the standing wavelength changed only by .06 Mm the position of the standing wave pattern changed by .30 Mm which is greater than 10% of the standing wave length. At distances nearer to the transmitter, the shift in the null will have even a larger magnitude. It should now be obvious that with a relatively small change in frequency and hence in standing wave length we nevertheless get a significant change in the position of the standing wave null. Due to the structure of the transmitter's modulator, it is constrained to change frequency in steps of 1 Hz. Hence the next step is to determine the number of frequencies that we will require to make a reasonable approximation for $|H_{\varphi}|_{\rho}$ at 45 Hz.

Figure G-1 is a general set of curves which show how the maxima move both as a function of frequency and c/v_{ph}. The minima (which are not indicated) are half way between the maxima curves. The vertical axis is the distance from the transmitter antipode normalized by the free space wavelength $\lambda = c/f$. It should be evident by looking at this figure that for any fixed value of c/v_{ph}, if we change frequency over a 10 Hz bandwidth between 40 and 50 Hz the position of the standing wave pattern will change by more than a standing wave length with respect to either of the site locations. (In fact we could even select only those integer frequencies 41 to 49 Hz and be

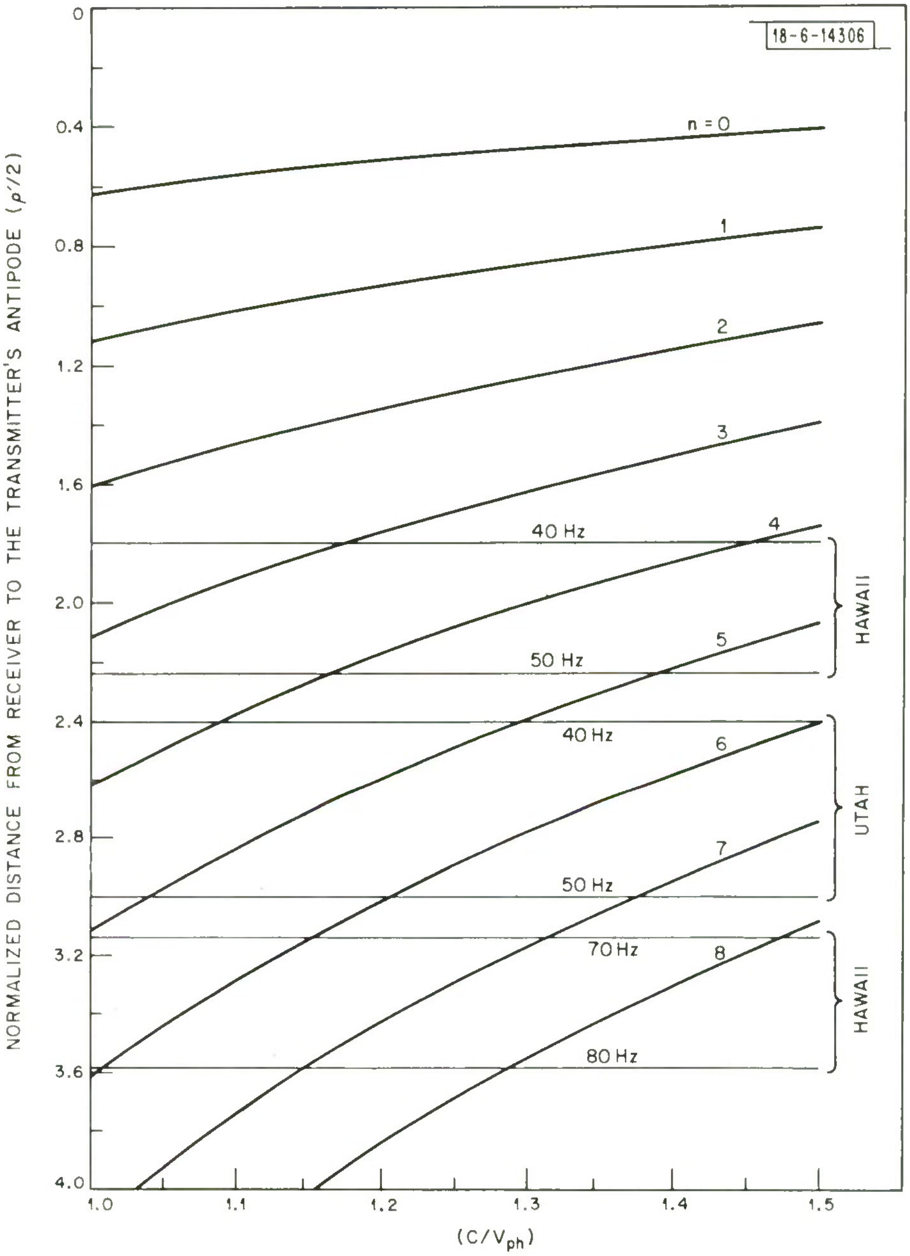

Fig. G-1. Location of standing wave maxima.

reasonably sure that we have a shift of more than a full standing wave length.) The argument can even tolerate small changes of (c/v_{ph}) with frequency.

Accordingly, we have selected a five frequency experiment with frequencies at 41, 43, 45, 47 and 49 Hz. The frequency band then is 8 Hz (~ 18% center frequency of 45 Hz). The expected decrease of c/v_{ph} over this band is of the order of only 2%. Hence there is little risk in equation 4 that the product $f(c/v_{ph})$ is a constant over the frequency range and as a result the step frequency changes should result in significant shifts of the standing wave pattern.

The preceding comments can also be applied to the 70-80 Hz range in an attempt to determine say $|H_{\varphi}(75)|_{\rho_0}$. The number of transmissions in the 70-80 Hz range was only 1/3 of those in the 40-50 Hz range. As a consequence no attempt was made to perform as comprehensive an analysis.

APPENDIX H

Transmission Schedule

Due to matters of economy the transmitter was operated only for two eight hour periods per day. One period was chosen to maximize the number of daylight hours for the entire Noval Scotia to Hawaii path and the other period the number of nighttime hours for the same path. We thus have purposefully avoided whenever possible the sunrise and sunset periods (where we know the signal level changes rather rapidly). The Nautical Almanac (1971) can be used to give local sunrise and sunset times for the period of experimentation. (An equally useful set of tables which also include the high latitudes is reference [17].) The time which we consider ionospheric sunrise or sunset corresponds to when the sun's zenith angle $\lambda = 99^\circ$ (this would correspond to the time when an observer who is stationed at an altitude of 85 km would begin to observe the limb of the sun over the bulge in the earth). The estimated ionospheric sunset and sunrise times are roughly interpolated from the local astronomical twilight and ground sunset (sunrise) times. Longitudinal corrections are made and then all the times are converted to GMT. Table H-1 shows the times for the reference date March 26, 1971.

Table H-2 shows graphically the day-night segments for all the sites and hence gives an indication of how the transmission times were chosen. An effective integration time T = 1. 42 hrs. was chosen for the bulk of this experiment. The position of the corresponding sample times with respect to the relevant all day or all night path is shown as well.

The transmission intervals were thus scheduled for

0300 - 1100 GMT (Nighttime transmissions)
1615 - 0015 (Daytime transmissions)

Table H-1. Sunrise and Sunset Times

Ref. Date March 26, 1971

		Sunrise			Sunset		
Location	Latitude °N Longitude °W	Begin Astronomical Twilight	Est. Ionospheric Sunrise	Sunrise $\lambda = 91°$	Sunset $\lambda = 91°$	Est. Ionospheric Sunset	End Astronomical Twilight
Hawaii	19° 15' N 155° 15' W	0447 * 0508 †	0523 * 0544 † 1544 GHT √	0600 0621	1813 1834	1850 1911 0511	1927 1948
Wendover Utah	40.66° 114.1°	0425 0401	0510 0446 1246	0555 0531	1817 1753	1857 1833 0233	1947 1925
β-Site Wisconsin	46° 04' 90° 53'	0415 0419	0504 0508 1108	0553 0557	1819 1823	1909 1913 0113	1959 2003
Nova Scotia	44° 26' 65° 13'	0415 0429	0504 0518 0918	0553 0607	1819 1833	1909 1923 2323	1959 2013

λ = Zenith Angle of Sun

Astronomical Twilight at $\lambda = 108°$

Est. Ionospheric Sunset or Sunrise $\lambda \simeq 99°$ (corresponds to $h = 85$ km)

* Std Local Time for Specified Latitude and Longitude of 15° (n) $n = 0, 1, \ldots 23$

† Std Local Time with Longitude Correction

√ GMT with Longitude Correction

* Values are from American Epherimis

TABLE H-2

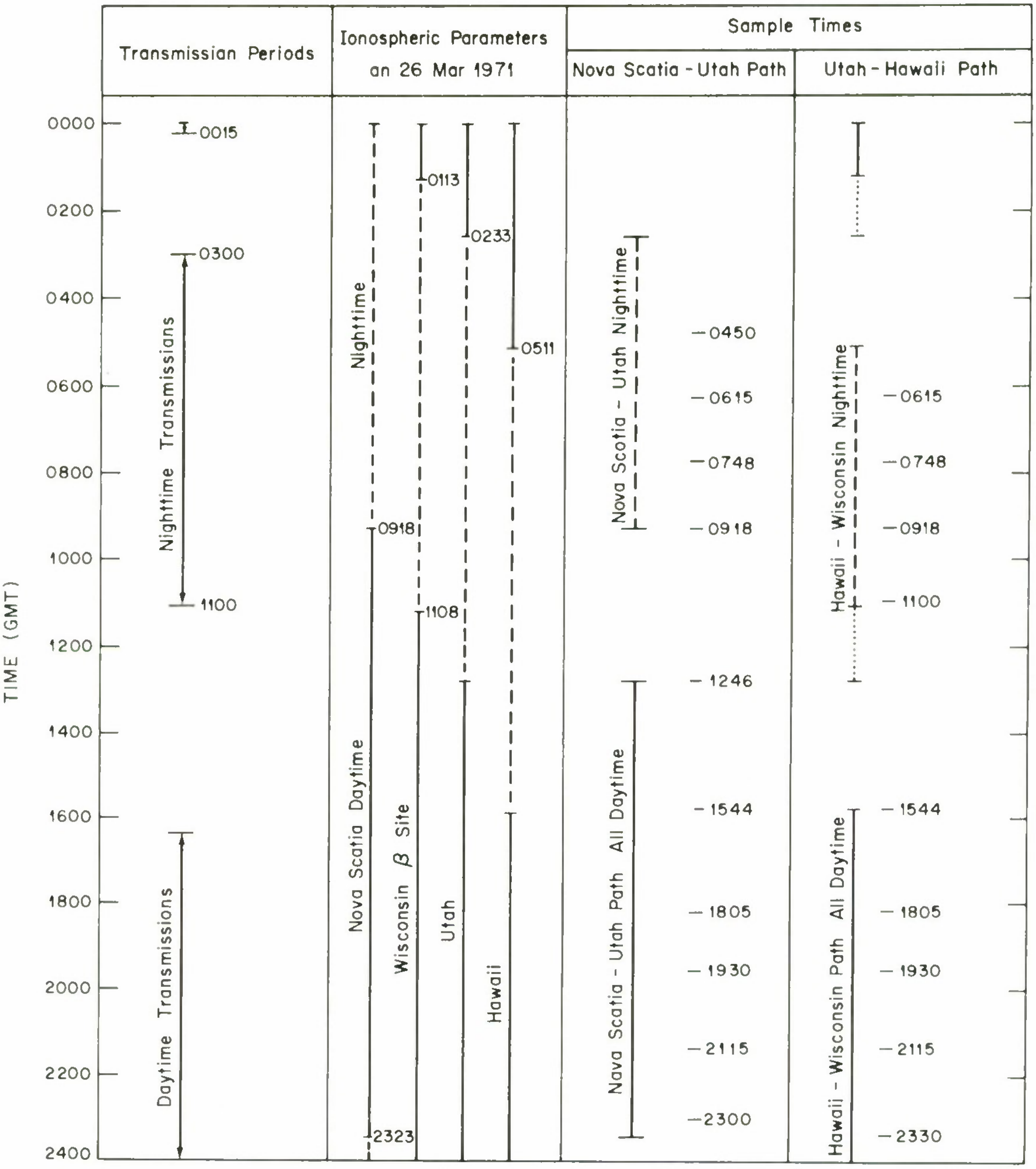
Transmissian Periods
Ionospheric Parameters an 26 Mar 1971
Sample Times
Nova Scatia - Utah Path
Utah - Hawaii Path
TIME (GMT)
0000
0200
0400
0600
0800
1000
1200
1400
1600
1800
2000
2200
2400
0015
0300
Nighttime Transmissians
1100
Daytime Transmissions
Nighttime
0113
0233
0511
0918
1108
2323
Nova Scatia Daytime
Wisconsin β Site
Utah
Hawaii
Nova Scatia - Utah Nighttime
0450
0615
0748
0918
1246
1544
1805
1930
2115
2300
Nova Scatia - Utah Path All Daytime
Hawaii - Wisconsin Nighttime
0615
0748
0918
1100
1544
1805
1930
2115
2330
Hawaii - Wisconsin Path All Daytime

APPENDIX I

Error Budget

The following is a discussion of the known error sources which contribute to error in a single measurement at a particular site. It should be noted that signal estimates are usually based on a number of individual measurements, the effect of which is to average some of the errors discussed herein. This effect will be discussed later.

Turns Area Product - The number of turns on the antenna is known exactly (471). It is estimated that the mean diameter can be measured to within ±.25 inches. Estimated error due to inexact turns area product is 0.8%.

Calibration Pad - An attenuation pad is employed to reduce the injected calibration signal to a known level and is injected in series with the antenna. The attenuation is constructed with a combination of .01 and .05% resistors. The overall estimated error is 0.1%.

Calibration Level - Field Measurement - The calibration level applied to the calibration attenuator is measured in the field and is used to determine the system gain. As discussed elsewhere the meters are calibrated against a secondary standard at the voltage where they will be employed. In view of this, the maximum error will accrue from meter reading and is estimated as 1.0%.

Frequency Gain Difference - The calibration signal is injected 1 Hz removed from the received signal frequency and used to calculate system gain. Since the gain at the two frequencies is not necessarily the same a correction is required to properly reference the two gains. This measurement is made with a shorted antenna at the field site before and after a measurement period. Calculations are based on the average of the two measurements. Error is estimated as 2%.

Calibration Level - Laboratory Measurement - The calibration signal must be estimated from the tapes during playback at the laboratory. Two factors enter into the error calculations: (1) Calibration of the instrument which is used to estimate the level and (2) accuracy of the squaring circuits used to form sum of squares. A signal substitution method is employed to estimate the calibration level. Under these conditions a calibrated voltmeter is used to measure the substitution signal and the error is due to meter reading (1%). The squaring circuits have an accuracy of 1% and two are employed. Assuming, worst case, that all errors are cumulative the error due to this effect is 3%.

Signal Level - Laboratory Measurement - The same methods are employed in signal estimation as for calibration level and the error is estimated to be 3%.

Crosstalk - Since it is necessary to generate a reference signal corresponding to the received signal frequency at the receiving site there is always a possibility of the undesired addition or subtraction of the reference signal from the received signal. This may occur in several ways including crosstalk between tape recorder heads, poor ground returns particularly in the front end, common mode coupling in power supplies, and magnetic coupling to the antenna. For our purposes any or all of the above will be considered as crosstalk and an error estimate for the combined effect stated. It should be noted that a well designed system will have low crosstalk and therefore it will be difficult to measure this level. Measurements of crosstalk on the systems employed in these tests have only been possible when the antenna was shorted and integration times of two hours were employed.

Crosstalk level has been observed to be constant for a particular piece of equipment, but not necessarily the same from one unit to another. Given a fixed crosstalk level the degree of degradation will be greatest at those frequencies and sites where the received signal is lowest. If Hawaiian operation at 45 Hz is chosen as an example of worst case condition the signal estimate may be in error by as much as 1.6%. Since the received signal phase is random with respect to the reference frequency phase this represents the worst possible or peak error, and will vary from run to run.

Contamination From Other Transmitted Fields due to Antenna Misalignment

The measurements are intended to measure the transverse horizontal magnetic field component H_φ since it is this component which will dominate as the range from the transmitter is increased. It is true, however, that both a radial (H_ρ) and a vertical (H_v) component are present; their strength being dependent on both range and bearing relative to the transmitter antenna pattern. If the receiving antenna is aligned perfectly (aligned along the vertical, and pointing precisely at the transmitter) then the H_ρ and H_v components will not influence the signal estimates. It is estimated that an angular mis-alignment of $\pm 2^\circ$ relative to the range vector between transmitter and receiver could exist at given site. This error could result from various causes, among them unknown local magnetic anomalies which could affect compass readings, mis-reading the compass, and errors in sighting in the antenna. An error in the vertical alignment of the loop would most likely result from the use of an inaccurate level, or a lack of care in antenna erection. This error is believed to be small and will be ignored henceforth.

The effect of small antenna misalignment from the true bearing will introduce an error into the estimate of H_φ since the H_φ and H_ρ fields will combine vectorially. Assuming that the receiving loop antenna is misaligned by θ_e the worst case resultant voltage induced into the loop antenna can be expressed as (see equation a-1)

$$V_{oc} = \omega N \mu_o A \left[|H_\varphi| \cos \theta_e \pm | H_\rho | \sin \theta_e \right] \qquad \text{(i-1)}$$

where H_ρ is the magnetic field component along the propagation path direction. For the single horizontal antenna, the far field ratio between H_φ and H_ρ is the following (Bannister [18])

$$\left| \frac{H_\rho}{H_\varphi} \right| = \left| \frac{c}{\omega d S_o} \tan \theta_b \right| \qquad \text{(i-2)}$$

where θ_b is the angle between electrical axis of antenna and propagation direction

S_o is the complex propagation constant

$\omega = 2\pi f$

d - distance from receiver to transmitter

The errors introduced by H_ρ are seen to greater for the closer in site locations. Table I-1 shows what we believe to be the maximum errors in signal estimation due to antenna misalignment.

Table I-1

Maximum Error in Signal Estimation due to Antenna Misalignment

	45 Hz	75 Hz
	East-West Antenna	East-West Antenna
Utah	1.06db	.59db
Hawaii	.27db	.15db

It is concluded that the maximum error at any site presently used or contemplated will not exceed 1.06db and this estimate is adopted as representative of this class of error.

Discussion of Total Error

For the purpose of this discussion all errors are expressed as percentage of the quality in question. All measurements are assumed to have Gaussian distribution about their mean value. Although there is some justification to assume that the stated error is seldom exceeded and therefore can be considered to represent two or three standard deviations (2σ, 3σ) we will employ the errors as representative of one standard deviation. It should be pointed out that those types of error which are not constant from measurement to measurement will be reduced by independent measurements. For these errors the standard deviation will be reduced by $\sqrt{N}$ where N is the number of independent measurements.

Based on a single measurement at a single frequency, the most probable error in estimating signal strength in the absence of noise is ± 5.23% (± .44 dB). Additional measurements under the same conditions will act to reduce the error. For example, if each of the reduceable sources of error was derived after 3 independent measurements then the probable error would be 3.21% (± .27 dB). In actuality, each number derived in this report would have to be examined as to the number of component measurements that went into its makeup, an error estimated for it, and then combined appropriately with other estimates with which it is subsequently used. In order to avoid this complexity we have adopted the course of assigning a worst case error which may be applied to all results.

Synopsis of Error Budget

Fixed Sources of Error

Turns Area	.8 %
Calibration Pad	.1 %
Antenna Misalignment	1.06%
Sub Total RMS	1.33%

Reduceable Sources of Error
(Reduceable by $\sqrt{N}$ where N ≡ no. of measurements)

Calibration Level - Field	1.0 %
Frequency Gain Difference	2.0 %
Calibration Level - Laboratory	3.0 %
Signal Level - Laboratory	3.0 %
Crosstalk	1.6 %
Sub Total RMS	5.06%

Total RMS Error Based on One Measurement	5.23% .44 dB
Probable RMS Error After N = 6	2.46% .21 dB

After careful consideration of the total number of measurements needed to obtain an estimate at a single frequency it was concluded that the average number was 6 (N = 6) and that the error to be associated with a single frequency estimate should be ± 2.46% (± .21 dB). Of course all ancillary estimates which make use of more than one single frequency measurement will have less error attached to them.

An example of the use of the error estimate as it pertains to the estimation of the propagation constant follows. Assuming that Utah and Hawaii are the two sites of interest, we assume that the signal estimate in Utah is high by .21 dB while the corresponding estimate in Hawaii for that measurement at that frequency is low by .21 dB. This leads to a differential error of .42 dB. Noting that 4.52 megameters separates Utah and Hawaii we conclude that the error in estimating the propagation constant in the absence of noise is

$$\frac{.42}{4.52} = .093 \approx .1 \text{ dB/Mm.}$$

Increasing the baseline measurement distance will reduce the error due to measurement error but will decrease signal strength at the distant station with a corresponding increase in uncertainty due to a lower S/N ratio.

ACKNOWLEDGEMENTS

We wish to acknowledge those people who directly or indirectly contributed to this experiment. First and foremost are Kenneth Hamilton and John Saia who built the equipment, collected the data and greatly assisted in the processing of the tapes. We thank our colleague, Harold Hoover, who helped evaluate and maintain the equipment as well as aided in the collection of the data.

We thank Colonel Kyle at Hill Air Force Base and the firecrew at Wendover Air Force Base for their invaluable help in locating a suitable site. Park manager, Edward Moses, of the Plum Island National Wildlife Refuge has been extremely tolerant over the past year in allowing us to use an area for the purposes of evaluating our systems.

REFERENCES

1. F. W. Chapman, et al., "Observations on the Propagation Constant of the Earth-Ionosphere Waveguide in the Frequency Band 8 c/s to 16 kc/s," Radio Sci. 1 (1966).

2. D. L. Jones, "Schumann Resonances and ELF Propagation for Inhomogeneous, Isotropic Ionospheric Profiles," J. Atmos. Terr. Phys. 29 (1967).

3. J. Galejs, "Propagation of ELF and VLF Waves Below an Anistrophic Ionosphere with a Dipping Static Magnetic Field," J. Geophys. Res. 73 (1968).

4. H. G. Hughes and J. F. Thiesen, "Diurnal Variations in the Apparent Attenuations of ELF Atmospherics over Two Different Propagation Paths," J. Geophys. Res. 75 (1970).

5. H. G. Hughes, "Nonreciprocal Attenuation Rates at ELF from 'Slow Tail' Measurements," J. Geophys. Res. 72 (1967).

6. D. P. White and D. K. Willim, "ELF Propagation Study (Phase I - Summer 1970)," Technical Note 1971-3, Lincoln Laboratory, M.I.T., (11 January 1971), DDC AD-718100.

7. J. R. Johler and R. L. Lewis, "Extra Low-Frequency Terrestial Radio-Wave Field Calculations with the Zonal Harmonic Series," J. Geophys. Res. 74 (1968).

8. J. Wait, Electromagnetic Waves in Stratified Media (Pergamon, New York, 1962).

9. J. Wait, "Earth-Ionosphere Cavity Resonances and the Propagation of ELF Radio Waves," Radio Sci. 69D (1965).

10. D. L. Jones, "Numerical Computations of Terrestial ELF Electro-Magnetic Fields in the Frequency Domain," Radio Sci. 5 (1970).

11. J. E. Evans, "Preliminary Analysis of ELF Noise," Technical Note 1969-18, Lincoln Laboratory, M.I.T. (26 March 1969), DDC AD-691814.

12. F. M. Greene, "NBS Field Strength Standards and Measurements (30 Hz to 1000 MHz)," Proc. IEEE 55 (1967).

13. S. Letzler and N. Webster, "Noise in Amplifiers," IEEE Spectrum (1970).

14. J. W. Craig, "Practical Designs for RC Active Filters Using Operational Amplifiers," Technical Note 1968-26, Lincoln Laboratory, M.I.T. (21 August 1968), DDC AD-674599.

15. J. Holsinger, "Confidence Intervals over Sample Sizes in the Measurement of Signal and Noise Powers, Signal-to-Noise Ratios and Probability of Error," Group Report 34G-9, Lincoln Laboratory, M.I.T. (3 January 1963), DDC AD-295133.

16. H. L. Van Trees, Detection, Estimation and Modulation Theory - 'Part I' (Wiley, New York, 1968).

17. United States Naval Observatory, Tables of Sunrise, Sunset and Twilight - Supplement to American Ephemeris 1946 (U. S. Government Printing Office, Washington, D. C., 1945).

18. P. R. Bannister, private communication.

DISTRIBUTION LIST

Chief of Naval Operations
Attn: Capt. Wunderlich (OP-941P)
Department of the Navy
Washington, D. C. 20350

Chief of Naval Research (Code 418)
Attn: Dr. T. P. Quinn
800 North Quincy St.
Arlington, VA 22217

Computer Sciences Corp.
Systems Division
Attn: Mr. D. Blumberg
6565 Arlington Blvd.
Falls Church, VA 22046
(3 copies)

IIT Research Institute
Attn: Dr. D. A. Miller, Div. E
10 W. 35th Street
Chicago, Illinois 60616

Institute for Defense Analyses
Attn: Mr. N. Christofilos
400 Army-Navy Drive
Arlington, VA 22202

Naval Civil Engineering Laboratory
Attn: Mr. J. R. Allgood
Port Hueneme, CA 93043

Naval Electronics Laboratory Center
Attn: Mr. R. O. Eastman
San Diego, CA 92152

Naval Facilities Engineering Command
Attn: Mr. G. Hall (Code 054B)
Washington, D. C. 20390

New London Laboratory
Naval Underwater Systems Center
Attn: Mr. J. Merrill
New London, CT 06320

Naval Electronic Systems Command
Attn: Capt. F. L. Brand, PME-117
Department of the Navy
Washington, D. C. 20360

Naval Electronic Systems Command
Attn: Mr. J. E. Don Carlos, PME-117T
Department of the Navy
Washington, D. C. 20360
(2 copies)

Naval Electronic Systems Command
Attn: Cmdr. K. Hartell, PME-117-21
Department of the Navy
Washington, D. C. 20360
(25 copies)

Naval Electronic Systems Command
Attn: Dr. B. Kruger, PME-117-21A
Department of the Navy
Washington, D. C. 20360

Naval Electronic Systems Command
Attn: Capt. J. V. Peters, PME-117-22
Department of the Navy
Washington, D. C. 20360
(2 copies)

Naval Electronic Systems Command
Attn: Mr. E. Weinberger, PME-117-23
Department of the Navy
Washington, D. C. 20360
(2 copies)

The Defense Documentation Center
Attn: DDC-TCA
Cameron Station, Building 5
Alexandria, VA 22314

DOCUMENT CONTROL DATA – R&D

(Security classification of title, body of abstract and indexing annotation must be entered when the overall report is classified)

1. ORIGINATING ACTIVITY *(Corporate author)* Lincoln Laboratory, M.I.T.	2a. REPORT SECURITY CLASSIFICATION Unclassified 2b. GROUP None

3. REPORT TITLE

ELF Propagation Study (Phase II – Fall 1971)

4. DESCRIPTIVE NOTES *(Type of report and inclusive dates)*

Technical Note

5. AUTHOR(S) *(Last name, first name, initial)*

White, David P. and Willim, Donald K.

6. REPORT DATE 15 February 1972	7a. TOTAL NO. OF PAGES 166	7b. NO. OF REFS 18

8a. CONTRACT OR GRANT NO. F19628-70-C-0230 b. PROJECT NO. 1508A c. d.	9a. ORIGINATOR'S REPORT NUMBER(S) Technical Note 1972-1 9b. OTHER REPORT NO(S) *(Any other numbers that may be assigned this report)* ESD-TR-72-54

10. AVAILABILITY/LIMITATION NOTICES

Approved for public release; distribution unlimited.

11. SUPPLEMENTARY NOTES None	12. SPONSORING MILITARY ACTIVITY Department of the Navy

13. ABSTRACT

An experimental measurement program has been undertaken to determine the parameters for propagation in the 40 and 70 Hz range. A transmitter in Wisconsin (WTF) transmitted simple sinusoidal signals for two eight-hour periods per day for 20 days. The radiated power was 1/4 watt at 45 Hz and 1/2 watt at 75 Hz. Receiver sites were located in Utah, Nova Scotia and Hawaii.

Subject to the constraints detailed in the text, estimates of the attenuation rates and the mode excitation factors have been determined with high accuracy. The daytime attenuation rates were found to be higher than those estimated previously on the basis of theoretical calculations. The nighttime excitation factor was also found to be a few dB smaller than previously expected. A careful analysis shows that directional differences in the attenuation rates ($|\alpha_{EW} - \alpha_{WE}|$) are less than 0.2 dB|Mm for both the 40 and 70 Hz range.

14. KEY WORDS

ELF propagation
sinusoidal signal